



 **Helmholtz-Zentrum
Geesthacht**
Zentrum für Material- und Küstenforschung

Effect of Dimensionality on Function: Fibers vs Films

Dissertation

zur Erlangung des akademischen Grades

Doktor der Ingenieurwissenschaften
(Dr.- Ing.)

Ahnaf Usman Zillohu

Kiel

2014

Gutachter 1: Prof. Dr. Mady Elbahri

Gutachter 2: Prof. Dr. Martin Müller

Datum der mündlichen Prüfung: 18.12.2014.

Declaration

I declare that this thesis has been prepared by me and I have not used any helping material other than that cited. This thesis has never been submitted to any university or examining body for evaluation. A major part of the thesis has already been published, as mentioned below, and is reproduced here after permission from the publisher.

- A. U. Zillohu, R. Abdelaziz, M. K. Hedayati, T. Emmler, S. Homaeigohar, M. Elbahri, Plasmon-mediated Embedding of Nanoparticles in a Polymer Matrix: Nanocomposites Patterning, Writing and Defect Healing, *The Journal of Physical Chemistry C* 2012, *116*, 17204.
- A. U. Zillohu, N. Alissawi, R. Abdelaziz, M. Elbahri, Thermo-plasmonics for Localized Graphitization and Welding of Polymeric Nanofibers, *Materials* 2014, *7*, 323.
- M. Jamali, M. K. Hedayati, B. Mozooni, M. Javaherirahim, R. Abdelaziz, A. U. Zillohu, M. Elbahri, Photoresponsive Transparent Conductive Metal with a Photobleaching Nose, *Advanced Materials* 2011, *23*, 4243.
- A. U. Zillohu, R. Abdelaziz, S. Homaeigohar, I. Krasnov, M. Müller, T. Strunskus, M. Elbahri, Biomimetic Transferable Surface for a Real Time Control over Wettability and Photoerasable Writing with Water Drop Lens, *Scientific Reports* 2014, *4*, 7407.

The thesis has been prepared maintaining the ‘Rules of Good Scientific Practice of the German Research Foundation’.

Ahnaf Usman Zillohu
Kiel, 04.08.2014

Dedicated to my Parents

Preface:

Due to the rapid scientific progress, today's advanced materials would be considered inferior according to tomorrow's requirements. This puts a tremendous pressure on material scientists to develop new materials that can cope with the design requirements of future. Thus, not only that new materials have to be developed but also attention has to be given on the ways to modify those which are currently available.

Physical restructuring is an efficient route to achieve this goal. One can observe in nature, that surfaces of many objects are structured for some specific functions, for example structuring on grass or lotus leaf for specific wetting properties; structuring on butterfly wing which not only is the source of its visually beautiful colors but also helps in directional flow of rain drop for easy drying, etc.

Since nature has perfected these techniques over millions of years, it would be wise to investigate how we can benefit from structured surfaces. Over the past decades, much work has been done on nanomaterials and their novel properties are beyond imagination. This thesis is an attempt to investigate and highlight the properties obtained when a surface is nanostructured compared to a flat one. The structuring is produced by electrospun nanofibers and the surface chemically similar but in the form of a flat film is used as a comparison to see the effect of dimensionality.

This is to be noted that in this thesis, dimensionality does not mean what is conventionally considered from nanomaterials, i.e., down to a few nanometers or a few atomic cluster. Rather, dimensionality is considered in a broader sense and more application oriented as concerning present day life. Thus, the nanofibers used may range from a few hundred nanometers up to a micron, however, compared to a water drop, for example, this structure is still very fine and can be regarded as a structured system compared to the flat surface of a film.

The first part of the thesis (Chapter 1) gives a brief introduction to the topic. The next three chapters, each starting with a detailed background to the topic of the chapter, discuss in the form of published/submitted research articles, the affect of dimensionality on materials' response in wetting, optical and plasmonic applications. Thus, Chapter 2, consists of a published paper dealing with the dimensionality and wetting properties; Chapter 3 deals with the optical properties particularly regarding the photochromic compounds and consists of one published and one submitted paper; whereas, thermoplasmonics are discussed in Chapter 4 which consists of two published papers.

Finally, in Chapter 5, is presented an introduction to experimental methods used for synthesis and characterization of samples. This is followed by summary of results and outlook for future work, constituting the Chapter 6.

I find myself deeply in debt and wish to thank all those who helped me during my thesis work. I hope that the contents of this thesis would serve its purpose and add to the overall human knowledge.

Ahnaf Usman Zillohu

Contents

Abstract.....	1
1 Introduction.....	3
1.1 Functionality and size:.....	5
1.2 Dimensionality:.....	6
1.3 References:.....	7
2 Wetting Properties of Films and Fibers.....	9
2.1 Background:.....	11
2.1.1 Wetting of Electrospun fibers vs. Film.....	13
2.2 Biomimetic Transferable Surface for a Real Time Control over Wettability and Photoerasable Writing with Water Drop Lens.....	15
2.2.1 Introduction:.....	15
2.2.2 Results and Discussion:.....	16
2.2.3 Conclusion:.....	24
2.2.4 Experiments:.....	24
2.2.5 Acknowledgements:.....	25
2.2.6 References:.....	25
3 Photochromic Films and Fibers.....	29
3.1 The light-matter interaction:.....	31
3.1.1 Light and Photochromic molecules:.....	31
3.2 Specular Reflection by Oscillating Photochromic Molecules with Tailored Photoswitchable Brewster Wavelength and Molecular Photonic Coupling.....	37
3.2.1 Introduction:.....	37
3.2.2 Results and Discussion:.....	38
3.2.3 Conclusion:.....	46
3.2.4 Experiments:.....	46
3.2.5 Acknowledgements:.....	47
3.3 Photoresponsive Transparent Conductive Metal with a Photobleaching Nose....	49
3.3.1 Introduction:.....	49
3.3.2 Results and Discussion:.....	50
3.3.3 Conclusion:.....	55
3.3.4 Experiments:.....	55
3.3.5 Acknowledgements:.....	56
3.3.6 References:.....	56
4 Plasmonic Heating of Films and Fibers.....	59
4.1 Light and metal nanoparticles:.....	61
4.2 Plasmon-Mediated Embedding of Nanoparticles in a Polymer Matrix: Nanocomposites Patterning, Writing, and Defect Healing.....	67
4.2.1 Introduction:.....	67
4.2.2 Results and discussion:.....	68
4.2.3 Conclusion:.....	73
4.2.4 Experiments:.....	74
4.2.5 Acknowledgements:.....	74
4.3 Thermo-Plasmonics for Localized Graphitization and Welding of Polymeric Nanofibers.....	77
4.3.1 Introduction:.....	77
4.3.2 Results and Discussion:.....	80
4.3.3 Conclusion:.....	83
4.3.4 Experiments:.....	83
4.3.5 Acknowledgments:.....	84
4.3.6 References:.....	84

5 Materials and Methods	87
5.1 Electrospinning:	89
5.2 Spin coating:	91
5.3 Sputter deposition process:	91
5.4 Optical microscope:	93
5.5 Scanning electron microscope:	94
5.6 Transmission electron microscope:	96
5.7 Atomic force microscopy:	97
5.8 Raman spectroscopy:	99
5.9 UV-Vis spectroscopy:.....	100
5.10 X-ray diffraction:	101
5.11 Contact angle measurement:	102
5.12 Ellipsometry:.....	104
5.13 Profilometry:	105
5.14 Materials and other specifications:	106
5.15 References:	106
6 Summary and Outlook	109
6.1 Summary:.....	111
6.2 Outlook:	115
Publications	117
Submitted papers.....	117
Published papers	117
Conferences:	118
Acknowledgements	119
List of Figures:	121
List of Tables:	122

Abstract

Decreasing the size of materials down to nanometer regime can result in unique properties not obtainable in their bulk counterparts and a tremendous effort has been invested in the ever expanding field of nanotechnology for its full utilization in a variety of applications. However, it is not only the size but also the dimensions (for example, either 1D fibers or 2D films etc) of the material that influence its function and this effect needs to be explored as well. In this thesis, the effect of dimensionality on the functional properties of submicron-sized systems is explored. In particular, polymer-based systems with and without a photochromic compound or metal nanoparticles, were prepared in the form of 1D electrospun nanofibers as well as 2D thin film, and the effect of their shape on the wetting, optical and plasmonic properties was investigated.

Regarding the wetting properties, it was found that where the polymer film was barely hydrophobic, the fibers were nearly superhydrophobic due to the roughness formed by the fibrous structure. Moreover, when the physical form of the fibers was changed by twisting them into the form of yarns, their wetting properties also changed from hydrophobic/sticky state to hydrophobic/slippery state. Further control over the wetting properties was demonstrated by structural modification of polymer by incorporating photochromic molecules.

Although not obviously, but the wetting properties of a material are affected by many of the variables that also affect its optical properties, e.g., its chemical nature, roughness, dimensionality etc. It was found that by controlling the size of photochromic fibers, their refractive index could be modulated with a result that their properties, after suitable optical stimulus, were either ‘enhanced absorptive’ or ‘enhanced transmissive’. The reflection rather than absorption based optical methodology was used to control the wavelength of reflected light by incorporating the interference effect in the reflected light and modulating the real part of refractive index. Moreover, a huge difference in Brewster wavelength of the polarized light reflected from photochromic molecules embedded in polymeric matrices of different polarity was observed. This polarity dependent difference in the wavelength of reflected light was much more pronounced compared to the polarity dependent difference in the wavelength of the absorbed light, thereby offering more sensitive method to evaluate polarity of different matrices.

Another unconventional affect of photochromic polymer film was discovered in the form of enhanced, photo-tunable, transparency of the hybrid system consisting of polymer-photochromic film coated on a thin metal film. The coupling between the dipole of embedded

photochromic molecule with its image in the thin metal film led to plasmonic tunneling which resulted in enhanced transmittance of the system. Moreover, the transmittance of light through the hybrid could be switched on/off by exposure to UV light and white light. Due to its high conductivity offered by the thin metal film, this hybrid can be a potential candidate for transparent conductor applications.

In modern functional materials, not only the photochromic compounds but also metal nanoparticles and films play a major role in light gathering and manipulation due to their plasmonic properties. In this work, the light gathering and heating effect offered by sputter coated silver nanoparticles to locally melt the underlying polymer film was studied. The polymer films, without any silver coat, could withstand exposure to laser without melting. However, a silver coated polymer film melted at a much weaker laser power, which resulted in the embedment of silver nanoparticles in the polymer at the point of laser exposure, thus forming a nanocomposite in submicron dimensions. Utility of this method in the submicron patterning, defect healing and welding/filling of microcracks in polymer films was also demonstrated. Even more, the ratio of different crystalline phases present in the structure of the polymer film also changed after resolidification, thereby demonstrating a control over local conformation and properties of the polymer. The utility of the thermoplasmonics was demonstrated by welding two polymeric nanofibers at a single point, thus paving the way for a process which may be useful in future optics and fiber based membranes technology. The heating effect was found to be so high as to locally graphitize the polymer.

In short, this thesis is an effort to highlight the utility of dimensional control to enhance the functionality of the materials according to the application and it is hoped that it would open the way for many new applications.

Chapter 1

Introduction

1.1 Functionality and size:

With increasing scientific progress, the demands from the high performance materials became so complex that conventional materials were of no further use and needed to be modified for a specific function or application. This raised the need for a new class of materials called the “functional materials”. Thus any materials, be it an alloy, a polymer or a ceramic etc., can be known as functional materials if it is used for specific function e.g., a gas sensor, light collector etc, not possible with conventional materials.^[1]

Until the end of 20th century, the topic of applied research was mainly conventional bulk materials even though nanostructure materials have been with us since centuries; for which an often given example is the colorful glass paintings found in Cathedrals. However, the scientific study of nanomaterials can be traced back to Richard Adolf Zsigmondy, the Nobel laureate in chemistry in 1925, for his research regarding individual gold "nano" colloids.^[2,3] Gradually, nanotechnology has already started to influence our lives, with over 1600 nanobased product that have been introduced only since 2005, which includes 24 percent boom after 2010.^[4] These include pharmaceuticals, stain and water repellent textiles, UV protection skin care, corrosion protection coatings, conductive coatings, sporting goods, etc. In order to fully utilize the potential of this new field, one needs to know what is a nanomaterial and where its properties come from?

The word ‘Nano’ actually comes from ‘dwarf’ in Greek and is equal to 10^{-9} m. So a human hair is like 65000 nm on average or about 108 gold atoms can be contained in 1 nm^3 .^[5] Conventionally, nanomaterials have at least one dimension below 100 nm,^[6] however, many submicron structures are also called nano because they are produced in some ‘nanosynthesis’ method or have some properties or applications not fulfilled by their bulk counterparts. Going down to micro-regime is simply miniaturization of systems, but going down to nano level results in completely novel properties. The remarkable properties of nanomaterials stem from very high surface area,^[7] a change in lattice constants in surface atoms due to relaxation and reconstruction,^[8] as well as due to the fact, that the many of the physical phenomena, such as electron mean free path, diffusion lengths, wavelength of light etc. are of the order of this length scale and as a result become irrelevant/critical in the case of nanoparticles. A higher fraction of surface atoms and ions naturally means increase reactivity, so gold which is considered inert would become a catalyst when it is in the form of nanoparticles.^[7] A change in lattice constants would mean a change in physical properties of the material. These effects together result in strange properties, like, the melting point of nanocrystal may be very low, even by a 1000 °C compared to bulk, semiconductor

nanocrystals would turn insulator, ferromagnetic materials lose their magnetism,^[7] or metal nanoparticles would become strong absorbers rather than scatterers of light etc.

1.2 Dimensionality:

However, it is not only the size that matters but also the shape (or its dimensionality) of functional materials affect their properties. The use of dimensionality by nature is easy to observe, for examples, the feather of a bird rather than being a continuous film, is made up of directional fibrous structure which not only gives it flexibility but also directional wetting properties. It naturally raises many interesting questions, whose answer is important not only to satisfy scientific curiosity but also because it can lead to many new products which can solve today's problems. For instance, if one needs a non-wetting surface, for scientific, industrial or domestic use; does the solution lie only in creating a new material, or is there a way to structure the surface that results in novel wetting properties not present in unstructured surface. It is here, that the importance of dimensionality becomes prominent as it affects the materials response regarding thermal,^[9] surface properties (wetting and reactivity), optical and mechanical properties^[10] and so on. As an example, the conductivity of thin film of carbon nanofibers has been shown to be anisotropic by a factor of 15. This value is much higher than the anisotropy generated by the oriented film of carbon nanotubes.^[11] In the optical regime, aligned nanofibers have been shown to act like a polarizer whereas the films of the same material are not.^[12] It is hoped that the present thesis contributes to broaden our understanding regarding dimensionality, as here, its effect on wetting, optical and plasmonic properties is presented.

It is worth mentioning here, that within this thesis, a 1D material would not be of the dimensions of a carbon nanotube or 2D would not be considered as a graphene sheet. Here, the meaning is a bit unconventional, as the behavior of films is compared with fibers that are hundreds of nanometer thick. One finds the importance of this study in view of practical requirements. As an example, one should be more interested in knowing the behavior of a water drop on a sheet of polymer and compare it with the mat of nanofibers rather than going down to the dimensions of molecular chains.

The reason for giving special attention to wetting and optical properties is their direct affect on our daily life in the form of many promising applications. For example, the photochromic systems have a potential use in optical switches,^[13] data storage and handling; thermoplasmonics are useful for localized chemistry and catalysis^[14] as well as in disease treatment;^[15] and surface with speciality wetting properties may be useful for self cleaning purposes, microdrop delivery, low drag^[16] etc. Polymers were selected as the test materials because of their ease of manufacturing into nanofibers or spin coated nanofilms. Moreover,

they can be loaded with different materials like photochromic compounds or sputtered with metal nanoparticles. Together with their good resistance to water/chemicals and transparency as well as colorability they serve equally good for testing the effect of dimensionality on optical as well as on wetting properties. However, it is worth mentioning that the motivation of this study was not only the promised applications but also a pure scientific curiosity.

1.3 References:

- [1] S. Banerjee and A. Tyagi, *Functional materials: Preparation, processing and applications*, Elsevier **2012**.
- [2] R. Zsigmondy, *Journal of the American Chemical Society* **1909**, *31*, 951.
- [3] D. Pile and J. Krenn, Perspective on plasmonics, in *Nature Photonics*, Nature Publishing Group, **2012**, *6*, 714.
- [4] <http://www.wilsoncenter.org/article/inventory-finds-increase-consumer-products-containing-nanoscale-materials>, Aug. 2014.
- [5] F. J. Owens and C. P. Poole, *The physics and chemistry of nanosolids*, John Wiley & Sons **2008**.
- [6] A. Tiwari, *Bioengineered nanomaterials*, Taylor & Francis **2013**.
- [7] G. Cao and Y. Wang, *Nanostructures and nanomaterials: Synthesis, properties, and applications*, World Scientific **2011**.
- [8] K. Hermann, *Crystallography and surface structure: An introduction for surface scientists and nanoscientists*, Wiley **2011**.
- [9] A. Henry *et al.*, *Physical Review B* **2010**, *82*, 144308.
- [10] L. Berhan *et al.*, *Journal of Applied physics* **2004**, *95*, 4335.
- [11] W. A. De Heer, A. Chatelain and D. Ugarte, *Science* **1995**, *270*, 1179.
- [12] D. Li, Y. Wang and Y. Xia, *Nano Letters* **2003**, *3*, 1167.
- [13] M. Irie, *Chemical Reviews* **2000**, *100*, 1683.
- [14] P. Christopher, H. Xin and S. Linic, *Nature chemistry* **2011**, *3*, 467.
- [15] G. Baffou and R. Quidant, *Laser & Photonics Reviews* **2013**, *7*, 171.
- [16] B. Bhushan and Y. C. Jung, *Progress in Materials Science* **2011**, *56*, 1.

Chapter 2

Wetting Properties of Films and Fibers

2.1 Background:

Surfaces with controlled wetting are of great importance as they promise a solution to a variety of today's problems. These specialized surfaces may either be water loving or water repelling. Water repelling surfaces can be used on boats to reduce drag,^[1,2] or protection against icing on aircrafts, dish antenna, wind mills and power lines, or would serve as self-cleaning surface just like the legendary lotus leaf, or would play a vital role in next generation scientific and home equipment, for example microdrop delivery in analytical systems,^[3-5] water directional collection systems^[6], etc. It is to be noted here, that not only water repellency (hydrophobicity) but also the ease of sliding of water drop on these surface is one of their crucial characteristics. On the other hand, surfaces with 'water-loving' (hydrophilic) characteristics would be of use in their own way, for example, easy cleaning surfaces simply by water, or as anti-fogging window glasses.^[7,8] Good biocompatibility of some 'water-loving' surfaces, such as titania, has also been shown for better cell adhesion^[9,10] and find use in bio-applications, etc. In short, surfaces with wetting characteristic specialized for intended use would sharply undercut the time, effort and money wastage.

In order to produce desired wetting properties, mostly the surfaces of natural objects are mimicked as these have been perfected over millenniums. Some of the surfaces are increasingly hydrophobic so that water drop balls up on them and easily slide, for example, the feather of a pigeon^[11] or the lotus leaf which is famous for its self-cleaning abilities,^[12,13] or wing of butterfly which have directional wettability.^[14] The hydrophobic nature and easy rolling of the water drop over these surface helps in keeping them dry and clean. Besides random rolling, the motion of the drop can also be directional, for example on a grass or rice leaf for self-irrigation purpose and cleaning along the entire length, etc. On the other hand, some of the natural surfaces are hydrophobic but still water drop tends to stick to them, an example being a rose petal on which even though the drop would ball up but still would not leave the surface even on an up side down tilt of the petal.^[15-17]

This means that two terms are required to quantify the wetting properties of a surface, i.e., contact angle (CA) and sliding angle (SA). Both these values depend upon the surface free energy as well as its physical structure or roughness. CA is the angle at which the solid-liquid interface intersects the liquid-air interface of a drop resting on a surface. It is the measure of interaction of liquid with the surface, thus for example, a surface with a high surface energy (because of free bonds etc) would tend to decrease its energy by having itself covered by the liquid as much as possible, resulting in a very low contact angle. The surface free energy term is explained by Young's equation for wetting behavior of perfect, homogenous surface while the roughness effects are covered by the Cassie and Wenzel

theories which are discussed in Section 5.11. Surfaces can be categorized as hydrophilic ($CA < 90^\circ$), hydrophobic ($CA \geq 90^\circ$) and superhydrophobic ($CA \geq 150^\circ$).^[18] The other term, i.e., sliding angle not only depends upon affinity of the surface with water as indicated by contact angle value but also on the penetration of the drop into the surface roughness features.

The wetting properties of natural functional surfaces are directly related with their chemical nature (surface energy)^[19,20] and more importantly to their physical structure (roughness)^[21] which is mostly hierarchical in nature. Considering again the lotus leaf, its surface is not only covered with wax (chemical effect) but also has microbumps, each with secondary roughness in the form of nanometer size hair (physical effect).^[22,23] When a drop of water is placed on this surface, some air is trapped in the rough features and drop cannot come in full contact with the surface which makes for the drop easy to roll over it. On the other hand, the bumps on a grass or rice leaf are aligned along the length, thus creating a groove like structure. A rolling drop on such a surface would need to cross higher energy barriers in order to move across the length of the leaf, which thus becomes an unfavorable flow direction. The effect of roughness in the structure of a lotus leaf can be highlighted by looking at the CA values. A flat wax surface shows a contact angle of only 74° (i.e., primarily hydrophilic) and the CA on a leaf with micropatterned wax is about 126° (i.e. hydrophobic). However, when the wax is nano-structured (as found in dry or fresh leaves) the contact angle rises to superhydrophobic value of 163° , with sliding angle as low as only 3° .^[12,24]

In the man made things, one observes the same influence of surface chemistry and physical structuring. So Teflon, which is one of the best bulk produced hydrophobic materials has a very low surface energy (18 mJ/m), while glass has a high surface energy (250 mJ/m).^[25] As a result, water would ball up on Teflon ($CA 108^\circ$)^[26] and would spread on glass ($CA \sim 35^\circ$). However when the surface of Teflon is roughened by RF-sputtering, its CA value may go as high as 165° with a very low hysteresis of only 3° .^[27]

After a successful structuring of a superhydrophobic surface by Onda *et al.* in 1996,^[29] a lot of research has been carried out by various groups to produce a specially structured roughness on surfaces intended for specific wetting applications, mostly mimicking nature. There is a variety of processes available^[30-33] like laser ablation and photolithography based microfabrication,^[34-36] solidification of dimers,^[29] microwave plasma enhanced CVD,^[37] phase separation related roughness,^[38] oxygen plasma treatment,^[39] sol-gel,^[40] large area template rolling,^[41] template extrusion,^[42] electrohydrodynamic technique,^[43] electrochemical deposition^[43,44], and so on.

Many of these methods are specific to certain materials (for example carbon nanotubes or some particular class of polymer and so on) or require some treatments which

actually damage the surface of the object for roughness formation and the process is irreversible. A better process would be one, which can be applied to a variety of materials, is simple, economical and most importantly does not damage the surface. Keeping these demands in view, electrospinning turns out to be one of the best candidates as it can be used to make micro- or nanofibers from a variety of material, like polymer, ceramic or composites. Moreover, the surface structure of individual fiber as well as, their collective arrangement on the surface can be easily controlled. Above all, the fibers can be laid on any surface and then removed on demand. A detailed description of electrospinning is given in the Chapter 5.

In the present work, electrospinning was used to produce fiber of a polymer and these were then subsequently given the form of yarns. The wetting properties of the structure formed by these yarns were then compared with that of random fiber mat as well as a thin film of the same polymer. Following is the brief summary of results while the details of the work (in the form of submitted published paper) follow it.

2.1.1 Wetting of Electrospun fibers vs. Film

The CA of water drop on a film of polyvinylidene fluoride (PVDF) was compared with that on the electrospun fibers of PVDF as a randomly collected mat as well as specially structured yarn. It was found that PVDF film was hardly hydrophobic as its contact angle was only 80° . However, when the roughness was added to the same materials, the contact angle immediately turned into almost superhydrophobic with a CA of 130° .

The wetting behavior of surface with loose fibers mat mimicked the surface of a rose petal as it would not let the drop to roll over it, rather it could be turned up side down without letting the drop fall. The sticking of the drop originates from the capillary driven penetration of water in the pores between fibers.

The same fiber mats were then rolled and pulled into a form of yarns, which were laid on the random fiber mat. The water drop could roll on such a surface with a tilt angle of around 45° . This was attributed to the reduced contact of the drop with the surface as well as to a decrease in pores between fibers after their compaction into the form of yarn. The polymer became dominantly amorphous and less polar after a photochromic compound, spirophenanthroxazine or SPO, was blended in it (please see section 3.1.1, page 33-34 for some information about SPO). This resulted in further decrease in sliding angle. Thus the control on wetting was demonstrated based on physical structuring as well as chemical. The water drops on the fibers-chromophore system acted as a lens for the UV light, concentrating it on the water-fibers interface due to multiple reflection and interference. The amplification effect enables to use even low power UV sources to carry out UV driven processes to the confinements of the water drop without endangering the rest of the surface by the unwanted

Wetting Properties

UV exposure. The use of water lens as a removable template for patterning as well as a qualitative tool, used for in detecting any UV absorbing species added in water, was also demonstrated.

2.2 Biomimetic Transferable Surface for a Real Time Control over Wettability and Photoerasable Writing with Water Drop Lens

*Ahnaf Usman Zillohu, Ramzy Abdelaziz, Shahin Homaeigohar, Igor Krasnov, Martin Müller, Thomas Strunskus and Mady Elbahri**

Scientific Reports, **2014**, 4, 7407. DOI:10.1038/srep07407 (2014)

We demonstrate a transferable device that can turn wettability of surfaces to sticky or slippy, as per requirement. It is composed of polymeric yarn with a fibrous structure, which can be lifted and placed on any surface to render it the unique wettability properties. We introduce polyvinylidene fluoride (PVDF) random fibers as biomimetic rose petal surface. When it is decorated with PVDF nanofibers yarns, the random mesh transform from rose petal sticky state into grass leaf slippy state. When it is placed on sticky, hydrophilic metal coin, it converts the surface of the coin to super hydrophobic. Adjustments in the yarn system, like interyarn spacing, can be done in real time to influence its wettability, which is a unique feature. Next, we load the polymer with a photochromic compound for chemical restructuring. It affects the sliding angle of water drop and makes the fibers optically active. We also demonstrate a “water droplets lens” concept that enables erasable writing on photochromic rose petal sticky fibrous surface. The droplet on a highly hydrophobic surface acts as a ball lens to concentrate light onto a hot spot; thereby we demonstrate UV light writing with water lenses and visible light erasing.

2.2.1 Introduction:

Regarding the wetting properties, there has been a growing interest to mimic natural surfaces, as these have perfected for specific purposes over a time of millions of years. So one observes a lotus leaf which is superhydrophobic, i.e. water drop contact angle of more than 150° , on which a water drop can roll randomly for cleaning purposes.^[45,46] The surface of a grass leaf is also superhydrophobic but is structured in such a way that water drop rolls along the length of the leaf for self irrigation of the plant.^[47] On the other extreme one finds a rose petal leaf to be superhydrophobic but posing so sticky surface to a water drop that it can be tilted upside down without letting the drop go.^[48] Such highly specific properties of naturally occurring surfaces are based not only upon their chemical nature but also on a certain physical structure.

For ideal solid surfaces, i.e., one which is perfectly smooth, flat, rigid and which is also chemically homogeneous, insoluble and nonreactive, the wetting characteristics are defined by the Young's equations as a function of the interfacial free energies.^[49] However,

most of the real surfaces existing in nature or fabricated in laboratories are rough and/or chemically heterogeneous. In such a case the Young's equation has been modified according to Cassie or Wenzel model.^[50,51]

In the Cassie state, the drop is not in full contact with the surface and is partly supported on air pockets that are existing between surface features. Thus, it is in a so-called "composite state". In contrast to this, the Wenzel drop penetrates into the surface feature which results in an increase in contact area. Since the contact line is anchored between the surface features, the surface holds onto the drop and steeper tilt angles are required to initiate its sliding. Similarly, the opposing wetting behaviors of grass leaf and rose petal stem mainly from their surface roughness features.^[52,53] In general, both of these surfaces have microbumps but these bumps are present in a different arrangement and therefore behave differently towards a water drop. So grass leaf has a Cassie-Baxter surface on which the water drop easily slides but rose petal surface shows a hybrid of Cassie-Baxter/Wenzel surface where droplets could partly penetrate at least the sublevel of the hierarchical roughness by physical mean (i.e. capillary action of microporous micro/nano scale structures) or chemical mean (i.e. hydrophilic interaction) and hence sticks to the petal.^[54]

There is a variety of methods available to mimic these structures, which range from templating and molding, plasma etching, electrospinning to acid or solvent treatment and phase separation, besides others.^[55-60] These processes restructure the surface in the form of nanotubes,^[61,62] bumps,^[63] fibers^[64,65] or spheres^[55] etc., which is as important for special wetting characteristics as is its chemical nature.^[66-68] The progress in artificially made natural surfaces has resulted in a plethora of applications, such as self cleaning coatings on big structures, coatings against snow collection,^[69] coatings on boats for low drag,^[54] etc. On the other hand, coatings with sticky characteristics can be used as a mechanical hand for microdrop delivery,^[61] as an example, but are still in a state of infancy.

Going beyond nature, i.e. acquiring the ability to change wetting properties of a surface in real time would lead to many new applications. Even more, integration of sticky hydrophobic droplet in controlling light has potential applications in field of optics but has not been introduced so far.

2.2.2 Results and Discussion:

PVDF was selected as a test polymer in this study. It is a fluoropolymer and consequently shows a very good chemical and moisture resistance. This ability is necessary for its potential application, e.g., in microcapillary fluid delivery, etc, where a polymer may come in contact with different liquids. Moreover, it easily lends itself to electrospinning – the method used for making nanofibers in this study. Electrospinning is a simple and fast method

for producing fibers of different composition, surface texture and size. These 1D fibers can be oriented/aligned in 2D to 3D forms either individually or in the form of yarns. Theoretically, these flexible fibers/yarns can be laid on many types of substrate along with their specific wetting properties. The electrospun fibers used for preparing the functional surface had an average fiber diameter of about $1\ \mu\text{m}\pm 200\ \text{nm}$, **Figure 2.1a**, and were collected in the form of a loose mesh. The surface of individual fibers was rough due to presence of nanobumps of size approximately 100 nm or less. PVDF random fiber mat was found to be highly hydrophobic with water drop contact angle of $130\pm 3^\circ$, which is much higher compared to that found on its film, i.e., 80° . This increase in contact angle is because of increased surface roughness.^[70-73] Considering a high contact angle, one might expect that a water drop should simply slide on the fibers, but, on contrary, water drop stayed sticking to them and the fibrous surfaces could even be tilted upside down without letting the drop to fall, **Figure 2.1b**. Actually, if the drop was pulled away from the fibrous mesh, the fibers would pull out of mesh along the drop **Figure 2.1c**. Thus, we have a highly hydrophobic but sticky surface which resembles a rose petal wherein the stickiness came from the porous nature of the electrospun fiber mat,^[74] which acts as capillary channels where water could seep into the spaces between the fibers and lock the drop to the surface.

An increase in contact angle of polymer nanofibers compared to that of the bulk film is already known.^[75-77] However, turning the same fiber from being sticky to a slippy, has not been introduced so far to best of our knowledge. For many applications, a surface not only needs to be superhydrophobic but also water should not stick to it, i.e., it should show the so-called grass leaf effect.

As mentioned earlier, that a surface can be modified from a being a sticky to a slippy one by several methods, like plasma treatment,^[78] electrochemical deposition,^[79] or chemical vapor deposition,^[80] etc. However, here we convert a rose petal like, hydrophobic sticky character of the surface to a grass leaf like slippy one, by physical restructuring. This was carried out by lying on the random mesh, a hierarchical structure composed of yarns prepared with electrospun nanofibers. To prepare a yarn, the fibers were simply twisted and pulled manually in the form of threads of $\sim 250\ \mu\text{m}$ average diameter. Twisting of the fibers into yarn brought the fibers densely close together and they appeared as dense nanostructured ridges on random fiber mats, as seen in the SEM micrograph, **Figure 2.1d**. These yarns were then laid on the random fiber mat with interyarn spacing of about $500\ \mu\text{m}$ (called "medium packing" onwards), **Figure 2.1e**. The structure thus formed can be called an artificial grass leaf on which the drop could slide at a tilting angle of about 45° , **Figure 2.1f**.

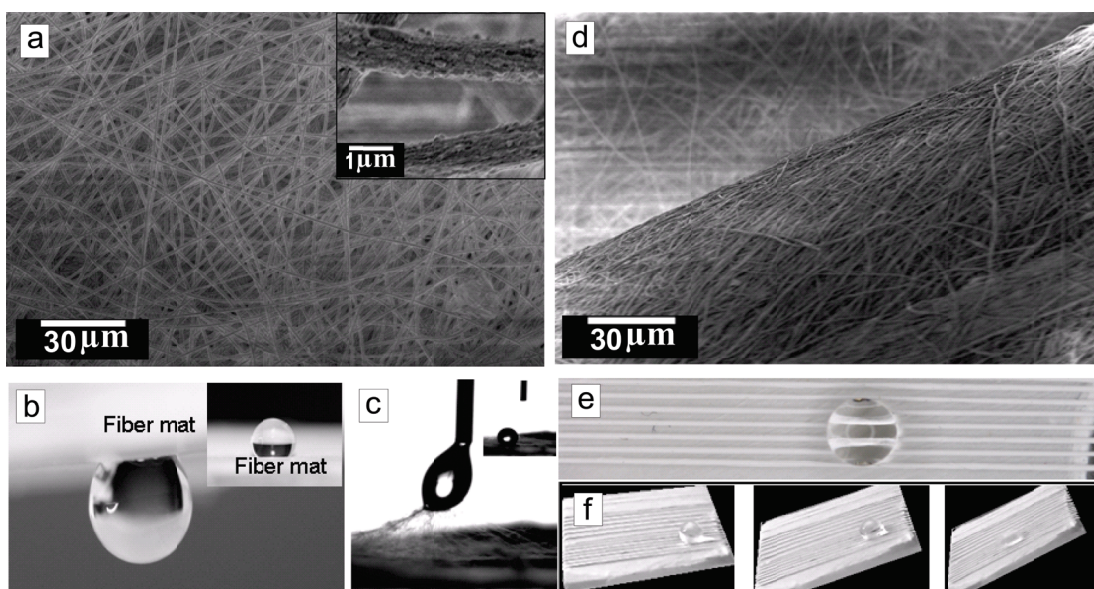


Figure 2.1 a) SEM micrograph of PVDF random fiber mat. Inset shows the rough surface of individual fibers. b) Water drop sticking to a random fiber mat. Inset shows same water drop when right side up. c) Camera pictures showing fibers being pulled out of random fiber mat, along with the water drop. Inset shows the drop ultimately staying with fibers mat. d) SEM micrograph showing the surface of half of the yarn. Random fiber mat under the yarn is visible in the background. e) Top view of a water drop sitting on PVDF yarn that was arranged on PVDF random mesh. f) Sequence of pictures showing water drop sliding on yarn when it is tilted.

The sliding of the drop on a yarn like surface roughness could be attributed to the fact that the drop was not completely touching the surface rather it was supported by the yarn only at some points and the rest was suspended in air, **Figure 2.2a**. Therefore, it was in a kind of "composite state". The twisting and rolling carried out during yarn formation also decreased the number of loose fibers on its surface which otherwise could act as pinning sites against the drop sliding. The compaction of structure and a decrease in loose fibers on yarn surface made the surface slippery towards a water drop. This, together with the presence of air pockets under the drop and between the yarns eased the sliding of the drop. Even though the yarn had much lesser pores which otherwise could be the pinning site for the drop as in the case of random mesh, but still these pores were not completely eliminated, **Figure 2.1d**. As a result, the sliding started only after breakage of the anchor points and the drop accelerated during its motion on the yarn like features. When a drop was placed slowly on the surface its contact line could come to equilibrium with a course of time after its capillary seepage into the tight pores between the nanofibers composing the yarn and got pinned there,^[81] **Figure 2.2b**. On a tilt, the drop was attached to these points by so-called microcapillary bridges and its movement was only possible by necking and rupture of these bridges. After detachment, the drop accelerated on the surface, unlike its slow motion on a smooth film, due to reduced dynamic friction. The accelerated motion of a moving drop starts due to additional energy stored in the stretched column, which was released on its breakage. Further pinning of the

drop during its travel on the yarn was sometimes observed, but was generally absent due to momentum of the drop so that it could not track the surface inhomogeneities, giving rise to dynamic hydrophobicity.^[81]

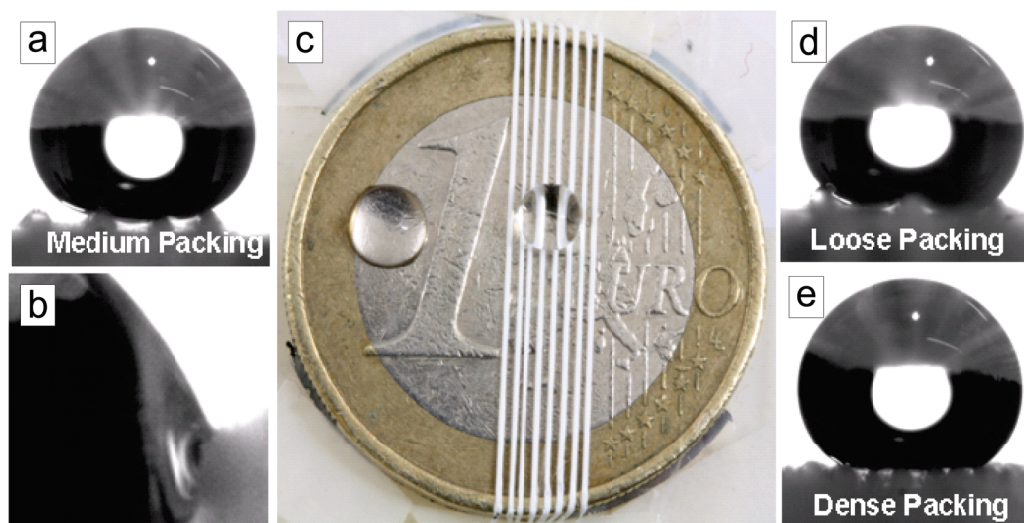


Figure 2.2 a) Water drops sitting on yarns with medium packing density. b) Anchoring of water drop on a yarn. c) A coin covered with yarns with water drops on the coin and the yarns. d) Water drops sitting on yarns with loose packing density. e) Water drops sitting on yarns with dense packing density.

A big advantage of yarn like setup is that it can be removed from one surface and placed onto another along with its hydrophobic properties. As an example, the same yarn was removed from random fiber mesh and placed on a metal surface (a coin) to convert it into a slippery hydrophobic surface, **Figure 2.2c**. It is obvious that the contact angle of the drop with yarn was hydrophobic but with the bare metal surface, it was hydrophilic. On tilting the coin the drop slipped on the yarn at around 42° tilt while it did not leave the bare coin even on an upside down tilt. In fact, our setup can be devised to change the interyarn spacing in real time so as to affect the sticky/slippy behavior of the surface.

Having proved the switching of the surface from rose petal (random fiber mesh) to grass leaf (yarn on top of random mesh) by surface restructuring, we further demonstrate the ability of our device to change the sliding angle by simply adjusting the distance between yarn, which can be done in real time by proper arrangements. We placed the yarn on the random mesh with almost no interyarn spacing (called “dense packing”) and with 1mm spacing (called “loose packing”) which was about double to that used in the “medium packing”. The average tilt angle required to initiate sliding of drop on yarn with different packing density is presented in **Table 2.1**. The medium packing arrangement of yarn seemed to be the most efficient as yarn with both “loose packing” and “dense packing” needed steeper tilt angle to initiate the drop slide. A small ($\sim 8\%$) variation in the results was observed which might have arisen from the dynamic nature of the test. Despite that the core

concept of switching the sticky/slippy state of the surface just by physical restructuring of the same fibers into yarns, remains firm.

Table 2.1 Tilt angles required to initiate the drop rolling on surfaces with different roughness

	Loose packing	Medium packing	Dense packing
Tilt angle for slip	64°±5°	45°±3°	53°±5°

It can be seen in **Figure 2.2d** that in the case of “loose packing” the distance between the yarns was so big that the drop could curve into the space between the yarns and could touch the random fiber mat under the yarn. This not only increased the contact area of the drop with the surface but also brought in the sticking effect offered by the random fiber mat lying under the yarn. That is why; a drop sitting on the “loose packing” required the steepest tilt angle to slide. “Dense packing”, **Figure 2.2e**, presented a behavior that was average between “medium packing” and “loose packing”. Here, even though the drop was not in contact with the random fibers mat as in the case of “loose packing” but still the air pockets under the drop, as offered by “medium packing”, were also missing. An increase in the contact area with the surface meant more anchoring sites that hindered the easy sliding of the drop. The contact angle hysteresis ($\Delta\theta$), i.e. the difference of advancing (θ_a) and receding (θ_r) contact angles of a drop on a tilted surface, is generally taken as an indicator of the drop’s resistance against sliding, with a pinned drop showing higher values of $\Delta\theta$. The measured $\Delta\theta$ values for the two extreme cases, i.e., loose packed and dense packed yarn were 67° and 45° respectively. The higher hysteresis value for the loose packed yarn system may be attributed to the pinning of the drop as it curves between the widely spaced yarns and touches the random fiber mat. However, as mentioned earlier that the surface of the yarns still had some pores even after twisting and rolling. These pores were also acting as pinning sites for the drop, **Figure 2.2b**. That is why; the hysteresis was high even for the dense packing yarn where the drop was not in a direct contact with the random fiber mat.

The physical restructuring of the surface, as presented above, is a versatile and easy way to control its wetting properties. On the other hand, the wetting properties of a surface can also be controlled depending upon its chemical restructuring. In short, water being a polar molecule should show stronger adhesion to a polar surface. PVDF can be either polar or non-polar depending upon the conformation of its chains and its crystallinity.^[82,83] Its crystalline β -phase, which has all the fluorine atoms on one side of the chain is highly polar.^[84] On the other hand, the surface of amorphous PVDF would be less polar because the chains are laid in a random fashion and cancel the effect of each other. So an amorphous structure is expected to pose a less binding surface towards a water drop and its sliding on such a surface is supposedly easier. In contrast to wide wisdom, we believe that even in a highly crystalline

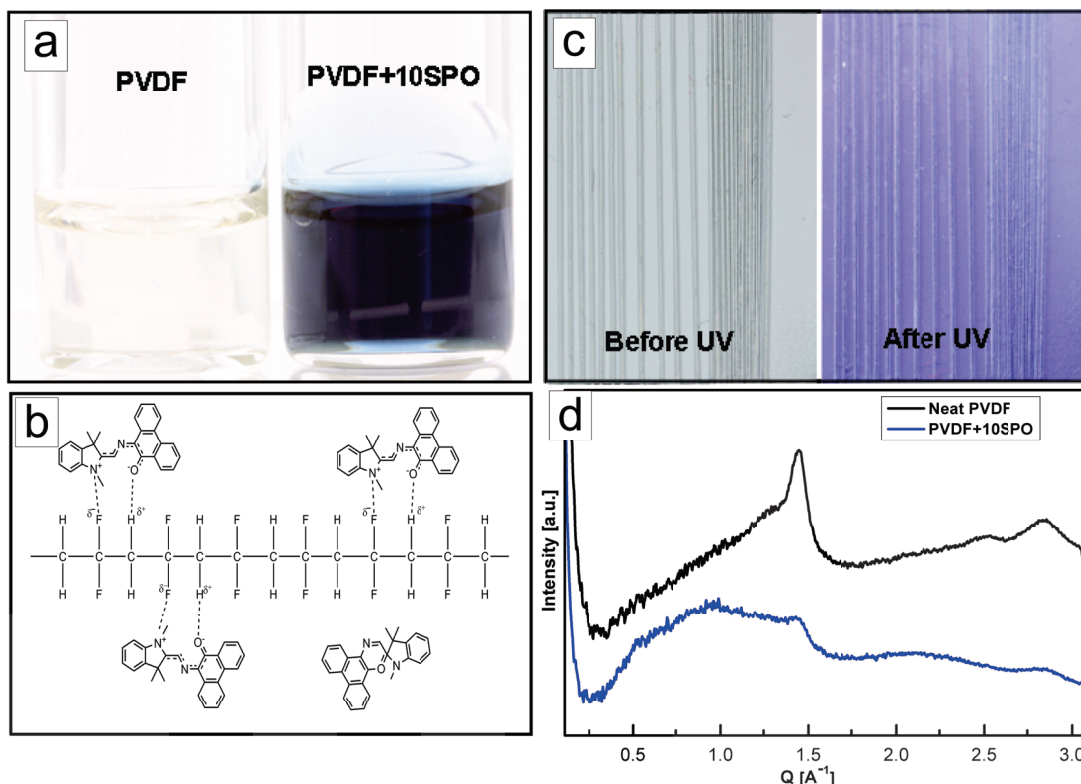


Figure 2.3 a) Blue solution of PVDF+10 wt.% SPO with DMF as a solvent in comparison with colorless solution of neat PVDF. b) Schematic showing interaction of SPO open form with the PVDF. c) PVDF yarns with 10 wt.% SPO, before and after UV exposure. d) WAXS analysis results for neat PVDF fibers and those containing SPO.

polymer, foreign polar molecules can weaken and replace the polymer–polymer interactions with polymer–molecule interactions and hence decrease its crystallinity.^[85] Indeed SPO can be switched between "opened, highly polar" and "closed, less polar" form not only on exposure to UV and white light respectively but its open form is also stable in its solvents.^[86]

Accordingly, 10 wt.% spirooxazine (SPO) was blended with the polymer solution in Dimethylformamide (DMF) that acted not only as a common solvent for polymer and SPO but also caused the SPO molecules to convert into their "open, highly polar" form by creating a polar environment around them. This was evident by the dark blue color of PVDF-10 wt.% SPO solution, **Figure 2.3a**. DMF evaporated during electrospinning but in the mean time part of SPO open form was stabilized by a dipole-dipole interaction with the polymer, **Figure 2.3b**. That is why, the fibers had a grayish blue color right after electrospinning, **Figure 2.3c**. After blending SPO with the polymer, it was expected that the molecules of the photochromic compound could disturb the regular chain arrangement required for a crystalline structure since they acted as side branches and hindered the alignment of chains required for crystallinity,^[87] **Figure 2.3b**. This could result in fibers being dominantly amorphous with consequent effects on the sliding angle of drop. Indeed, change in crystallinity after adding SPO was seen in the wide angle X-ray scattering (WAXS) analysis.

For the neat PVDF fibers, a strong peak was observed, which suggested that they were dominantly crystalline in either β -phase or its resembling γ -phase, **Figure 2.3d**. These two phases are difficult to distinguish from each other by X-ray diffraction, but share a common property that both are polar and thus can ensure good stability of open form of SPO which is also polar.^[85] With the addition of SPO, the strong peak representing crystalline phase was eliminated. As discussed above, the amorphous PVDF being less polar, should offer a surface to the droplet that is only weakly sticky. Thus, the drop could slide on it at a lower tilt angle compared to that in the case of neat crystalline PVDF yarn, **Table 2.2**.

Table 2.2 Tilt angles required to initiate the drop rolling on different surfaces with added SPO

	Loose packing	Medium packing	Dense packing
Tilt angle for slip	$55^{\circ} \pm 2^{\circ}$	$43^{\circ} \pm 5^{\circ}$	$43^{\circ} \pm 5^{\circ}$

However, since a part of SPO embedded in the PVDF fibers was already in the open form, exposure to UV did not bring about such a big change in sliding angle which could be taken as a trend. This was supported by static contact angle measurement, which showed a very small effect, i.e., a change from 135° before UV to 131° after UV exposure.

Here it is worth mentioning that only slippy state of a hydrophobic surface is not important but also the sticky state has its own applications. We demonstrate here, the ability of random fibers mat to arrest a drop as a novel way to create two-dimensional patterns by using water drops as tiny ball lenses, **Figure 2.4a**. The drops were deposited on a mat of PVDF fibers containing 10 wt.% SPO, to write the word "LENS". Upon orthogonal UV exposure, water droplets that acted as lenses, deviated the light, concentrating it on the point where the drop was in contact with the fiber mat, thus creating a kind of "UV hotspot", **Figure 2.4b**. Each individual spot consisted of an inner dark blue area, ('Region A', **Figure 2.4b**) because of exposure to highly concentrated UV dose. As the water lens concentrated the light in the centre, the area surrounding the darker region, directly under the curve of the water lens, did not receive any UV exposure and remained in the faint grayish blue color of original fibers ('Region B', **Figure 2.4b**). The rest of the area ('Region C', **Figure 2.4b**) also had a blue color but it was lighter than the 'Region A' because here, UV was not concentrated. The image formed by selective UV exposure was erasable by intense white light, after which the surface was ready for the next patterning, **Figure 2.4a**.

On the other hand, a similar pattern could also be made on PVDF film containing 10 wt.% SPO but since the film was not superhydrophobic therefore the contact area of water drop with the film surface was bigger compared to that in the case of fibers, **Figure 2.4c**. Here, the darker area in the middle of impression made by the drop after UV exposure was

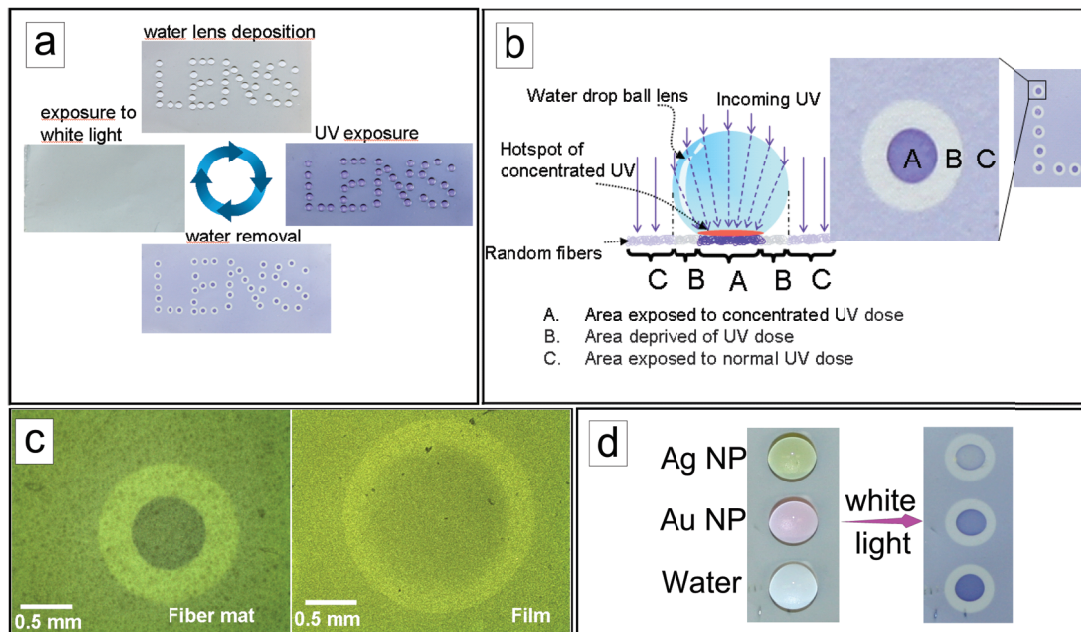


Figure 2.4 a) Erasable writing with water lens on 'PVDF-10 wt.% SPO' random fiber mat. b) Schematic of the water lens system along with enlarged, top view of one of the spots constituting the letter 'L'. c) Optical micrograph of the impression made by water lens on SPO loaded PVDF fibers and film, after UV exposure. d) PVDF-10 wt.%SPO fibers with water lenses of pure water and that loaded with silver and gold nanoparticles, before (left) and after (right) exposure to white light containing a weak part of UV. Water drop removed after exposure to light in order to show the intensity of the dark impression made by the exposure.

about four times bigger more than that observed in the case of fibers. This meant that the light concentration effect and the minimum feature size producible on the film were far less than that on the fibers. The advantage of using water is the availability, ease of application and removal and no damage to the delicate substrate, which may be a concern if using other type of lenses.

Enhancement in the field, accompanying as oscillating dipole, due to its proximity with a metal mirror has already been shown.^[88] In the present case, water drop acts as a mirror near the oscillating dipoles created by photochromic molecules and a low intensity electromagnetic field of incident UV is intensified (hot spot generation) by multiple reflection/scattering and interference at the interface between the drop and the fibers. Thus, the UV flux can be enhanced on a small area on which potential UV assisted reactions can take place while the rest of the sample surface remains free of any collateral damage. As a potential application of the drop lens we demonstrate here a local switching using white light that has only a weak part of UV and simultaneously the detection of UV absorbents dispersed in the drop. The intensity of the dark impression made after exposure to light would indicate the nature/concentration of the dispersed species, as shown in the **Figure 2.4d**, where water drops containing silver and gold nanoparticles are compared. After exposure to light, the drop

which was loaded with gold nanoparticles showed lesser absorption than the drop containing silver nanoparticles. This is because the plasmon of silver (at nearly 400 nm) is very near to the UV range compared to that of gold (which is at nearly 530 nm). This enables one to separate visually, different solution depending upon their UV absorptivity. It can also be seen that UV did not affect the area surrounding the drops as much strongly as it did within the hot spot as seen for the pure water droplet, which actually intensified the UV. The concept of water lens would open a new vein of research ranging from photonic sensors to thermophoresis based on loaded droplets. However, to put these ideas into practice, an in depth investigation of the phenomenon is needed which is beyond the scope of this paper.

2.2.3 Conclusion:

To conclude, it was demonstrated in this work that the wetting properties of a system can be manipulated both by its physical and chemical structure. Sticking of water drop on random mat of polymer nanofibers, and its sliding on the yarn made out of the same nanofibers showed the influence of physical structuring. The method of transforming the wetting properties of a surface, as presented here, is simple and unique, with added benefit that this device is removable and can be employed to different types of substrates without causing any permanent change in them. Moreover, it can be switched between the sticky to slippy state instantly. Further control on wetting properties of the system was shown by its chemical modification with a photochromic compound that resulted in crystalline to amorphous transformation of the system with consequent decrease in sliding angle of the water drop. As a novel application of the stickiness of a hydrophobic surface, we used water drop as a lens for writing or making patterns.

2.2.4 Experiments:

Polymer solution for electrospinning was prepared by dissolving 11 wt.% of Polyvinylidene fluoride (PVDF) in N,N-Dimethylformamide (DMF). For fibers loaded with 1,3-Dihydro-1,3,3-trimethylspiro[2H-indole-2,3'-[3H]phenanthr[9,10-b](1,4)oxazine] (*i.e.*, SPO), 10 wt.% of it was added to the polymer solution. Electrospinning was done by pushing the polymer solution through a needle that was connected to a high voltage source of 8kV. Because of electrohydrodynamic nature of the process, the polymer stretched into the form of fibers, which were collected at the base plate in the form of a mat. This mat was simply lifted from the target, spread over a glass plate, and subsequently tested for its wetting properties. Yarns were made by manually rolling and stretching a thin layer of mat collected on the target plate. These yarns were then laid over the glass plate, which was already covered with a layer of random fiber mat. The polymer film was made by blade casting method, from the same solution of PVDF that used for electrospinning of fibers.

Contact angle and sliding angles were measured on OCA15 machine from 'Dataphysics' using 14 μL water drops. To study the UV effects on contact angle and sliding angle, a UV lamp (Labino AB, 35 W) with its peaks intensity in the range of 365 nm was used. The writing with "water lenses" was carried out by manually delivering of 2 μL water drops on the random fiber mat surface in the form of a pattern. After the first writing, the surface was recovered by exposing it to white LED light source. For analyzing the effect of UV absorbents, suspended in the water, drops of colloidal silver and gold solution containing nanoparticles of size range 5-10 nm were placed over PVDF nanofibers containing 10 wt.% SPO. These were then exposed to a white light (Labino AB, 35 W) for one minute.

For structural characterization, the fibers were glued to a sample frame and consequently exposed to synchrotron X-rays of wavelength 0.65250 Å. The diameter of the beam was about 700 μm . The illumination was done by scans along the direction perpendicular to the fiber axis. The scattered radiation was recorded with a CCD-detector.

For microstructure characterization, the fibers were first sputtered with silver and were consequently examined in Field Emission SEM, Carl Zeiss ULTRA Plus.

2.2.5 Acknowledgements:

We acknowledge the partial financial support by German Academic Exchange Service (DAAD) and by German Research Foundation (DFG) through SFB677 (C09). M.E. thanks the Initiative and Networking Fund of the Helmholtz Association (grant No. VH-NG-523) for providing the financial base to start his research group.

2.2.6 References:

- [1] B. Bhushan, *Beilstein journal of nanotechnology* **2011**, 2, 66.
- [2] K. Liu and L. Jiang, *Nanoscale* **2011**, 3, 825.
- [3] L. Ionov *et al.*, *Advanced Functional Materials* **2006**, 16, 1153.
- [4] B. Zhao, J. S. Moore and D. J. Beebe, *Science* **2001**, 291, 1023.
- [5] K. Liu *et al.*, *Nanoscale* **2012**, 4, 768.
- [6] Y. Zheng *et al.*, *Nature* **2010**, 463, 640.
- [7] N. Nuraje, *et al.*, *Langmuir* **2010**, 27, 782.
- [8] J. A. Howarter and J. P. Youngblood, *Macromolecular Rapid Communications* **2008**, 29, 455.
- [9] J. He *et al.*, *Journal of materials science: materials in medicine* **2008**, 19, 3465.
- [10] D. S. Kommireddy *et al.*, *Journal of nanoscience and nanotechnology* **2005**, 5, 1081.
- [11] E. Bormashenko *et al.*, *Journal of colloid and interface science* **2007**, 311, 212.
- [12] Y. T. Cheng *et al.*, *Nanotechnology* **2006**, 17, 1359.
- [13] W. Barthlott and C. Neinhuis, *Planta* **1997**, 202, 1.
- [14] Y. Zheng, X. Gao and L. Jiang, *Soft Matter* **2007**, 3, 178.
- [15] M. Nosonovsky and B. Bhushan, in *Green tribology*, Springer, **2012**, 25.
- [16] L. Feng *et al.*, *Langmuir* **2008**, 24, 4114.
- [17] M. Dawood *et al.*, *Langmuir* **2011**, 27, 4126.
- [18] K. Koch *et al.*, *Soft Matter* **2009**, 5, 1386.

- [19] S.-W. Lee and P. E. Laibinis, *Journal of the American Chemical Society* **2000**, *122*, 5395.
- [20] F. D. Dos Santos and T. Ondarcuhu, *Physical review letters* **1995**, *75*, 2972.
- [21] L. Feng *et al.*, *Advanced materials* **2002**, *14*, 1857.
- [22] J. Wang *et al.*, *Plant science* **2009**, *176*, 687.
- [23] H. Zhang *et al.*, *Colloids and Surfaces A: Physicochemical and Engineering Aspects* **2012**, *413*, 314.
- [24] Y.-T. Cheng and D. E. Rodak, *Applied physics letters* **2005**, *86*, 144101.
- [25] T. S. Sudarshan and J. J. Stiglich, "Surface modification technologies: Proceedings of the 19th international conference on surface modification technologies," Minnesota, USA, ASM International, **2005**.
- [26] F. MacRitchie, *Chemistry at interfaces*, Elsevier Science **1990**.
- [27] R. Jafari, R. Menini and M. Farzaneh, *Applied Surface Science* **2010**, *257*, 1540.
- [29] T. Onda *et al.*, *Langmuir* **1996**, *12*, 2125.
- [30] T. Sun *et al.*, *Accounts of chemical research* **2005**, *38*, 644.
- [31] M. Ma and R. M. Hill, *Current Opinion in Colloid & Interface Science* **2006**, *11*, 193.
- [32] K. Liu, X. Yao and L. Jiang, *Chemical Society Reviews* **2010**, *39*, 3240.
- [33] S. Nishimoto and B. Bhushan, *Rsc Advances* **2013**, *3*, 671.
- [34] J. Bico, C. Marzolin and D. Quéré, *EPL (Europhysics Letters)* **1999**, *47*, 220.
- [35] C. Extrand, *Langmuir* **2002**, *18*, 7991.
- [36] B. He, N. A. Patankar and J. Lee, *Langmuir* **2003**, *19*, 4999.
- [37] Y. Wu *et al.*, *Chemical Vapor Deposition* **2002**, *8*, 47.
- [38] H. Y. Erbil *et al.*, *Science* **2003**, *299*, 1377.
- [39] K. Teshima *et al.*, *Langmuir* **2003**, *19*, 10624.
- [40] N. J. Shirtcliffe *et al.*, *Langmuir* **2003**, *19*, 5626.
- [41] C. Guo *et al.*, *ChemPhysChem* **2004**, *5*, 750.
- [42] L. Feng *et al.*, *Angewandte Chemie* **2002**, *114*, 1269.
- [43] L. Jiang, Y. Zhao and J. Zhai, *Angewandte Chemie* **2004**, *116*, 4438.
- [44] M. Li *et al.*, *The Journal of Physical Chemistry B* **2003**, *107*, 9954.
- [45] Y. T. Cheng, *et al.*, *Nanotechnology* **2006**, *17*, 1359.
- [46] X. Liu, *et al.*, *Soft Matter* **2012**, *8*, 2070.
- [47] A. Roth-Nebelsick, *et al.*, *J. R. Soc. Interface* **2012**, *9*, 1965.
- [48] B. Bhushan and E. K. Her, *Langmuir* **2010**, *26*, 8207.
- [49] T. Young, *Phil. Trans. R. Soc. Lond.* **1805**, *95*, 65.
- [50] R. N. Wenzel, *Industrial and Engineering Chemistry Research* **1936**, *28*, 988.
- [51] A. Cassie and S. Baxter, *Trans. Faraday Soc.* **1944**, *40*, 546.
- [52] T. Sun, *et al.*, *Accounts of Chemical Research* **2005**, *38*, 644.
- [53] M. Nosonovsky and B. Bhushan, in *Green tribology*, Springer **2012**.
- [54] M. Callies and D. Quéré, *On water repellency* **2005**, *1*, 55.
- [55] L. Jiang, Y. Zhao and J. Zhai, *Angewandte Chemie* **2004**, *116*, 4438.
- [56] S. Ramakrishna, *et al.*, *An introduction to electrospinning and nanofibers*, World Scientific **2005**.
- [57] Z.-G. Guo and W.-M. Liu, *Applied Physics Letters* **2007**, *90*, 223111.
- [58] X.-M. Li, D. Reinhoudt and M. Crego-Calama, *Chemical Society Reviews* **2007**, *36*, 1350.
- [59] H. Teisala, M. Tuominen and J. Kuusipalo, *J. Nanomater.* **2011**, *2011*, 33.
- [60] S. S. Homaeigohar and M. Elbahri, *Journal of Colloid and Interface Science* **2012**, *372*, 6.
- [61] M. Jin, *et al.*, *Advanced Materials* **2005**, *17*, 1977.
- [62] Y. Lai, *et al.*, *Advanced Materials* **2009**, *21*, 3799.
- [63] L. Feng, *et al.*, *Langmuir* **2008**, *24*, 4114.
- [64] T. Pisuchpen, *et al.*, *Langmuir* **2011**, *27*, 3654.

- [65] G. Gong, *et al.*, *Journal of Materials Chemistry* **2012**, 22, 8257.
- [66] X. Yao, Y. Song and L. Jiang, *Advanced Materials* **2011**, 23, 719.
- [67] D. Xia, L. M. Johnson and G. P. López, *Advanced Materials* **2012**, 24, 1287.
- [68] W.-G. Bae, *et al.*, *Advanced Materials* **2013**, 26, 675.
- [69] A. Nakajima, K. Hashimoto and T. Watanabe, *Monatshefte für Chemie* **2001**, 132, 31.
- [70] D. Han and A. J. Steckl, *Langmuir* **2009**, 25, 9454.
- [71] H. Wu, *et al.*, *Soft Matter* **2008**, 4, 2429.
- [72] H. Y. Erbil, *et al.*, *Science* **2003**, 299, 1377.
- [73] K. Liu, X. Yao and L. Jiang, *Chemical Society Reviews* **2010**, 39, 3240.
- [74] F. Zheng, *et al.*, *Journal of Colloid and Interface Science* **2014**.
- [75] L. Feng, *et al.*, *Angewandte Chemie* **2002**, 114, 1269.
- [76] M. Zhu, *et al.*, *J. Mater. Sci.* **2006**, 41, 3793.
- [77] A. Singh, L. Steely and H. R. Allcock, *Langmuir* **2005**, 21, 11604.
- [78] B. Balu, V. Breedveld and D. W. Hess, *Langmuir* **2008**, 24, 4785.
- [79] X. Zhang, *et al.*, *Journal of the American Chemical Society* **2004**, 126, 3064.
- [80] K. Teshima, *et al.*, *Applied Surface Science* **2005**, 244, 619.
- [81] E. Gauthier, *et al.*, *ACS Appl. Mater. Interfaces* **2012**, 4, 761.
- [82] M. Broadhurst and G. Davis, *Ferroelectrics* **1984**, 60, 3.
- [83] H. S. Nalwa, *Ferroelectric polymers: Chemistry, Physics, and applications*, Taylor & Francis **1995**.
- [84] L. Yu and P. Cebe, *Polymer* **2009**, 50, 2133.
- [85] J.-S. Lin, *European Polymer Journal* **2003**, 39, 1693.
- [86] M. Jamali, *et al.*, *Advanced Materials* **2011**, 23, 4243.
- [87] D. Kline, J. Sauer and A. Woodward, *Journal of Polymer Science* **1956**, 22, 455.
- [88] M. K. Hedayati, *et al.*, *Advanced Optical Materials* **2014**, 2, 705.

Chapter 3

Photochromic Films and Fibers

3.1 The light-matter interaction:

An important aspect of nanomaterials is their interaction with light, not only aesthetically or because vision is one of our most important senses but also because it opens a door to a large number of fascinating applications like, light sensitive remote controlling, high speed data handling, high capacity data storage, colorful displays etc. Additionally, light can be used simply as energy transfer media for bulk or localized heating which can be used in tumor treatment,^[1-3] solar cells,^[4,5] localized welding, defect healing and composite making^[6] in polymers etc.

The interaction of light with matter may result in its scattering, reflection or absorption depending upon the size, shape and nature of matter and wavelength of light. Rayleigh scattering is the dominant phenomenon when the particle size is very small in comparison to the light wavelength. The scattering cross-section, σ_{Ray} , is given by:^[7]

$$\sigma_{Ray} = \frac{8\pi}{3} \left(\frac{2\pi n_{med}}{\lambda_0} \right)^4 a^6 \left(\frac{m^2 - 1}{m^2 + 2} \right)^2 \quad \text{Equation 3.1}$$

Where, λ_0 is the wavelength of light in vacuum, a is the particle radius, $m = n_{sph}/n_{med}$ is the ratio of refractive index of the particle to the surrounding medium. This is rather a simplified view of scattering from a fiber as any periodic disturbances can also act as coherent scattering centers.

Another effect is polarization caused by the fiber which can be explained with the help of Maxwell-Garnet model.^[8] According to this model, the attenuation of light is stronger for electric field polarized parallel to the long axis of an infinite cylinder than that when it is perpendicular to the cylinder. Thus fibers would strongly attenuate light which is polarized parallel to their length.^[9] Both these effects which purely originate from the size and shape of the fibers, are absent in the case of thin film as the latter are a continuous homogenous structure. Other differences between film and fibers are found when light sensitive materials, for example a photochromic compound or metal nanoparticles, are added to the system.

3.1.1 Light and Photochromic molecules:

“Photochromism is a reversible transformation of a chemical species, induced in one or both directions by absorption of electromagnetic radiation between two forms, A and B, having different absorption spectra”.^[10] In a positive photochromic process, irradiation causes the thermodynamically stable ‘form A’ (or educt) to transform into a ‘form B’ (product), with the absorption wavelength of B being longer than that of A, **Figure 3.1**. That is why many of the photochromic compounds are yellowish or colorless in their ‘form A’ and their

photoproduct is bluish. The reversion of 'form B' back to 'form A' takes place either photochemically or thermally.^[10]

The earliest report of reversible color change in tetracene dates back to Fritzsche in 1867. Since then a great variety of compounds, which reversibly change color in response to light exposure, have been discovered. There are at least thirteen different families of artificially made organic compounds showing positive photochromism, besides a large number of inorganic or naturally occurring photochromic compounds.^[10] Out of these,

spirooxazine family was chosen since it possesses many of the desired properties in one system, including fatigue resistance,^[11,12] high colorability,^[13] and fast switchability.

The change in molecular structure after interaction with light results not only in a change in its absorption spectrum, but also in its dipole moment,^[14] refractive index, geometry and size. These changes can be used in a variety of devices like controlling conductivity, wettability,^[15] transparency,^[16] etc by light or heat stimulus. This is now in the focus of modern research due to many fascinating applications like, 3D data storage,^[14,17] holographics,^[18,19] optical electronics,^[20] solar cells, light driven mobility, optical tweezers^[21] and so on. In order to understand and utilize the full potential of photochromic phenomenon, one has to consider how light interacts with matter.

When light interacts with a molecule of a photochromic compound, many different phenomena may take place. Firstly, the electric field of light can polarize molecules, and since light is an oscillating electric field, it can initiate vibrations of charge carriers in the molecule. This results in the molecules acting as small antennas radiating their electromagnetic signal seen as 'reflection'.

Besides this, a part of energy is absorbed in the form of electronic transition within the photochromic molecule or breakage of bonds. There is an energy gap between the 'Highest Occupied Molecular Orbital' or HOMO (an equivalent of valence band in atoms^[22]) and 'Lowest Unoccupied Energy Level' or LUMO (an equivalent of conduction band in atoms). Electrons, in the ground state of a molecule, occupy the HOMO which is the highest energy level occupied by electrons in a molecule. Most of the organic photochromic molecules have σ and π bonding due to conjugation. Since electrons in sigma orbital are tightly bound, the electrons from π orbital of a conjugated bonded molecules, like those of

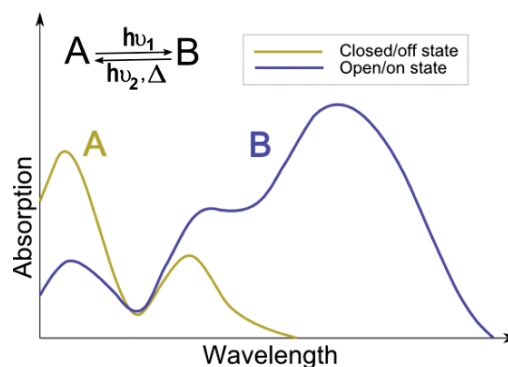


Figure 3.1 Reversible conversion of a photochromic compound between its two states which absorb at different parts of the spectrum.^[10]

many organic photochromic compounds, occupy the HOMO energy level. The visible part of the spectrum spans from 380-700 nm with a corresponding energy in the range of 40-75 kcal/mol. This energy is sufficient for lower energy electronic transitions, like $\pi \rightarrow \pi^*$ or $n \rightarrow \pi^*$, **Figure 3.2**. The molecule ultimately relaxes back to its ground states by dissipating the acquired energy in the form of phosphorescence, fluorescence or by thermal relaxation processes. Since the relaxation processes (radiative and non-radiative) are in competition with the photochromic process, the quantum yield is always less than one.

The charge transfer, say from n orbital (localized on oxygen) to π^* orbital (delocalized on carbon and oxygen) results in a change in dipole moment. Moreover, the presence of π^* electron in first singlet (S_1) and triplet (T_1) can result in change of hybridization from sp^2 to sp^3 -similar structure. As a result, the bond lengths between carbon and oxygen may increase. These all factors contribute to a change in chemical properties of the photochromic molecule after photoexcitation.^[23]

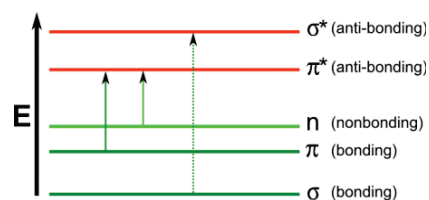


Figure 3.2 Excitation of electron into higher energy molecular orbitals after absorption of light.

On the other hand, a photon of higher energy light, like UV, can cause bond breakage. The weakest bonds in organic molecules have energy around 35 kcal/mole (for example O–O bond) while stronger bonds can have energy up to 100 kcal/mole (for C–H bond).^[23] The breakage of bonds by UV is highly selective because of localization of electronic excitations and the way these excitations play their role to break a bond.^[23]

The spirooxazine (SPO) photochromic molecules properly called (1,3-Dihydro-1,3,3-trimethylspiro[2H-indole-2,3'-[3H]phenanthr[9,10-b](1,4)oxazine]) that was used in the present work, is shown in the **Figure 3.3** along with its structural components and typical sequence of photochromism when it is exposed to UV light.

In the ground state of SPO (also called OFF or closed state), the indoline and oxazine parts of the molecule are orthogonally joined at sp^3 bonded spiro carbon. Transition from spiro (SP) form to merocyanine (MCN) form (the so-called ON or open state) occurs upon UV exposure which results after the breakage of the bond between spiro carbon and oxygen and as a result, the molecule rotates and acquires a planar configuration of 'open or ON state'. The open molecule may exist in zwitterionic (or charged form) or in isomeric quinonic forms.

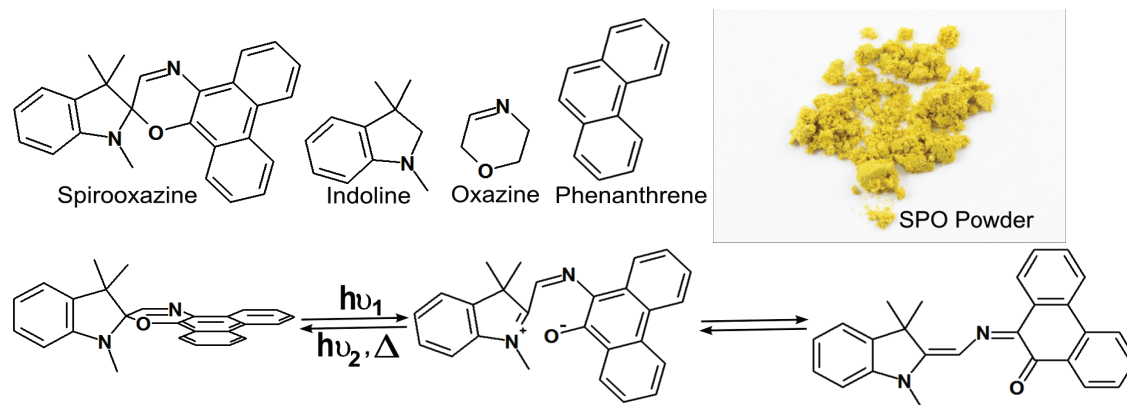


Figure 3.3 **Top left)** Molecular structure of photochromic molecule ‘spirooxazine (SPO)’ used in this thesis. **Top middle)** Individual structural components of SPO. **Top right)** SPO powder in basic form. **Bottom)** Reversible conversion of SPO (right) into its open form which may exist in **(middle)** zwitterionic or **(right)** quinoidal structure.

The opening and planarization of the molecule increases its conjugation length which in itself represents the π electron delocalization. A longer conjugation length shows a red shifted absorption spectrum of the molecule and the energy difference between HOMO and LUMO may decrease down to the energy of the visible quanta.^[24,25] When a part of optical spectrum is absorbed, the complementary of the absorbed color is seen as the color of the compound. In comparison to that, the molecule absorbs in UV range when it is in closed form that is why many of the photochromic compounds are either colorless or yellow.

The color (or the quantum of light) absorbed by a photochromic compound not only depends upon its structure but also on its environment. There have been several empirical rules, e.g. Woodward-Fieser rule^[26] or Fieser-Kuhn rule^[27], to predict the absorbed color by a dye depending upon its structure, substitutions and its solvent. The change of color (emissive or absorptive) of a compound, depending upon the nature of its surrounding environment and the phenomenon is called solvatochromism.^[28] In reference to solvatochromism, the current use of the word ‘solvent’ has been extended to include gels, micelles, polymers and various surfaces.^[28] The observed shifts are due to a variation of solvation energy of the ground and excited state in different solvents, which in turn depends upon the solvent’s polarity.^[28] Polarity includes a number of physical phenomena such as, solvents dipole moment, polarizability, H-bonding capability, Lewis acidity/basicity etc.^[28] It is generally observed that when the excited state of molecule is more polar than the ground state (**Figure 3.4a**), then a more polar solvent would tend to ease the formation of excited state with a resulting red (bathochromic) shift in absorption. This is also known as positive solvatochromism. On the other hand, when the ground state of the molecule is more polar

than its excited state, a blue (hypsochromic) shift in absorption wavelength is observed on increasing the polarity of the solvent (**Figure 3.4b**).

The spirooxazine used in this thesis showed a positive solvatochromism as its solution showed a red shift in absorption as the solvent for SPO was changed from nonpolar toluene (middle) to protic polar ethanol (left) or

aprotic polar N,N-Dimethylformamide (right) solvent, **Figure 3.5**. The same behavior was observed when SPO was blended in polymers of different polarity. This leads to a very useful way of detecting the polarity of the matrix in which SPO is dissolved/embedded.

However, it is not only absorption, which takes place when light interacts with matter, rather it may also be scattered (reflected) or absorbed/reemitted (fluorescence, phosphorescence). Light, having an oscillating electric field, when interacts with the SPO molecules, induces oscillating dipoles in it. According to the Lorentz model, the molecule would now act as a radiative source (called secondary radiation), the frequency of which would depend upon the dipole moment of the molecule and its environment.^[29] On the other hand, as a result of non-radiative coupling, a part of incident energy would be lost (absorption) to the surrounding medium as vibrations induced in the molecules of the surrounding medium (thus creating heat). Mostly, it is the change in ‘absorption’ maxima of the photochromic compound that is considered when an effect of its environment is studied,^[30-33] even though, as shown in the present thesis, a process based on reflection by the photochromic molecules shows a better sensitivity to the polarity change.

The work presented in this part of thesis emphasizes the effectiveness of ‘reflection based’, refractive index modulated systems. The advantage gained by the reflection based method is obvious as the difference in reflection minima at Brewster angle of the photochromic system, using s-polarized light, was around 40 nm for polymer matrices of

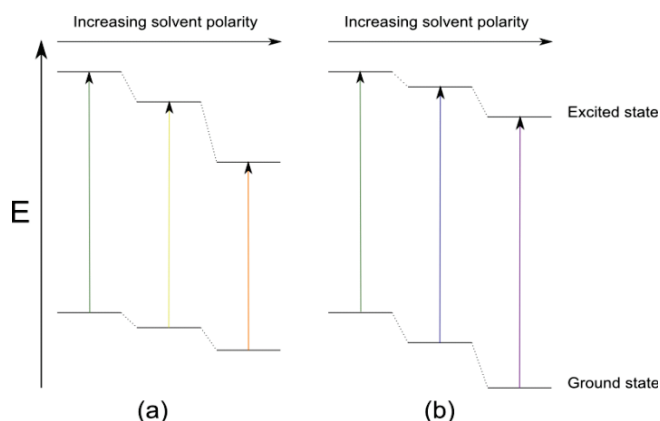


Figure 3.4 a) A red shift in absorption energy with increasing solvent polarity (Positive solvatochromism). b) A blue shift in absorption energy with increasing solvent polarity (Negative solvatochromism).

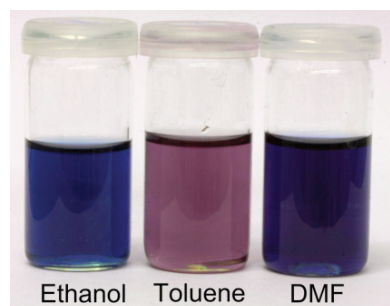


Figure 3.5 Different colors of SPO solution depending upon polarity and proticity of the solvent.

increasing polarity in comparison to a mere 11 nm difference in absorption maxima with the same change in polarity of the matrix.

Another interesting finding presented in this part of the thesis is enhanced transmittance by the photochromic fiber based system in its photo-excited state, which is contrary to enhanced absorbance generally observed in film based systems. By proper control of the size of the fibers, the extinction maxima could be tuned to correspond to either the real or imaginary part of the refractive index. Whereas in the latter case the photochromic fibers showed increase in absorption, in the former case an increase in transmission was observed. Moreover, a control through interference and refractive index modulation, over the color reflected by a thin film, is also demonstrated. The details are presented in the following paper, which has been submitted to “*Light: Science & Applications*” (reference number: LSA2014133), and is in the process of peer review. This is followed by another publication (*Advanced materials*, **2011**, 23, 4243) regarding the photoactivated transparency in polymer films.

3.2 Specular Reflection by Oscillating Photochromic Molecules with Tailored Photoswitchable Brewster Wavelength and Molecular Photonic Coupling

*Mady Elbahri**, **Ahnaf Usman Zillohu**, Bastian Gothe, Mehdi Keshavarz Hedayati, Ramzy Abdelaziz, Hala Jarallah El-Khozondar, Muhammad Bawa'aneh, Moheb Abdelaziz, Andrei Lavrinenko, Sergei Zhukovsky and Shahin Homaeigohar

Submitted to: "Light: Science & Applications" (reference number: LSA2014133)

3.2.1 Introduction:

Photoswitching is a highly desired feature for modern applications^[34] ranging from memory devices,^[35-38] smart windows,^[39,40] to optoelectronic and chemo-mechanical devices.^[41] Photochromic molecules incorporated in a polymeric matrix compose a versatile system that has been investigated and developed for the construction of novel dynamic materials^[42,43] wherein the desired properties are not only tunable but also reversible.^[44] Yet most of the progress is solely based on the optical absorption of the molecules. Despite its wide range of applications, some fundamental aspects and properties are still unclear or unexplored, for example, the photoswitchable reflection, which would open up entirely new possibilities in the ever advancing fields of smart and active optical sensing, photonics and plasmonics.

When electromagnetic (EM) waves illuminate a dipole that is much smaller than their wavelength, the field is considered homogenous. This approximation, first introduced by Rayleigh,^[45] is called a quasi-static approximation. Accordingly, the electric field inside the dipole will drive the electrons cloud relative to positive core, **Figure 3.6a**. The attraction between the negative charges and the core ions originates a restoring force that establishes oscillations. The resonance frequency depends on the polarizability of the surrounding medium. In the simplest case, the alternating surface charges form an oscillating dipole that radiates electromagnetic waves. At this point, the energy of light converts into the oscillation energy of the electronic cloud, where the dipole acts as an antenna that oscillates and re-radiates light to the far field. In the same way, an oscillating sheet of charges^[46] will generate electric and magnetic fields, due only to the local change in the electric field that in turn induces, for instance, electric dipole and quadrupole moments, which eventually cause the reflection from objects.^[47,48]

Specular reflection is raised or diminished depending on the polarization of light and the angle of incidence as first demonstrated by É.-L. Malus in 1808 and further confirmed by D. Brewster in 1815. Indeed this effect has been shown and discussed as purely geometrical

one, neglecting the illuminated matter enclosed.^[49] It makes some contradictions with the electromagnetic dipole radiation concept that is used to explain the phenomenon, as recognized by several physicists.^[50-54] However, while the origin of the phenomenon is not yet fully understood, here we restrict ourselves to experimental demonstration of the phenomenon aiming to implement it for designing a novel photoactive optical device.

Here, we introduce the first experimental evidence of the photoswitchable specular reflection at the visible frequencies exhibited by the excited state photochromic molecules embedded randomly in a polymeric matrix. Moreover, we demonstrate the first photoswitchable Brewster wavelength phenomenon that can be used as a new type of a remote polarity detector. Based on the photoswitchable optical effects; reflection, modulation of real part of the refractive index and the interference, we introduce the design of a tunable active photonic device and a new class of photoswitchable photonic transparency.

Indeed, for the case of radiating dipoles (i.e. chromophores) embedded in a transparent polymeric matrix, a molecular Brewster phenomenon for specular reflection would occur, controlled by the oscillating dipoles of the molecules, **Figure 3.6b**. In this context whenever the electric dipoles oscillate perpendicular to the electric field's direction of propagation, there will be no radiation reflected back into the first medium. Therefore, a reflection minimum for the p-polarized wave exists at a certain grazing angle, which gives rise to the Brewster phenomenon.^[48] Since it is controlled on the molecular level, a switching in molecular behavior should effect both the reflection and Brewster phenomenon. Thus, by using chromophores, the Brewster phenomenon would be solely controlled by the dynamic light switching and the polarizability of the medium enabling the development of what we referred to as the molecular Brewster wavelength.

3.2.2 Results and Discussion:

To confirm it, we used a photoswitchable compound blended in transparent polymeric matrices, and found that the specular reflection and Brewster phenomenon are controlled by UV light illumination. A schematic illustration of the molecular structure of spirooxazine (SPO) that was used in this work is shown in **Figure 3.6c**.

SPO belongs to the family of molecules that displays photochromic properties. The SPO 'closed form/OFF state' has absorption only in the ultraviolet (UV) spectral region. Upon illumination with UV, the C-O bond of the closed form breaks, and the molecule transforms to its planar merocyanine state (or 'open form/ON state').

Owing to its planar structure and an extended π -conjugation, merocyanine shows a delocalized transition in absorption shifted to the visible region. This shift originates from the electron promotion from the bonding level (π) to anti-bonding level (π^*) under UV illumination.^[42] **Figure 3.6d** shows a typical dipole and quadrupole nature of the oscillating chromophores originating from π - π^* transition.^[55] The spirooxazine used in this work showed a pronounced response in absorption and reflection at around 600 nm wavelength after exposure to UV **Figure 3.6e**. The photochromic molecules can be switched back to their original closed form by illumination with white light giving them the ability to be dynamically controlled by light.

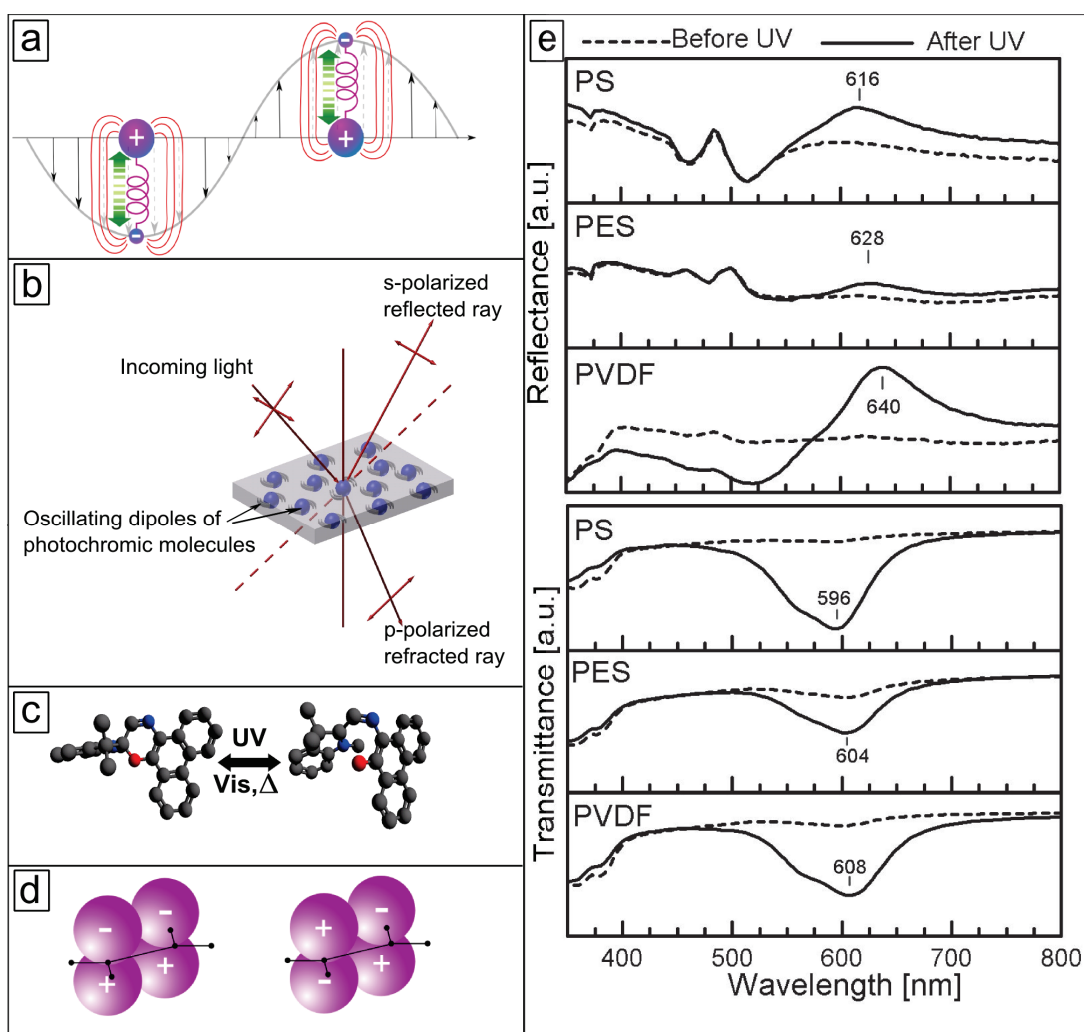


Figure 3.6 The photochromic dipole. **a)** Sketch showing that the fluctuating electric field drives the charges of a dipole relative to each other. **b)** Sketch illustrating that the oscillation dipoles (blue spheres) in the matrix material originate the Brewster phenomenon. **c)** Sketch of a photoreversible C-O bond breakage in a spirooxazine (SPO) molecule upon UV exposure. **d)** Sketch of dipoles and quadrupole generated after π - π^* transition in a chromophore. **e)** Reflection and transmission response of SPO loaded films of different polymers in the 'off state' (before UV) and in the 'on state' (after UV). The full names of the polymer matrices can be seen in the Table 1.

The photochromic system was fabricated by spin coating, on glass substrates, 50 nm films of different polymers doped with SPO. The polymers used for spin coating are listed in the **Table 3.1**, along with their respective refractive indices and dipole moments. The matrices were selected in such a way that there was only a slight difference in their refractive index but a significant difference in their dipole moments, with a view to prove our concept of Brewster wavelength.

For a deeper understanding, the specular reflection properties of the films using s- (R_s) and p-polarized (R_p) light under oblique incidence were investigated. As shown in **Figure 3.7**, there was no resonance reflection peak in the visible range before UV illumination irrespective of the polarization.

However, upon UV exposure, a resonance reflection peak appeared at around 600 nm. It is well recognized that the dipole radiation at an interface differs significantly for p- and s-polarized waves^[48] and as a result, R_p - and R_s - showed quite different intensities. Under s-polarized light, the oscillation direction of electric dipoles is always parallel to the oscillation direction of the reflected light, hence R_s increased gradually with increasing angle of incidence.^[48] A similar trend was observed for p-polarized light; however, at certain angle where the dipole moments were parallel to the direction of the reflected light, a dip appeared in the intensity of light reflection owing to the absorption by the molecules.^[48] Although the reflection did not vanish completely, there was a minimum value at the same critical incident angle of 65° for all polymers matrices. Since the reflection peak/dip appeared/disappeared dynamically upon UV and white light illumination, respectively, the current finding can be considered as an important step towards designing novel photochromic devices.

Table 3.1 Refractive indices and dipole moments of the polymer matrices

Polymer	Real part of refractive index (n)	Dipole moment (D)
Polystyrene (PS)	1.58-1.61 ^[56]	0.2-0.3 ^[57,58]
Polyethersulfone (PES)	1.55-1.67 ^[59,60]	1.62 ^[61]
Polyvinylidene fluoride (PVDF)	1.42 ^[62]	2.1 ^[63]

Having introduced and proven the photoswitchable specular reflection in the glassy composite medium, we considered examining the polarity sensing using the unpolarized/polarized light reflection while introducing the Brewster wavelength sensor, first with p-polarized light. **Figure 3.8a** shows the comparison of the reflection spectra at oblique angles of 45° and 65° (at the Brewster dip) in a film of 30 wt.% SPO embedded in the non polar PS and polar PVDF matrices. While the reflection peaks (at 45° incidence) showed a spectral shift of 11.1 nm, the reflection dip that occurred at the Brewster condition (i.e., at 65° incidence) showed a huge amplified spectral shift of 40 nm.

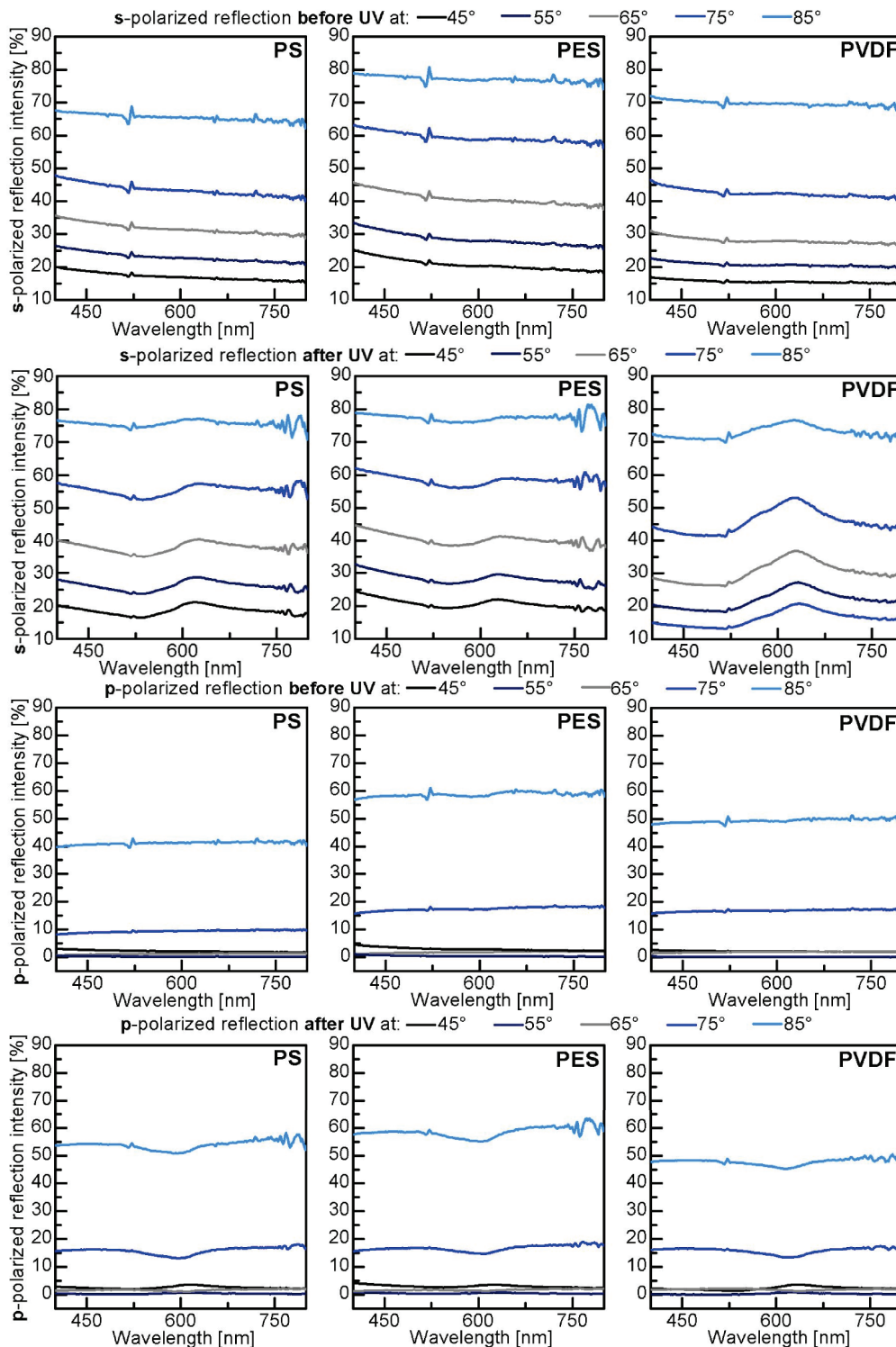


Figure 3.7 Ellipsometry analysis. Angular reflectance of p- and s-polarized light, from film composed of SPO embedded in three different polymeric matrices before and after UV exposure.

This demonstrates, to the best of our knowledge, the highest sensitivity of an optical sensor towards the matrix polarity and proves our concept of the Brewster wavelength. It is to be noted that the shift in Brewster wavelength seems to be more affected by the dipole moment rather than the real part of refractive index that is nearly the same for both the

polymers, nevertheless, more investigations are needed to understand the Brewster wavelength phenomenon.

To simplify the technique of reflection based polarity determination, we examined the detection of matrix polarity using unpolarized light. **Figure 3.8b** shows the comparison of the reflection maxima from films of SPO in different polymers, plotted against the dipole moment of each polymer. These measurements were made under normal incidence, as well as, at an incident angle of 45°. The sensitivities were determined from a linear fit, and show a change of 11.7 nm/Debye at normal incidence, and 11.1 nm/Debye at 45°. Indeed, while the reflection measurements can provide clear spectral differences between the polymer matrices

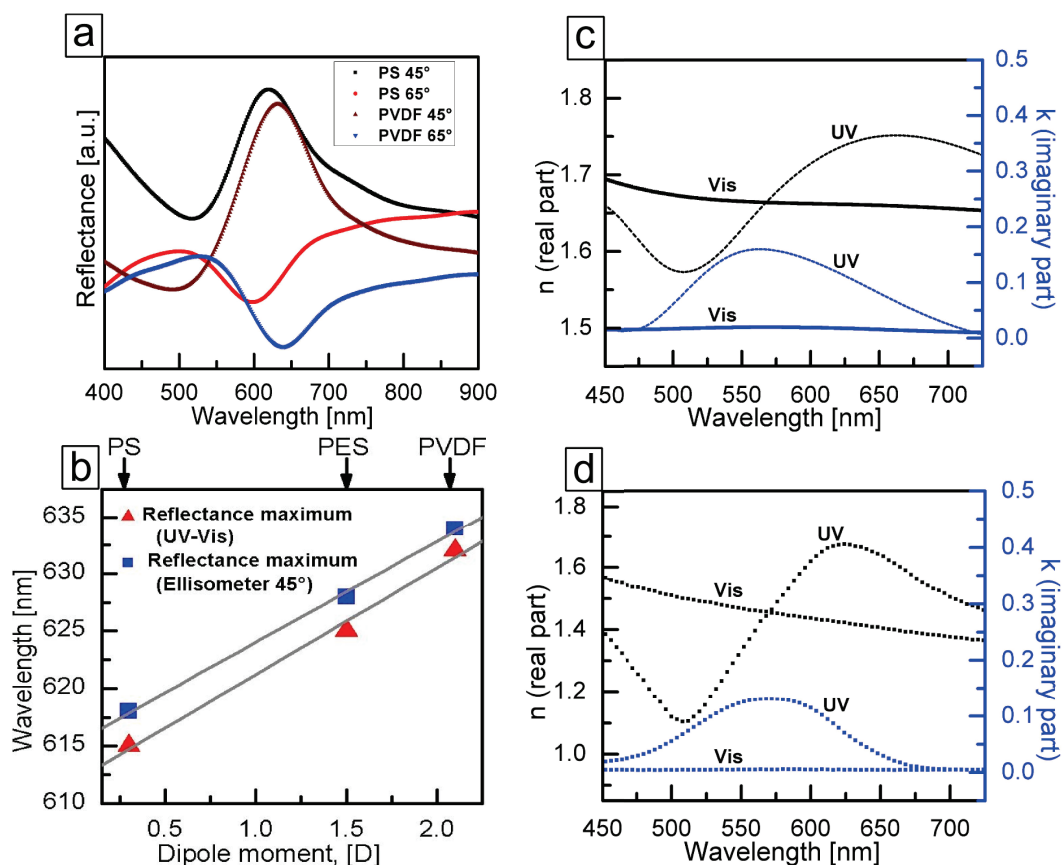


Figure 3.8 Reflectance and refractive index. **a)** Ellipsometry results of UV exposed samples showing a significant, matrix dependent change in Brewster wavelength, observed at Brewster angle of 65° (p-polarized light). **b)** UV-Vis and ellipsometry results showing an increase in reflectance maxima with increasing dipole moment of matrix polymers surrounding the SPO molecules. **c,d)** Real and imaginary parts of refractive index of PS-SPO Film under Vis/UV illumination: (c) using ellipsometry results; (d) numerical simulation.

especially the polar ones, the transmission technique was not sensitive enough as shown in **Figure 3.6e**. It is worth mentioning that the sensitivity based on the shift in reflection peaks' maxima was approximately similar to that obtained while using s-, p-polarized light but was less compared to that based on the Brewster reflection dip. Thus a novel analytical platform wherein the polarity of the host medium can be indentified and photo-detected with high

accuracy using reflection measurements, especially at the Brewster wavelength, has been demonstrated.

The finding of the photoswitchable reflection by photochromic molecules randomly embedded in a polymeric matrix as demonstrated here, would deepen our understanding of the refractive index modulation, which is to date extracted from the molecular absorption solely^[64-69] and could facilitate a novel strategy towards interference-based optical devices under UV illumination. **Figure 3.8c** shows a typical light modulated refractive index of ~20-30% SPO photochromic molecules embedded in a PS matrix before/after UV exposure, as measured by ellipsometry. While the imaginary part, which is attributed to the molecular absorption, showed a peak at 560 nm, the real part of the refractive index underwent an anomalous dispersion and peaked at 660 nm.

We stress here that, the dispersive curve of the real part is controlled by the dynamic reflection of the photochromic molecules. We further confirm it by calculating the refractive index modulation from the absorption and reflection coefficients by direct numerical simulations. The results of calculations are shown in **Figure 3.8d**. For the numerical calculations, the index of refraction was restored with the following relation,^[70]

$$n = \frac{1+R}{1-R} + \sqrt{\frac{4R}{(1-R)^2} - k^2} \quad \text{Equation 3.2}$$

where k is given by;

$$k = \frac{\lambda}{4\pi} \times \frac{A}{d} \quad \text{Equation 3.3}$$

Here, A is the normalized absorption coefficient, R is the normalized reflection coefficient, λ is the wavelength and d is the thickness. It is evident that the results are quite similar with minor differences owing to the difference in the adopted methods.

Most of photochromic devices presented to date are based on modulation of the imaginary part of the refractive index.^[64-69] However, we believe that our findings will change the picture, and novel optical devices can be designed by bringing together reflection, inferences and refractive index modulation. To highlight our findings without going into too much details, we would like to give two examples, namely, tailored coloration and photonic wavelength shift of a ‘photochromic film’ coated reflective substrate, and a new class of optically active photoswitchable photonic transparency using photochromic fibers.

To explore the role of refractive index modulation (real/imaginary) and consequently manifest our findings of photoswitching reflection, we spin coated PS-SPO film on silicon substrate with and without a spacer layer of silicon oxide. **Figure 3.9a** shows the sketch of the coating arrangement along with the different coloration of the coating before and after UV illumination. The UV-Vis analysis of the system wherein the photochromic film was directly coated on the silicon substrate is shown in **Figure 3.9b**. It can be seen that the film was brownish (**Figure 3.9a**) in ‘closed/off state’, and had the reflection maximum and minimum at around 665 nm and 462 nm respectively (**Figure 3.9b**), owing to the constructive and destructive interference.

However, once illuminated by UV light, a reflection dip appeared at around 604 nm and the color changed to green, **Figure 3.9a,b**. Moreover, the reflection peak underwent a pronounced red shift of more than 50 nm while the reflection dip blue shifted by about 12 nm, owing to the modulation of the real part of the refractive index. Yet, when a spacer layer of 50 nm silicon oxide between PS-SPO film and silicon substrate was introduced, the film color became light blue without UV exposure which changed to dark blue after UV exposure, **Figure 3.9a**. **Figure 3.9c** represents the UV-Vis analysis of this system where a broad reflection minimum occurred at around 620 nm. Upon illumination with UV light we observed a drop in reflection along with a slightly blue shifted reflection minimum at around 600 nm i.e., at the wavelength where absorption of photochromic molecules takes place, **Figure 3.9c,3.6e**. No splitting was observed as the reflection minimum was indeed in the range, where the imaginary part of the refractive index of the photochromic film was dominant. This result highlights the control of color and peak shift, based on the interference and refractive index of the photochromic film while introduces a very promising design map for controlling the optical properties of photochromic devices.

To manifest our finding of controlling the optical properties of a photoactive device and consequently introduce the concept of photochromic transparency as well, we designed another photochromic system based on nanofibers.

Photochromic fibers were fabricated by the electrospinning technique from a blend of polymer solution and SPO. A typical image of fibers is shown in **Figure 3.9d**. Electrospinning allowed us to control the fibers’ diameter and therefore, we were able to tune the resonance peak of fibers to coincide with the absorption resonance of molecules or to overlap with the peak of the real part of their refractive index (i.e. reflection dominant region). **Figure 3.9e,f** shows this situation using PVDF fibers having an average diameter of (d~950 nm) and (d~750 nm), which contained 20-30 wt.% SPO, possessing a broad resonance peak centered at 720 nm and 620 nm respectively. After the UV exposure, not only

the position of the resonance peak shifted but also the optical response of the system changed with the varying size of the fibers.

The UV-Vis analysis in the transmission mode of optically active PVDF fibers of coarser diameter ($d \sim 950$ nm) is shown in **Figure 3.9e**. The fibers have transmission minimum

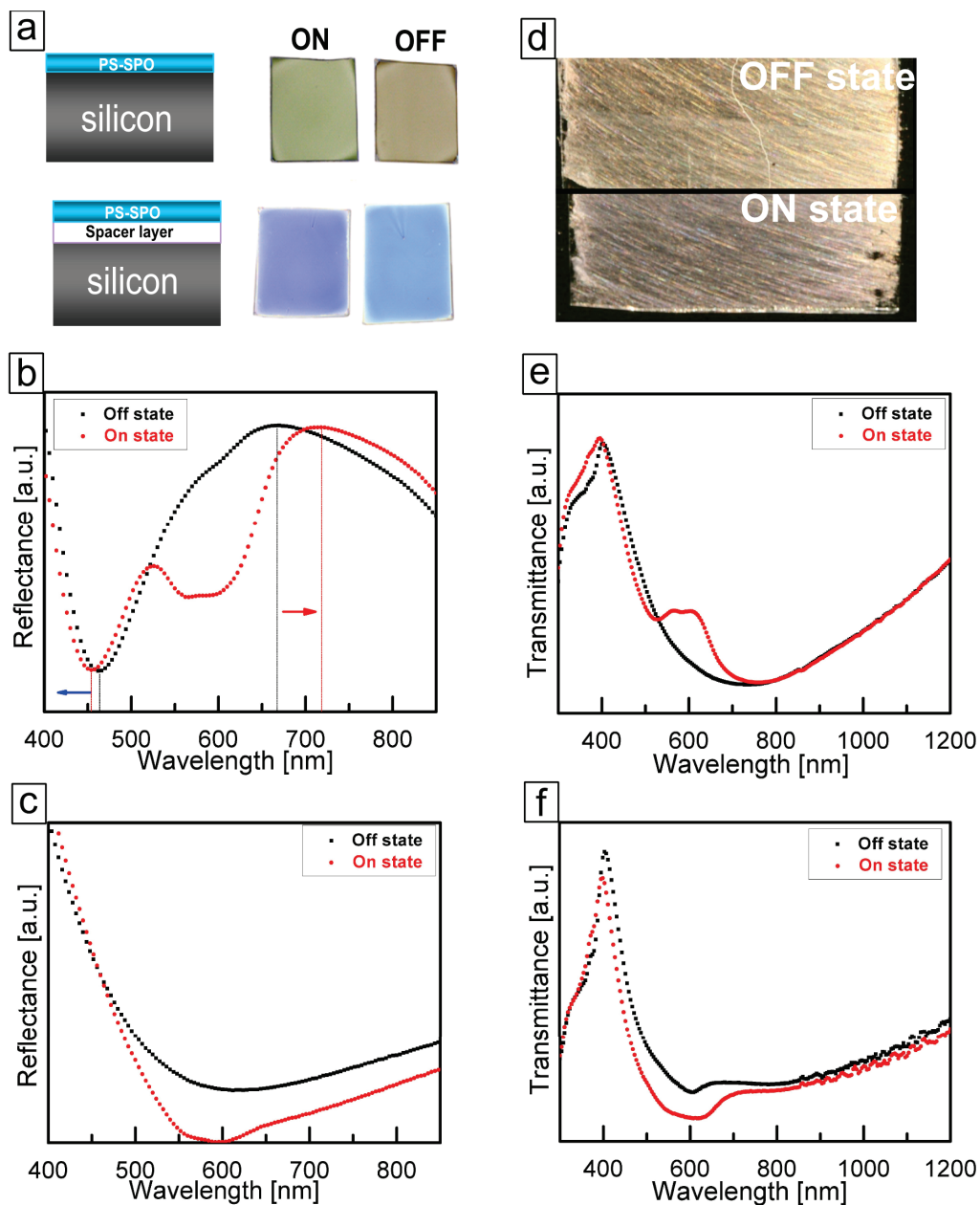


Figure 3.9 Color and transparency by refractive index modulation. **a)** Effect of a thin spacer layer of silicon oxide between ‘PS-SPO’ film and silicon wafer on the reflected color for “off state/before UV” and “on state/after UV” states. **b)** UV-Vis reflectance spectra of PS-SPO film coated on silicon wafer; “off state/before UV, black line” and “on state/after UV, red line”. **c)** UV-Vis spectra of PS-SPO film coated on silicon wafer with silicon oxide spacer layer; (off state/before UV, black) and (on state/after UV, red). **d)** Camera picture of part of fibers, in ‘off state/before UV’ and ‘on state/after UV’ states, as seen with transmitted light. **e,f)** UV-Vis spectra of PVDF-SPO fibers of different thickness (off state/before UV, black) and (on state/after UV state, red) : (e) ~ 950 nm thick fibers; (f) ~ 750 nm thick fibers.

at around 720 nm when the embedded chromophore was in ‘closed/off state’. Once illuminated with UV light, an enhancement in transmission appeared at around 600 nm, i.e., at the wavelength where absorption of photochromic molecules was expected. Even more pronounced was the resonance peak splitting, revealing two separate peaks at 568 and 604 nm. Such splitting allowed us to demonstrate a molecular photonic coupling, analogous to molecular plasmonic coupling.^[69, 71-73] On the other hand, in the case of finer fibers, a photo-absorption was observed after UV exposure (**Figure 3.9f**), which is generally expected from SPO molecules inside polymer films or solvent environments. For fine fibers neither an increase in transmission nor splitting was observed, and the system behaved similar to the silicon/spacer system (**Figure 3.9c**) because both were controlled mainly by the imaginary part of the refractive index. Thus, we show a new strategy for controlling the molecular coupling in an optically active system.

3.2.3 Conclusion:

Taken together, we demonstrated the first experimental evidence of specular reflection of a chromophore enabling the design of novel optically active systems, which as shown here for example, can be used as an indicator of the matrix polarity with a much higher sensitivity than an indicator based on transmitted color. Moreover, a control over the reflective colors of the polymer-chromophore film is shown by controlling the substrate properties. Furthermore, by refractive index modulation, the optical properties of a nanofibers based photochromic system could be changed from ‘absorptive upon UV exposure’ to ‘enhanced transmissive upon UV exposure’. Our experimental findings need further investigation in terms of numerical simulation to fully understand the phenomenon. Yet we believe our work would enhance our interpretation of several optical phenomena based on the photoswitchable molecules and would enable the design of new light-driven functional devices.

3.2.4 Experiments:

For the spin coating of films, solutions of the polymer (2 wt.% for PS, 3 wt.% for PES and 2 wt.% PVDF) together with 1,3-Dihydro-1,3,3-trimethylspiro[2H-indole-2,3'-[3H]phenanthr[9,10-b](1,4)oxazine] (i.e., SPO) were prepared by stirring in N,N-Dimethylformamide (DMF) at room temperature. Glass slides were cleaned in piranha solution (volume ratio: 5 H₂O + 1 NH₄OH + 1 H₂O₂), rinsed with de-ionized water and consequently dried with nitrogen. The spinning speed, ranged from 2000-3600 rpm. Film thickness was determined with a Bruker Dektak XT profilometer.

Solutions for electrospinning were prepared by dissolving 10-13 wt.% PVDF in DMF by stirring along with SPO. Electrospinning was carried out pushing the polymer solution at a

fixed rate through a needle that was kept at a high potential with respect to a grounded target that was in the form of two parallel wires. Due to electrostatic forces between the charged polymer and the grounded target, the polymer droplet took into the form of a jet which further thinned into nanofibers during its flight towards the target. The fibers were collected between the two wires constituting the target and were picked onto a glass plate.

For switching of SPO between its 'ON' and 'OFF' states, a UV lamp (Labino, 35 W) was used with its peak intensity at 365 nm with irradiation time of approximately 4 minutes.

Ellipsometry was performed on an M-2000 ellipsometer from J.A. Woollam Co., Inc. with an automated angle base. Measurements were done between 45° and 85° with a step size of 10°. Data acquisition was done with the company's CompleteEASE software. UV-VIS analysis of films and fibers was done Perkin-Elmer UV-VIS spectrometer (Lambda 900). The measurements were made after measuring glass as background.

3.2.5 Acknowledgements:

We gratefully acknowledge the financial support by the German Research Foundation (DFG) through SFB677 (C09) and the partial financial support by German Academic Exchange Service (DAAD). M.E. thanks the Initiative and Networking Fund of the Helmholtz Association (grant No. VH-NG-523) for providing the financial base to start his research group. We also would like to thank Mr. Stefan Rehders for drawing the schematics.

Transparent conductor:

Observation of molecular photonic coupling in photochromic systems naturally raised interest regarding the molecular plasmonic coupling and further work in this direction led to the development of a photoswitchable transparent conductor. The enhancement in transmittance along with a high conductivity is of particular interest, especially for solar cells and sensors. Metal films being highly conductive are inherently highly reflective, too. On the other hand, present day transparent conductors, like Indium Tin Oxide (ITO), are not only expensive but also cannot offer conductance of metal thin film. As a potential transparent conductor, a hybrid of metal thin film and photochromic molecules embedded in a polymer matrix was developed. It not only had high conductivity but also had photo-switchable transparency. The high transparency was obtained only at a certain content of SPO in the system, where it created strong enough wave vector that could couple with plasmonic wave vector generated by its mirror image in metal thin film. Upon coupling, an increase in transmittance and a strong decrease in reflection were observed. The transmittance could be blocked to a level that of a metal film by exposing the device to UV. Since switching back of SPO molecules to their closed state controlled the switching speed of transparency, a method to accelerate the switching of molecules with organic solvent vapors was also devised. Such a device could also be used as an optical sensor for the organic solvent vapors. This work was published in “*Advanced Materials*, **2011**, *23*, 4243”, and is presented next in the same form.

3.3 Photoresponsive Transparent Conductive Metal with a Photobleaching Nose

*Mohammad Jamali, Mehdi Keshavarz Hedayati, Babak Mozooni, Mojtaba Javaherirahim, Ramzy Abdelaziz, Ahnaf Usman Zillohu and Mady Elbahri**

Published paper: *Advanced Materials*, **2011**, 23, 4243. DOI: 10.1002/adma.201102353
Reprinted here with permission from: WILEY-VCH Verlag GmbH & Co. KGaA, Weinheim, ©2011.

3.3.1 Introduction:

Smart materials that respond to a stimulus or their environment to produce a dynamic and reversible change in critical properties are in focus of actual research.^[74] Among several stimuli, photochromism is receiving increasing attention because of its potential applications in molecular switching, lenses, and data storage among others.^[75] In general, photochromic molecules can turn any composite into a smart material provided the host matrix is soft enough (e.g., a polymer) to let the molecule rotate upon illumination. The unique properties of these molecules can be even more beneficially implemented into the devices whose optical properties are the matter of interest (e.g., optoelectronic devices) and to make them smart. In this regard, transparent conductors (TCs) can be a proper matter since their optical properties are crucial. Traditionally, indium tin oxide (ITO) has been widely implemented as a standard TC in different kinds of optoelectronic devices. However, having phototunable optical transparency along with high electrical conductivity would be potentially applicable for novel smart optoelectronic sensors. During the course of last decades, great efforts have been made to develop new kind of TCs to replace ITO.^[76–78] In this regard, different materials and composites have been proposed and studied, including conductive polymers,^[79] carbon nanotubes (CNTs),^[80–82] graphene,^[83] metal grids,^[84,85] and random networks of metallic nanowires.^[86,87] But to the best of our knowledge, no work has been reported concerning smart TCs. Our recent work showed that one can enhance the optical transparency of the thin metallic film with the aid of a plasmonic nanocomposite and make a novel transparent conductive metal (TCM).^[88]

Here, we demonstrate the first photoswitchable transparent conductor that functions via nanophotonic interaction. The newly developed photoresponsive TCM structure is a sputtering-deposited metal film spin-coated with spirophenanthrooxazine (SPO) molecules embedded in a polymeric matrix. Under a certain filling factor of SPO, the coating layer gives a high optical transparency to the metal substrate, which intrinsically has a high electrical conductivity (approximately an order of magnitude greater than typical TCs, e.g.,

ITO). Transmission enhancement up to 100% (relative to the intrinsic value of a thin metal film) is observed and can be diminished upon UV light illumination. Although the recovery time takes almost one day, we tremendously reduced it to few seconds by exposing the device to certain organic vapors, demonstrating a photobleaching gas sensor.

It is well known that light can be trapped between the polarized metallic nanoparticles (in proximity of a metal film) and the metallic film, giving rise to the highly concentrated electrical field.^[89] We have recently shown that nanocomposites that contain a nanoparticle polarizer embedded in a polymeric matrix can be used to excite plasmonic tunneling.^[88] The activation of the surface plasmon associated with the confinement of the electromagnetic waves results in a significant reduction of the reflection and at the same time the induced charges on the metal mirror by the dipole and image reduce the absorption and scattering of the structure and therefore raise the ratio of the light that can pass through, consequently making the metal film transparent.

In this work, we used the mentioned concept to make the metallic film highly transparent, however instead of using nanoparticles as the polarized medium, we implemented the idea by using photoswitchable molecules dispersed in a polymeric matrix. The photoswitchable molecules have dipole moments that can be switched on (open form) and off (closed form) upon UV and visible light illumination, respectively.

3.3.2 Results and Discussion:

Although spiro molecules are known as light absorbers, by proper design of the SPO-doped coating one can enhance the transmission of metal film as well. In **Figure 3.10a**, the transmission spectra of the films deposited with different concentrations of SPO molecule are illustrated. One can see that the transmission of 20 nm sputtered silver film^[90] spin-coated with 10 nm of polystyrene (PS), which is less than that of the bare silver film, is slightly increased when SPO molecules are introduced into the polymeric matrix to the critical filling factor of 50 vol.%. At this concentration the overall light transmission of the film is strongly enhanced in the most of the visible spectrum, whereas beyond this critical filling factor a rapid diminishing of transmission occurs.

Figure 3.10b shows the reflection spectra of the coated Ag film with different concentrations of SPO. It is obvious that the reflection of the metal film is slightly reduced when coated with PS/SPO (20 vol.%) compared to the bare metal film. However, the coating with PS/SPO (50 vol.%) results in a minimum in the reflection spectra at 486 nm in addition to the overall reflection reduction. By increasing the SPO content up to 70% the reflection intensity increases and becomes broader in a way that covers a wide range of the visible frequencies.

It is well recognized that spiro molecules (SPO) are chemical species in which the dipole moments change their conformation under UV illumination from close (off) to open (on) states.^[90,92] In the off state (not illuminated by UV light) the SPO molecules, which are distributed in the polymeric coating, are polarized due to thermal equilibrium with its open form.^[93] In addition to acting as dipoles in the polymeric film and dipole–dipole interactions, those molecules that are located in proximity of the silver (mirror) will induce also a dipole image on the film.^[94] The induced dipoles result in a new charge distribution in the metal layer, which can be assumed as an in-plane wave vector, k_{Ind} .^[95] This charge distribution is expected to vary with the SPO concentration, as is shown schematically in **Figure 3.11**.

Plasmonic coupling is achieved by matching between the induced wave vector and that required for the surface plasmon. The reflection minimum that appears in the case of PS/SPO (50 vol.%) is a sign of plasmonic coupling and indicates that SPO

molecules, at a certain filling factor, provide the surface momentum needed for surface plasmon excitation on the metal surface. The fact that the position of the reflection dip is almost at the same wavelength as the transmission peak for PS/SPO (50 vol.%) is a strong hint for the occurrence of a resonant plasmonic tunneling phenomenon.^[96] The dipole–image interaction of the chromophores strongly interacts with the free electrons of the metal,

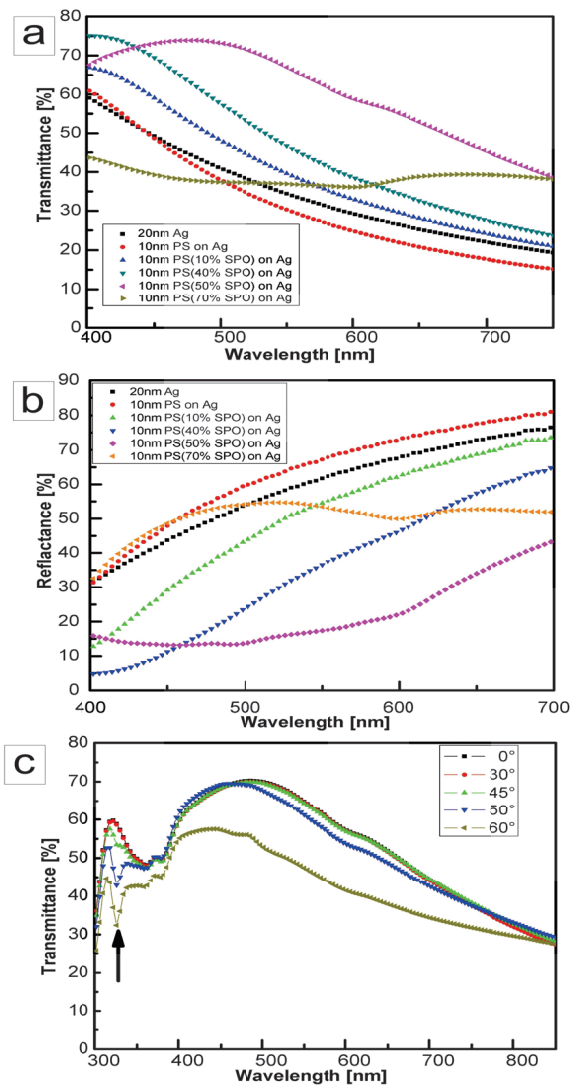


Figure 3.10 a) Transmittance spectra of 20 nm silver film coated with 10 nm PS doped with 20 vol%, 50 vol%, and 70 vol% SPO. The uncoated 20 nm silver film and the 10 nm PS film coated on a 20 nm silver film are shown as references. b) Reflectance spectra of a 20 nm silver film coated with 10 nm PS doped with 20 vol%, 50 vol%, and 70 vol% SPO. The uncoated 20 nm silver film and the 10 nm PS film coated on a 20 nm silver film are shown as references. c) Optical transparency of the stacks (10 nm PS (50%) on 20 nm silver) at different angle of incidence. The arrow shows the position of the drop in the spectra where it is due to the excitation of a plasmon.

creating a plasmonic state that is responsible for the broad drop in the reflectivity and appearance of the higher transmission.

To illustrate the role of surface plasmon in the optical transparency enhancement, angular measurement was carried out. As shown in **Figure 3.10c**, the coating shows an omnidirectional transmission (angular independency) up to critical angle of $\sim 50^\circ$ at which a drop in the transmission occurs due to the excitation of the radiative surface plasmon at 330 nm.^[97] This is shown by arrow in **Figure 3.10c**. This is a strong evidence that the surface plasmon phenomenon and its excitation type (i.e., evanescent, radiative, etc.) controls and determines the optical transparency of the system.

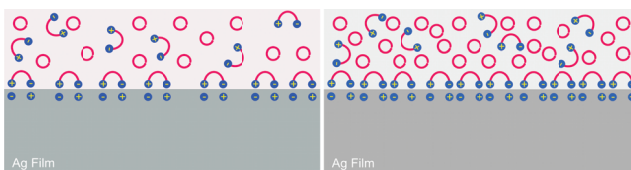


Figure 3.11 Simplified illustration of the SPO-doped, polymer-coated silver film showing the partial polarization of the molecules and the dipole image of the molecule in the base metal film: low SPO concentration (**left**) and high SPO concentration (**right**).

Increasing beyond the critical concentration leads to a larger wave vector, which is comparable or even larger than the wave vector of internal reflection of the sample, and hence high reflectivity in a broad area between 482 and 600 nm occurs. **Figure 3.10b**.

Additionally, the dipoles in the molecules also interact with each other and the magnitude of the interaction force depends on the intermolecular distance. In other words, for low concentration of SPO in the coating, the force is negligible, but for a highly concentrated film it might increase scattering or absorption and reflection.^[94]

Our results show for the first time that one can tune the metal/chromophores interaction by adjusting the filling factor of the chromophores in a way that results in either reflection or transmission enhancement. The relative transmission enhancement for the sample with (50 vol.%) is around 100% in most of the spectrum. One sees a clear difference in the brightness of the photograph of the logo of the Nanochemistry and Nanoengineering group taken through a piece of glass coated with a 20 nm silver film (right) and with a PS/SPO coating (left) due to the low and high transmissions of the film, respectively, **Figure 3.12a**.

SPO under UV illumination switches to photomerocyanine (PMC) form, which absorbs light at visible frequencies due to its highest occupied molecular orbital (HOMO) to lowest unoccupied molecular orbital (LUMO) transition.^[98] This switching behavior of SPO gives a novel property to the TC. Despite the enhanced transparency by means of the optimized coating concentration to 50% SPO, there is a drastic drop in transmission down to the transmission of the bare silver film upon UV illumination, **Figure 3.12b**. A photograph of

the sample of the mentioned sample before (left) and after (right) UV illumination is shown in **Figure 3.12c**.

One problem regarding application of SPO is that the recovery time of the system after illumination with UV light is fairly long (almost 1 day), which is illustrated in **Figure 3.13a**. Here, we demonstrate a fast recovery based on a photobleaching gas nose. Our strategy of fast response is based on the fact that the switching of the spiro molecules in the solution is very fast, while this phenomenon is hindered when the spiro molecules are embedded in a solid (polymeric) film. In other words, the polymeric solution as a viscous environment provides sufficient space for the molecules to switch forth and back upon the illumination with UV and visible light, respectively. On the other hand, the free volume inside the solid film is not enough for easy rotation of the molecules; therefore their movements are strongly suppressed. By exposing the sample to organic vapor of a good solvent, which acts as plasticizer for PS, the polymer film should expand and facilitate reverse-switching of SPO, i.e., a bleaching process.

The results of a photobleaching test (proof of- concept experiment), which was done simply by exposing the samples that were in the

on state (UV illuminated ones) to different organic vapors, is shown in **Figure 3.13b**. These kinetics curves show a highly specific photobleaching process with a rapid response for toluene and acetone, moderate response for ethanol, and very slow response for isopropanol. In other words, the response of the system depends strongly on the solubility parameter of the polymer and organic gas that were used. The results demonstrate a fast recovery of the photo- or gas-switchable device along with its potential use as an artificial nose.

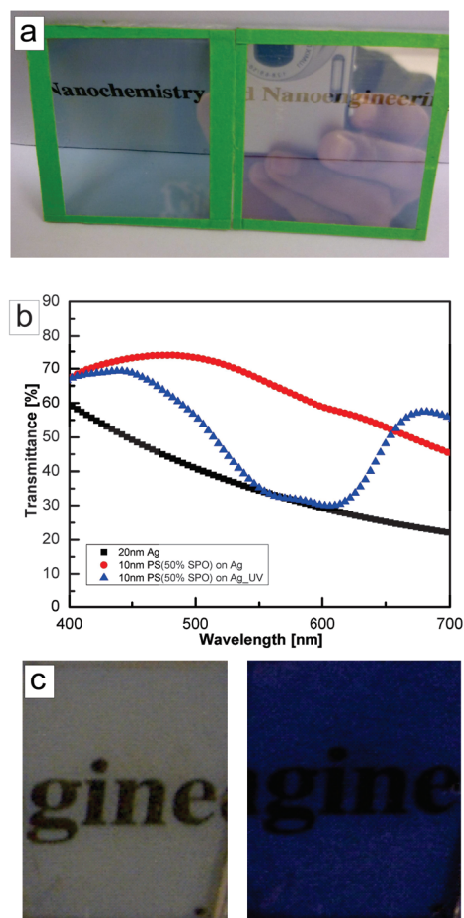


Figure 3.12 a) Photograph of the Nanochemistry and Nanoengineering logo taken through a piece of glass coated with a 20 nm silver film (right) and 10 nm PS (50 vol% SPO) coated on a 20 nm silver film (left). b) Transmittance spectra of 10 nm PS films doped with 50 vol% SPO coated on 20 nm silver film before and after UV illumination. The uncoated 20 nm silver film and the 10 nm PS film coated on a 20 nm silver film are shown as references. c) Photographs of the 20 nm silver film coated with 10 nm PS (50 vol% SPO) before UV illumination (left) and after UV illumination(right).

The photobleaching test with acetone vapor was cycled several times without any noticeable degradation of the polymer and/or segregation of the molecules (**Figure 3.13c**). To have an appropriate transparent conductor, in addition to a high transparency, significant conductivity is also needed. The measurements showed that the electrical resistivity of the coated silver film ($13.3 \mu\Omega\cdot\text{cm}$) is comparable to that of the bare silver film ($1.59 \mu\Omega\cdot\text{cm}$) but is an order of magnitude lower than that of commercial thick ITO films ($250 \mu\Omega\cdot\text{cm}$).^[99] Therefore one can say that using this technique a new transparent conductive film is fabricated that has superior electrical properties to the typical ITO. It means that this device can be used as a new photoswitchable transparent conductive film.

In summary, we have presented a new kind of smart transparent conductive metal based on a thin metallic film coated with spirophenanthrooxazine (SPO)/polymer composite. Transparency enhancement up to 100% (relative to the intrinsic value of thin metal film) is achieved in an optimum concentration of SPO, which was attributed to the image dipole phenomenon and excitation of a plasmon resonance of the thin film that diminishes the reflectivity of the stacks.

In addition to having a photoswitching property, fast recovery of the rotated dipoles to the original state is also achieved. This goal was achieved by exposing the UV-illuminated

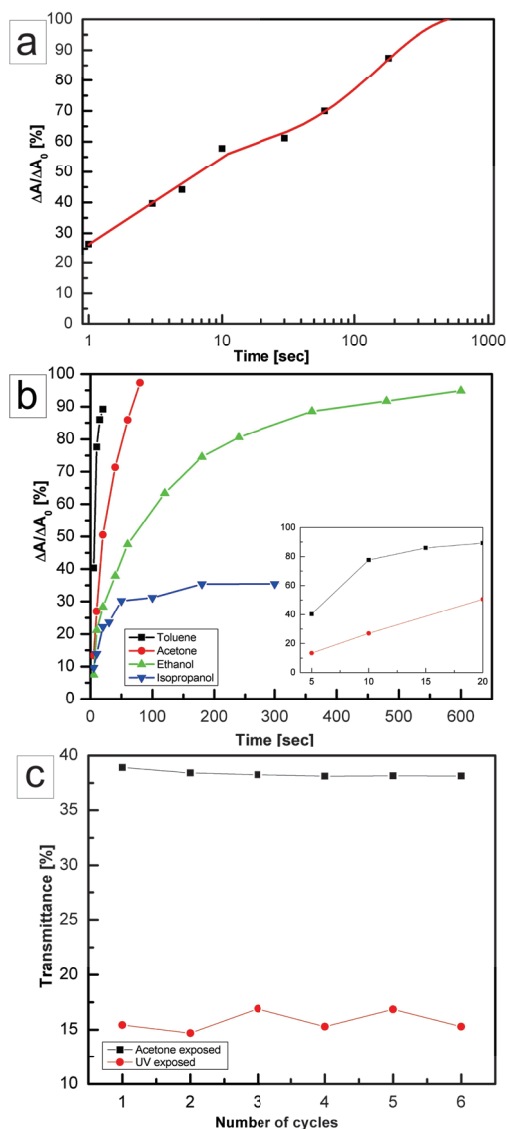


Figure 3.13 a) Photobleaching of a sample containing 50% SPO after exposure to the visible light in atmosphere. ΔA is the difference between the maximum absorption and the absorption at time t , ΔA_0 is the difference between the maximum absorption and the initial state. b) Photobleaching of a sample containing 50% SPO in the presence of different chemical vapors. The inset shows the magnified graph of toluene (rectangle) and acetone (circle). c) Reproducibility of switching back by exposing to acetone vapor. The sample was exposed to UV light and then to the acetone vapor several times. The transmission points were measured at a wavelength of 600 nm illumination (left) and after UV illumination (right).

samples (low transparency ones) to organic vapor gases. The recovery time of the SPO was remarkably reduced to a few seconds and a new photobleaching nose was demonstrated. In addition, the electrical conductivity of the device is comparable to the value of bulk silver.

With this technique one can benefit from enhancement of optical transparency together with the electrical conductivity of the thin metal film to realize a new smart transparent conductor with fast photoswitching properties.

3.3.3 Conclusion:

Here we make thin gold film highly transmissive by spin coating it with a blend of a polymer with a photochromic compound. The thin metal film is inherently highly conductive, and thus the hybrid can be used as a transparent conductor. The transmissive properties of the hybrid are omnidirectional and can be switched to a nontransmissive state by exposure to UV. Recovery back to the transmissive state can be accelerated by exposing the system to organic vapors of a solvent, which in turn demonstrates the applicability of the device as an electronic nose for organic vapor gases.

3.3.4 Experiments:

SPO, which was used as a photochromic dye, was obtained from Sigma Aldrich. General laboratory grade acetone was used as the solvent. A PS solution in toluene was utilized as the polymer matrix. Silver films (20 nm) were deposited on glass slides (1.5 cm × 2.5 cm) by sputtering,^[90] and used as the substrate. For that purpose, 4 min sputtering with a rate of 5 nm.min⁻¹ was used and the thickness of the film was further measured with profilometer.

The 0.026 M solution of SPO was prepared by dissolving SPO powder in acetone. The 1 wt.% PS solution was diluted with toluene to different concentrations in order to create different thicknesses after spin-coating.

The prepared solutions were spin coated on the silver coated glass plate by means of Spin coater (P6700 Series). The spin-coating was performed in a wide variety of speeds to find the optimum condition to have a uniform film with the desired thickness. As a result, spin-coating at 1000 rpm for 60 s was selected to prepare all of the samples.

The thicknesses of all of the samples were measured by means of profilometer (Dectak 8000 surface profile measuring system). To analyze the switchability of the coatings, a 35 W UV spot light lamp (LABINO-AB) was utilized. In all of the cases, the irradiation time was identical (i.e., 20 s). Optical measurements were done using a UV-Vis/IR spectrometer (Lambda 900). For all the spectrometry tests, the transmission of the glass, which was used as the substrate, was considered as the base data; i.e., the transmission intensity of every sample was normalized to that of glass in order to exclude the loss due to

the intrinsic reflection of the glass. To accelerate the switching of the device, we exposed the sample after UV illumination to acetone, isopropanol, toluene, and ethanol vapors. For that purpose, the samples were placed as the lid of a beaker containing 5 mL solvent and the distance between the lid and the surface of the solvent was held constant for all the samples (8 cm). Immediately after the vapor exposure process, the spectra were taken in order to observe the effect of the solvent vapor on the switching properties. To find the right switching time, the mentioned process was carried out for different time periods. Finally, the response time was calculated based on the resulting spectrum. This proof of concept experiment was carried out in air and was highly reproducible.

3.3.5 Acknowledgements:

The authors appreciate the financial support provided through SFB 677 funded by the German Research Foundation (DFG) and the financial support from the DAAD PhD fellowship for A.U.Z.; M.E. thanks the Initiative and Networking Fund of the Helmholtz Association for providing the financial base for the start-up of his research group. Additionally, the authors gratefully acknowledge Prof. Franz Faupel and Dr. Thomas Strunskus for their comments on the manuscript and S. Rehders for his technical help regarding the setup and operation of the sputtering chamber. The help of Mr. Ali Tavassolizadeh, for drawing the sketch, is also acknowledged.

3.3.6 References:

- [1] C. Yang *et al.*, *Cancer Nanotechnology* **2013**, *4*, 81.
- [2] Y. Wang *et al.*, *ACS nano* **2013**, *7*, 2068.
- [3] I. H. El-Sayed, X. Huang and M. A. El-Sayed, *Nano Letters* **2005**, *5*, 829.
- [4] S. Pillai *et al.*, *Journal of Applied physics* **2007**, *101*, 093105.
- [5] M. Grätzel, *Journal of Photochemistry and Photobiology C: Photochemistry Reviews* **2003**, *4*, 145.
- [6] A. U. Zillohu *et al.*, *The Journal of Physical Chemistry C* **2012**, *116*, 17204.
- [7] A. Cox, A. J. DeWeerd and J. Linden, *American Journal of Physics* **2002**, *70*, 620.
- [8] J. A. Rogers *et al.*, *Applied physics letters* **1997**, *70*, 2658.
- [9] D. Li, Y. Wang and Y. Xia, *Nano Letters* **2003**, *3*, 1167.
- [10] H. Dürr and H. Bouas-Laurent, *Photochromism: Molecules and systems: Molecules and systems*, Elsevier Science **2003**.
- [11] G. Baillet, G. Giusti and R. Guglielmetti, *Bulletin of the Chemical Society of Japan* **1995**, *68*, 1220.
- [12] T. Feczko, M. Kovács and B. Voncina, *Journal of Photochemistry and Photobiology A: Chemistry* **2012**, *247*, 1.
- [13] F. Ortica *et al.*, *Journal of Photochemistry and Photobiology A: Chemistry* **2001**, *138*, 123.
- [14] G. Berkovic, V. Krongauz and V. Weiss, *Chemical Reviews* **2000**, *100*, 1741.
- [15] B. L. Feringa and W. R. Browne, *Molecular switches*, Wiley **2011**.
- [16] M. Jamali *et al.*, *Advanced materials* **2011**, *23*, 4243.
- [17] Y. Liang, A. S. Dvornikov and P. M. Rentzepis, *Optics communications* **2003**, *223*, 61.
- [18] V. Weiss, A. Friesem and V. A. Krongauz, *Optics letters* **1993**, *18*, 1089.

- [19] V. Weiss, A. Friesem and V. Krongauz, *Journal of Imaging Science and Technology* **1997**, *41*, 371.
- [20] T. P. Saragi *et al.*, *Chemical Reviews* **2007**, *107*, 1011.
- [21] M. Takeshita and M. Irie, *Tetrahedron letters* **1998**, *39*, 613.
- [22] J. X. J. Zhang and K. Hoshino, *Molecular sensors and nanodevices: Principles, designs and applications in biomedical engineering*, Elsevier Science **2013**.
- [23] N. J. Turro, *Modern molecular photochemistry*, University Science Books **1991**.
- [24] F. Mohammad, *Specialty polymers: Materials and applications*, IK International Pvt Ltd **2007**.
- [25] B. Valeur and M. N. Berberan-Santos, *Molecular fluorescence: Principles and applications*, John Wiley & Sons **2013**.
- [26] R. B. Woodward, *Journal of the American Chemical Society* **1941**, *63*, 1123.
- [27] L. F. Fieser, M. Fieser and S. Rajagopalan, *The Journal of organic chemistry* **1948**, *13*, 800.
- [28] P. Bamfield and M. G. Hutchings, *Chromic phenomena: Technological applications of colour chemistry*, Royal Society of Chemistry **2010**.
- [29] J. R. Lorenzo, *Principles of diffuse light propagation: Light propagation in tissues with applications in biology and medicine*, World Scientific **2012**.
- [30] F. Ortica *et al.*, *Photochemical & Photobiological Sciences* **2002**, *1*, 803.
- [31] B. Hoo Lee *et al.*, *Dyes and pigments* **2004**, *61*, 235.
- [32] N. A. Murugan, S. Chakrabarti and H. Ågren, *The Journal of Physical Chemistry B* **2011**, *115*, 4025.
- [33] F. Ciardelli *et al.*, *Polymers for Advanced Technologies* **1995**, *6*, 32.
- [34] M. M. Russew and S. Hecht, *Advanced materials* **2010**, *22*, 3348.
- [35] M. Irie, *Chemical Reviews* **2000**, *100*, 1683.
- [36] R. Potember, T. Poehler and D. Cowan, *Applied physics letters* **2008**, *34*, 405.
- [37] A. Sawa, *Materials today* **2008**, *11*, 28.
- [38] J. Ouyang *et al.*, *nature materials* **2004**, *3*, 918.
- [39] C. Bechinger *et al.*, *Nature* **1996**, *383*, 608.
- [40] Y. Ohko *et al.*, *nature materials* **2002**, *2*, 29.
- [41] A. Grinthal and J. Aizenberg, *Chemical Society Reviews* **2013**, *42*, 7072.
- [42] M. Jamali *et al.*, *Advanced materials* **2011**, *23*, 4243.
- [43] M. K. Hedayati, *et al.*, *Advanced Optical Materials*, DOI: 10.1002/adom.201400105.
- [44] R. Klajn, *Chemical Society Reviews* **2013**, *43*, 148.
- [45] J. W. S. Rayleigh, *Phil. Mag.* **1871**, *41*, 274.
- [46] C. Kittel and E. M. Purcell, *Berkeley physics course*, McGraw-Hill **1966**.
- [47] S. Martin, *An introduction to ocean remote sensing*, Cambridge Univ. Press **2004**.
- [48] H. Fujiwara, *Spectroscopic ellipsometry: Principles and applications*, John Wiley & Sons **2007**.
- [49] M. Biot, *Journal of Applied physics* **2004**, *28*, 1455.
- [50] M. Kerker, *The scattering of light, and other electromagnetic radiation*, Academic Press **1969**.
- [51] C. F. Bohren and D. R. Huffman, *Absorption and scattering of light by small particles*, John Wiley & Sons **2008**.
- [52] M. Biot, *The Journal of the Acoustical Society of America* **2005**, *29*, 1193.
- [53] A. Movchan *et al.*, *SIAM Journal on Applied Mathematics* **2001**, *61*, 1706.
- [54] J. A. Stratton, *Electromagnetic theory*, John Wiley & Sons **2007**.
- [55] P. W. Atkins and R. S. Friedman, *Molecular quantum mechanics*, Oxford Univ. Press **2011**.
- [56] S. N. Kasarova *et al.*, *Optical Materials* **2007**, *29*, 1481.
- [57] A. Sen and L. Kandpal, *Proceedings of recent advances in polymers and composites*, Allied Publishers **2000**.

- [58] H. F. Mark, *Encyclopedia of polymer science and technology: Step-reaction polymerization to thermoforming*, Interscience Publishers **1970**.
- [59] Margolis, *Engineering thermoplastics: Properties and applications*, Taylor & Francis **1985**.
- [60] M. Biron, *Thermoplastics and thermoplastic composites: Technical information for plastics users*, Elsevier **2012**.
- [61] H. F. Mark, *Encyclopedia of polymer science and technology: Molding to petroleum resins*, Interscience Publishers **1968**.
- [62] R. Nussbaumer *et al.*, *Journal of materials science* **2005**, *40*, 575.
- [63] Q. M. Zhang, V. Bharti and G. Kavarnos, in *Encyclopedia of smart materials*, (Ed: M. Schwartz), John Wiley & Sons, **2002**.
- [64] Y. B. Zheng *et al.*, *Nano Letters* **2011**, *11*, 2061.
- [65] Y. B. Zheng *et al.*, *Nano Letters* **2009**, *9*, 819.
- [66] C. Bertarelli *et al.*, *Advanced Functional Materials* **2004**, *14*, 357.
- [67] J. Biteau *et al.*, *Chemistry of materials* **1998**, *10*, 1945.
- [68] E. Kim, Y.-K. Choi and M.-H. Lee, *Macromolecules* **1999**, *32*, 4855.
- [69] J. Dintinger, S. Klein and T. W. Ebbesen, *Advanced materials* **2006**, *18*, 1267.
- [70] J. I. Pankove, *Optical processes in semiconductors*, Dover Publications **2012**.
- [71] D. Dulić *et al.*, *Physical review letters* **2003**, *91*, 207402.
- [72] J. Dintinger *et al.*, *Advanced materials* **2006**, *18*, 1645.
- [73] S. J. van der Molen *et al.*, *Nano Letters* **2008**, *9*, 76.
- [74] M. A. C. Stuart *et al.*, *Nature Materials*, **2010**, *9*, 101.
- [75] M. M. Russew, S. Hecht, *Advanced Materials* **2010**, *22*, 3348.
- [76] A. Kumar, C. Zhou, *ACS Nano* **2010**, *4*, 11.
- [77] H. Wu *et al.*, *Nano Letters* **2010**, *10*, 4242.
- [78] X.-Y. Zeng *et al.*, *Advanced Materials* **2010**, *22*, 4484.
- [79] K. Fehse *et al.*, *Advanced Materials*. **2007**, *19*, 441.
- [80] E. M. Doherty *et al.*, *Carbon* **2009**, *47*, 2466.
- [81] Z. Wu *et al.*, *Science* **2004**, *305*, 1273.
- [82] M. Zhang *et al.*, *Science* **2005**, *309*, 1215.
- [83] K. Kim *et al.*, *Nature* **2009**, *457*, 706.
- [84] M. Kang *et al.*, *Advanced Materials* **2008**, *20*, 4408.
- [85] K. Chen *et al.*, *Organic Electronics* **2011**, *12*, 961.
- [86] S. De *et al.*, *ACS Nano* **2009**, *3*, 1767
- [87] X.-Y. Zeng *et al.*, *Advanced Materials* **2010**, *22*, 4484.
- [88] M. Elbahri *et al.*, *Advanced Materials* **2011**, *23*, 1993.
- [89] N. Liu *et al.*, *Nano Letters* **2010**, *10*, 2342.
- [90] F. Faupel *et al.*, *Advanced Engineering Materials* **2010**, *12*, 1177.
- [91] V. Malatesta *et al.*, *International Journal of Quantum Chemistry* **1992**, *42*, 879.
- [92] Y.-R. Yi, I.-J. Lee, *Journal of Photochemistry and Photobiology A* **2002**, *151*, 89.
- [93] A. K. Chibisov, H. Gerner, *Journal of Physical Chemistry A* **1999**, *103*, 5211.
- [94] A. Grigorenko *et al.*, *Nature* **2005**, *438*, 335.
- [95] J. R. Lakowicz, *Analytical Biochemistry* **2005**, 337.
- [96] Sergei Sidorenko and O. J. F. Martin, *Optical Express* **2007**, *15*, 6380.
- [97] N. Yamamoto *et al.*, *Surface and Interface Analysis* **2001**, *31*, 79.
- [98] A. I. Perrier *et al.*, *Journal of Physical Chemistry A* **2009**, *113*, 13004.
- [99] J. M. Phillips *et al.*, *Applied Physics Letters* **1995**, *67*, 2246.

Chapter 4

Plasmonic Heating of Films and Fibers

4.1 Light and metal nanoparticles:

Light cannot only be harnessed by colorful photochromic compounds but also metal nanoparticles have been recently under intense research for their light absorbing properties. Metals that have been traditionally been used as reflectors of light, behave as strong absorbers of light when in the form of nanoparticles, as is explained in the following.

It was Faraday in 1857, who first related the red color of gold colloid to the small size of the suspended gold particles.^[1] Later, following the work by Mie^[2] and Ritchi^[3] on electromagnetic properties of metal dielectric interface for small particles and thin films respectively, a lot of research effort has been devoted to this field.^[4]

The Drude model for conduction considers the electrons in metals to act as gas atoms so that they can wander around the static nuclei which makes the metals as a sort of plasma. The oscillating electric field of an incident electromagnetic radiation results in the oscillation of free electrons in the metal

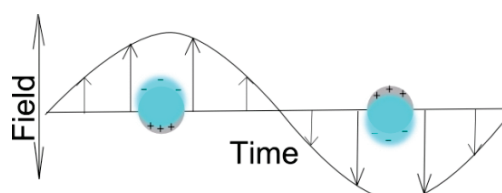


Figure 4.1 Oscillation of electron cloud (blue) around stationary nuclei (grey) due to incident oscillating electric field of electromagnetic radiation.

(**Figure 1.6**); the quantum of this charge density fluctuation being called ‘plasmon’. It can be excited in bulk metals (called Bulk plasmons), in individual metal nanoparticles (Localized surface plasmons/particle plasmon) or in thin metal film (Propagating surface plasmons). Applying the Drude model to the propagation of electromagnetic waves in a metal and using Maxwell’s equations, one gets the bulk plasma frequency, ω_p , of free charge carriers as:^[5]

$$\omega_p = \sqrt{\frac{ne^2}{m\epsilon_0}}$$

Equation 4.1

where, n is the electron density, e is their charge, m is the effective mass of the electrons and ϵ_0 is the permittivity of the free space. An incident radiation that has frequency higher than ω_p will pass through the metal but would be reflected back if it is lower than bulk plasmon frequency.^[6]

The electric field of the light incident on a nanoparticle that is very small compared to the wavelength of light, can be considered to be homogenous through out the particle (quasistatic approximation) which results in the formation of dipole on the nanoparticle. This condition is easily fulfilled by nanoparticles of size less than 100 nm upon their interaction with visible light. Contrary to propagating surface plasmons, which exist in thin metal films, localized surface plasmons confine the electric field to distinct particles. The curved surface

of the nanoparticles has two important consequences.^[7] Firstly it exerts an effective restoring force on the driven electron which results in resonance with consequent field enhancement inside the particle and also outside, in its near vicinity. Secondly, due to the curved surface, the plasmons can be induced with direct light illumination, without any need for phase matching which is necessary in the case of propagating surface plasmons on flat films. It is now well known that the bright colors of silver and gold nanoparticles are due the fact that the resonance frequency of their free electrons lies in the visible part of the spectrum which results in absorption of particular color and one perceives its complementary color as the color of the nanoparticles.

In order to determine the absorption efficiency of a particle of size $a \ll \lambda$, first one can calculate the polarizability considering the field to be homogenous and static and later can add time dependence to the results. The numerical procedure, the details of which are nicely presented by Maier^[7], results in the following relation stating the complex polarizability of a particle in quasistatic field:^[7]

$$\alpha = 4\pi a^3 \frac{\varepsilon - \varepsilon_m}{\varepsilon + 2\varepsilon_m} \quad \text{Equation 4.2}$$

Here ε is the complex frequency dependent, dielectric function of metal particle and ε_m is the real valued dielectric function of the surrounding matrix. It is clear that polarizability experiences a resonant enhancement (and consequently a huge absorption) when the denominator is minimum. Considering a small or slowly varying ‘Im ε ’, the results leads to Fröhlich condition for dipolar resonance in a small sphere:

$$\text{Re } \varepsilon_\omega = -2\varepsilon_m \quad \text{Equation 4.3}$$

For a sphere of Drude metal located in air, this condition is met when:

$$\omega_0 = \frac{\omega_p}{\sqrt{3}} \quad \text{Equation 4.4}$$

For other particle shapes, such as spheroids for example, the **Equation 4.2** is only valid when necessary corrections are applied. In the said case, one finds two separate resonances, a blue shifted resonance along the minor axis and a red shifted one along the major axis.

The nanoparticles not only absorb light but also a part of it is scattered. The scattering and absorption cross sections are given by the following relation:^[7]

$$\sigma_{sca} = \frac{k^4}{6\pi} |\alpha|^2 = \frac{8\pi}{3} k^4 a^6 \left| \frac{\varepsilon - \varepsilon_m}{\varepsilon + 2\varepsilon_m} \right|^2 \quad \text{Equation 4.5}$$

$$\sigma_{abs} = k \operatorname{Im}[\alpha] = 4\pi k a^3 \operatorname{Im} \left[\frac{\varepsilon - \varepsilon_m}{\varepsilon + 2\varepsilon_m} \right] \quad \text{Equation 4.6}$$

with $k = \frac{2\pi}{\lambda}$. Since scattering scales with a^6 , larger particles scatter more than small and above 100 nm particle size, scattering takes over absorption.^[8] The above-mentioned relation is valid even for dielectric particles provided the quasistatic approximation is valid. The total effect of absorption and scattering (called extinction) by a sphere of volume V can be given by:^[7]

$$C_{ext} = 9 \frac{\omega}{c} \varepsilon_m^{\frac{3}{2}} V \frac{\varepsilon_2}{[\varepsilon_1 + 2\varepsilon_m]^2 + \varepsilon_2^2} \quad \text{Equation 4.7}$$

where ε_1 and ε_2 are the real and imaginary parts of the dielectric function of the particle. The position and intensity of plasmon absorption maxima depends upon the size, shape, composition, mutual interaction of metal nanoparticles and the dielectric constant of the surrounding medium. Thus a red shift in absorption is observed as the particle size increases, their shape becomes elongated, when the interparticle distance decreases,^[9-11] or when the value of the dielectric function of the surrounding medium increases.^[12,13]

For particles of larger size, the quasistatic approximation does not hold any longer because of significant phase change over the particle volume. This problem was addressed by Mie in his solution to Maxwell's equations. It accounts for the effects such as depolarization fields and radiation damping, not covered by quasistatic approximation. On the other hand, the electron mean free path exceeds the particle size when it is below 10 nm, which leads to electron surface scattering (the so-called chemical interface damping^[7]) and consequent broadening of plasmon absorption peak.^[14]

The confinement of electric field in the form of plasma oscillation, forms the basis for many of the advanced applications such as surface enhanced spectroscopy,^[15,16] optical filter,^[17,18] sensors,^[19,20] solar cell application,^[21] and thermoplasmonic applications^[22-24] etc.

The deactivation of photo-excited nanoparticles may simply involve loss of coherence. Since plasmon is coherent oscillation, merely a change in plane of electron oscillation would result in extinguishing of plasmon. This process is ultrafast, of the order of femtosecond.^[25] However, the energy of the system remains the same and is only dissipated by radiative and non-radiative processes. The efficiency of radiative decay (by photoluminescence) is generally very low, being 10^{-4} in the case of gold nanoparticles.^[26] The reason may be that the radiative processes ($5d$ to $6sp$ band transitions) are much slower than the non-radiative processes which relax by coulomb interaction or electron-phonon scattering.^[26] Right after photoexcitation, the electron gas in a nanoparticle has a highly non-thermal energy distribution. Due to electron-electron collision, the energy is exchanged between electrons and finally they established a Fermi-Dirac equilibrium but at a very high Fermi energy level. This process is also very fast and takes place at the time scale of around 0.5 ps.^[27] The hot electron gas loses its energy to lattice thermalization by electron-phonon relaxation within the nanoparticle in the time scale (for gold nanoparticles) of about 0.7ps.^[28] Finally, the nanoparticle loses its energy to the surrounding by phonon-phonon relaxation that takes place in up to hundreds of picoseconds. Since the heat transfer is through surface, its rate is proportional to the square of the radius of the particles.^[29]

The heat Q generated by nanoparticles after exposure to light of amplitude (intensity) E_0 and angular frequency ω , is given by:^[30]

$$Q = \frac{\omega}{8\pi} E_0^2 \left| \frac{3\varepsilon_m}{2\varepsilon_m + \varepsilon} \right|^2 \text{Im} \varepsilon \quad \text{Equation 4.8}$$

The heat transferred to the surrounding matrix by phonon-phonon coupling, raises its temperature by ΔT_r , which is given by:^[31]

$$\Delta T_r = \frac{V_p Q}{4\pi k_s r} \quad \text{Equation 4.9}$$

Where V_p is the volume of nanoparticle, k_s is the thermal conductivity of the surrounding and r is the distance away from the nanoparticle.

The heat generation by plasmonic phenomenon has a huge potential of application especially because of localization near the particles. It is a potential candidate for cancer treatment, local catalysis, solar power collection, local chemical restructuring, welding of soft

materials and their defect healing, pattern making and composite formation in polymers etc.^[23,32-36]

The next part of the thesis, which is in the form of two published papers, deals with the thermoplasmonic effect on silver-coated PVDF (polyvinylidene fluoride) film and fibers. The film was a commercially available product of 50 μm thickness and had alpha dominant conformation. The fibers were made by electrospinning. Their size was in the range of 1 μm and they had a dominantly beta conformation. The film as well as the fibers were sputter coated with silver. The AFM analysis showed that the silver coating on the film was in the form of nanoparticles of up to 20 nm size range. Neat films could survive the laser up to its full available power (100 mW, 785 nm) without melting. However, melting spots could be produced on silver coated films with as little laser power as 2 mW, owing to plasmonically generated heat. The minimum spot size was around 500 nm meaning that this method could be used to make 2D submicron patterns on polymer surface. TEM analysis of spots showed embedding of the silver nanoparticles in the polymer, thus forming a local composite at submicron scale. More interestingly, by Raman analysis, an increase in the content of β -PVDF conformation in the region of resolidified spot was observed. This demonstrates local control over the conformation of the polymer. Another practical use of plasmonic heating was demonstrated by the repair/healing of cracks and defects. In a similar fashion, the uncoated PVDF fibers, which could survive the laser up to its maximum power, could be melted with a low power laser after receiving a silver coat. Since the thermal conduction decreases with system dimensionality,^[37] thus plasmonically generated heat would be more confined in nanofibers than in the films. Welding of two fibers together, after melting with thermoplasmonic heat, was demonstrated as a practical example. It was observed that the heat was sufficiently high to locally graphitize the polymer nanofibers.

4.2 Plasmon-Mediated Embedding of Nanoparticles in a Polymer Matrix: Nanocomposites Patterning, Writing, and Defect Healing

*Ahnaf Usman Zillohu, Ramzy Abdelaziz, Mehdi Keshavarz Hedayati, Thomas Emmeler, Shahin Homaeigohar, and Mady Elbahri **

Reprinted (adapted) with permission from *Journal of Physical Chemistry C*, **2012**, *116*, 17204. DOI:10.1021/jp3016358. Copyright (2012) American Chemical Society.

4.2.1 Introduction:

Plasmonics, as an emerging field, aims to exploit the unique optical properties of metallic nanostructures to enable routing and active manipulation of light on the nanoscale. Plasmonic heating is a phenomenon, which is recently recognized for its potential in photothermal therapy. Here we show the first proof-of-concept experiment based on plasmonic heating for selective and precise embedding of nanoparticles in a polymeric matrix. We demonstrate a unique way for in-situ fabrication of nanocomposites in different forms including patterning, writing, and defect healing in a controlled manner along with crystallinity control through light irradiation.

Plasmonics of the metal nanoparticles (NPs) has become the building block of a new generation of nanophotonic materials and devices with a myriad of applications ranging from waveguides (for confining and guiding electromagnetic energy at visible and near-infrared frequencies)^[38,39] to solar cells,^[40-42] transparent conductors,^[43,44] and biosensors.^[42,45] Metal NPs absorb and scatter light where the absorbed portion drives mobile charge carriers inside the NPs, and the energy gained by these carriers turns into heat, giving rise to novel phenomenon known as Plasmonic heating; a phenomenon that is recently recognized for its potential in cancer therapy^[46,47] and catalysis^[48]. Metallo-dielectric hybrids show numerous potential applications in areas ranging from catalysis^[49] and optics^[50] to electronics and biotechnology^[51]. Nanocomposites consisting of metal NPs embedded in a polymeric matrix are of particular interest because synergistic properties of their constituents give rise to novel applications.^[52] Whereas different physical and chemical synthesis routes of polymer-metal nanocomposites have been investigated,^[53,54] fabrication of nanocomposites using radiation is restricted to the photolysis^[55] under UV illumination, which is highly complex, time-consuming, expensive, and mainly causes a polymer degradation. We demonstrate a new plasmonic-based process that is not only capable of selective and precise embedding of NPs in a polymeric matrix to produce a nanoscale composite in intricate patterns but also can be used to heal/repair microdefects.

4.2.2 Results and discussion:

The as-sputtered metallic layer, as shown by AFM, consisted of separate and nonpercolating silver NPs, **Figure 4.2a**. The latter feature was proved after a conductivity measurement test (data not shown here). In terms of size, the NPs were mostly as large as 6–20 nm, **Figure 4.2b**.

It was observed that uncoated PVDF foil could survive the laser beam up to 100 mW before a softening or melting of the polymer subsurface could start. However, on the metalized foil, the heat generation by the plasmonic absorption was strong enough to premelt the polymer subsurface at only 2 mW power. Optical images of different patterns including simple 1D wire/line up to 2D closed loop, squares, or rectangle are shown in **Figure 4.3a (left)**. The AFM image, **Figure 4.3a (right)**, shows one of these patterns that is composed of a ~500 nm thick parallel-chains array.

Patterning was done using a spot-by-spot overlapping, but this could be done in a continuous mode if the instrument is capable of a real time display and control. Indeed, our process can even be utilized for controlled direct “Plasmonic Writing” of nanocomposites in more complicated shapes. **Figure 4.3b (top)** is an optical micrograph of the name of our group and our institutions, written with a 532 nm laser of 10 mW power on the silver-coated PVDF foil.

An AFM picture of the letter “S”, as an example, is shown in **Figure 4.3b (bottom right)** with confirmed embedding of the silver NPs in features of submicrometer size. High-magnification imaging with the aid of AFM, **Figure 4.3b (bottom left)**, revealed the embedding of the NPs in the melt pool of the polymer resulting in the formation of a nanocomposite. Regarding the effect of embedding, as seen in **Figure 4.3c**, the plasmonically embedded NPs induce a yellow color, whereas the nonexposed surrounding is reddish blue. Such an effect, observed in small spots, was expanded over a millimeter-sized area by joining thousands of spots (the inset picture in **Figure 4.4a, right**) and was subsequently examined with UV–Vis experiment. The results indicated a blue shift of the plasmonic response, which can be understood in terms of disruption of the plasmonic coupling “communication” between the NPs upon embedding and coating with the premelted polymer. A UV–Vis analysis of the silver coated polymer film in full spectral range showed that the plasmon resonance for our system was at ~500 nm, **Figure 4.4a (left)**. An increase in the plasmon frequency shown by a shift of absorption to a shorter wavelength (~420 nm) after embedment of the silver particles in the polymer supports the above mentioned observation, **Figure 4.4a (right)**.

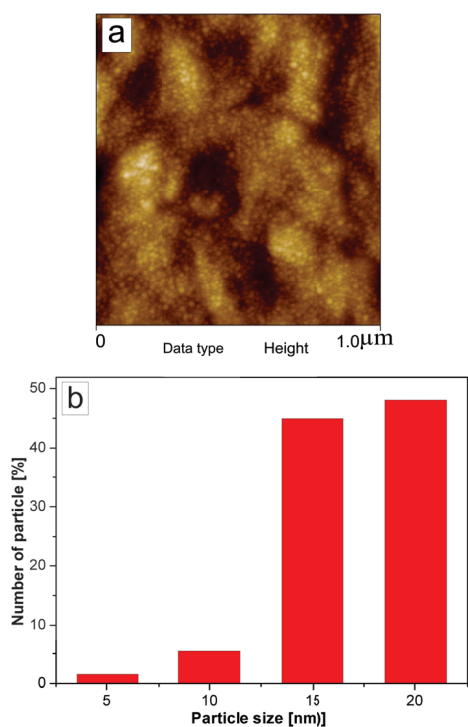


Figure 4.2 a) As sputtered silver on PVDF sheet-AFM height contrast, b) Histogram showing the size distribution of Ag nanoparticles deposited on the PVDF sheet.

The formation of nanocomposites is believed to be caused by softening and premelting of the subsurface layer of the polymer foil through a photon-thermal energy conversion process by the NPs. A large amount of heat can be accumulated by the NPs causing a dramatic temperature increase around them. Taking into account the fact that the surface of

polymers has physical properties that differ from those of the bulk material due to interfacial interaction and the effects of enhanced molecular dynamics at the surface,^[56,57] the temperature increase may be high enough to melt the subsurface of the polymer or at least bring it to premelting regime. Indeed, it was very difficult and challenging to measure the temperature increase at the surface of the NPs. At the same time, because of heat dissipation to the surrounding polymer, temperature calculation would not give a precise value. However, we calculated the temperature that originated from the particles, and the data were in agreement with the expected softening temperature of the polymer. The temperature increase is given by:^[58]

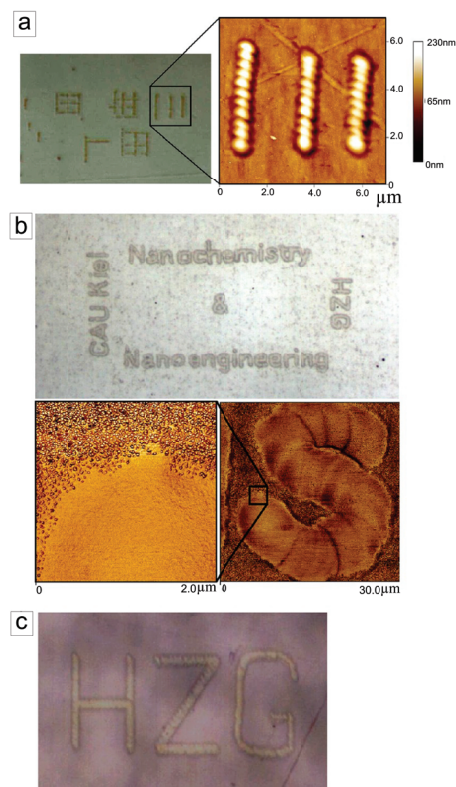


Figure 4.3 a) Optical micrograph (left) and AFM image (right) of the fine structures made on a silver coated PVDF film by exposing it to 532 nm laser at 2mW power. b) Names of our research group and institutes were patterned on the film with 532 nm laser at 10mW power (top). AFM image of the letter “S” (bottom right) with a further zoom on an area on the letter “S” (bottom left) showing complete embedment of the silver particles. c) “HZG” written by plasmonic heating. The blue shift in the plasmonic response of the particle after embedding in the polymer matrix is indicated by a change in color from reddish blue (surrounding) to yellow (the letters).

$$T_o = T_\infty + \frac{I_o K_{abs} r_o}{4k_\infty} [1 - \exp(-Bt)] \quad \text{Equation 4.10}$$

where T_o is the final temperature after exposure of NPs to light, T_∞ is the initial temperature (room temperature), I_o is the intensity of incident laser, K_{abs} is the absorption coefficient of NPs (which varies from ~ 0.8 for 6 nm particles to 2.5 for 20 nm particles^[59]), r_o is the size of NPs (radius), and k_∞ is the heat conductivity of PVDF (taken^[60] as 0.16 W/(mK)). In the **Equation 4.10**, the exponent term takes into consideration the exposure time for very short pulses and can be ignored for longer exposures, as is our case. The calculated final temperature when using a laser power of 0.2 mW ranged from 310 to 400 K depending on the particles size, which varied from 6 to 20 nm. This temperature was high enough to pre-melt the polymer because it was much higher than the lower glass transition but slightly below the melting temperature of PVDF, which was determined to be 433 K by DSC measurement (data not shown). The calculated temperature may only give an approximation as the exact temperature may vary depending upon particle size distribution, interparticle distance, and their mutual interaction, besides other factors.^[61,62]

The reduction in the high surface energy of NPs while they are coated with the polymer represents the driving force for the embedment. Once the particles are embedded, they reach a metastable state below the polymer surface where further movement slows down. This state corresponds to a minimum in free energy at a particle position just below the polymer surface, which results by the balance of two opposing forces, that is, long range van der Waals forces pulling the particles into the polymer and the entropic force pushing the particles back toward the surface.^[53,63] TEM analysis was used to prove the embedding process. Cross-sectional view by TEM, **Figure 4.4b**, showed that the particles exist at the interface. It is worth mentioning here that

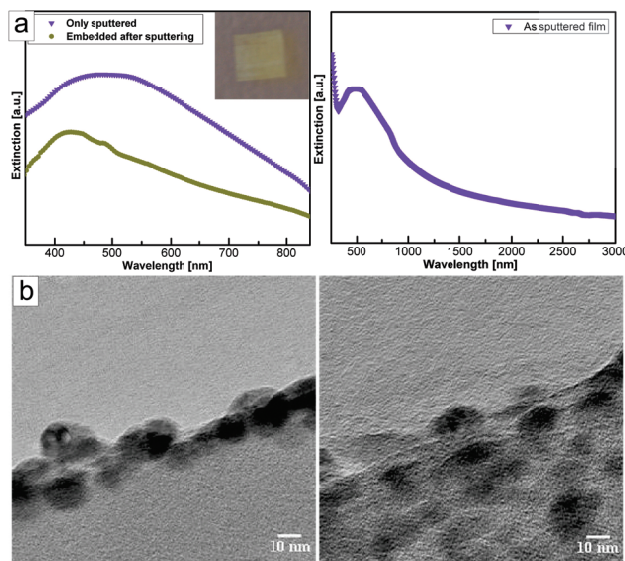


Figure 4.4 a) UV-Vis spectrum (full spectral range) of PVDF film sputter coated with 3 nm silver (left graph). A close view of UV-Vis spectrum in the plasmon spectral range for a comparison before (purple line) and after (green line) embedment of silver particles into the polymer (right graph). The inset picture shows the nanoparticle embedded area surrounded by the nonembedded one. b) Cross section of PVDF foil before (left) and after (right) exposure to laser (TEM image).

in this view the particles look very close to each other because the image is the 2D superposition of NPs in a 3D structure. Indeed, the polycrystalline NPs did not change their crystallinity upon embedding. The ability to control the spot size of nanocomposite is important because it determines the fineness of the final shape. Highly defined and localized nanocomposite spots of different sizes could be fabricated by adjusting the laser power, laser wavelength, and exposure time, as shown in **Figure 4.5**. Other factors like particle size, polymer crystallinity, magnification of the Raman microscope objective, and so on also affect the size of the nanocomposite spot, but they will not be considered in this stage. The effect of laser power is self-evident, and the size of the nanocomposite spot increases with increasing power of the incident laser.

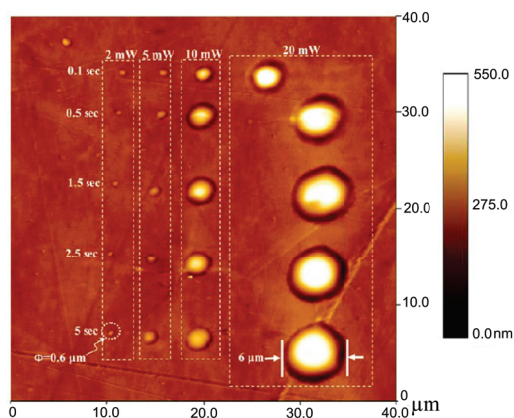


Figure 4.5 Spots made on the silver coated PVDF film with 532 nm laser, with different power and exposure time (AFM height profile).

It is shown in AFM image, **Figure 4.5**, where the nanocomposite spot size changes from ~ 0.6 to ~ 6 μm for laser power increase from 2 to 20 mW, keeping all of the other conditions constant (i.e., 5 s exposure with 532 nm laser). The exposure time for which the coated polymer surface is exposed to laser naturally should increase the size of the nanocomposite spot but only to the point when all surface particles are embedded in the softened polymer. This is why we could only notice appreciable change in spot size for a very small change in exposure time, that is, from 0.1 to 1.5 s exposure, after which there was no significant change in the resulting nanocomposite spot size even if the exposure time was increased to 5 s, **Figure 4.5**. It is worth mentioning here that the wavelength of the laser also plays an important role in controlling the size, crystallinity, and so on of the nanocomposite spots produced. For instance, to increase local temperature to the softening point of the polymer even at lower laser power, a coupling between the plasmon resonance of the NPs and the wavelength of applied laser is required. As previously discussed, our system of silver-coated PVDF foil had a plasmon resonance at ~ 500 nm, **Figure 4.4a (left)**. Consequently, green laser with 532 nm wavelength should have better coupling/heating response than the red laser with 785 nm wavelength.

To explore that, we did the same experiment using 785 nm laser. Indeed no spots were observed until a power of 25 mW was applied using the red laser. However, 532 nm laser could make spots even at 2 mW power. Local control and tuning of polymer

crystallinity is a concept that could open a new way for controlling properties. High magnification imaging by AFM, of a spot made by a green laser at a higher power (10 mW), showed a local recrystallization of polymer, **Figure 4.6a (left)**. A magnified view of the surface of the same spot shows the formation of fine structure, **Figure 4.6a (right)**. It turned out that the generated heat

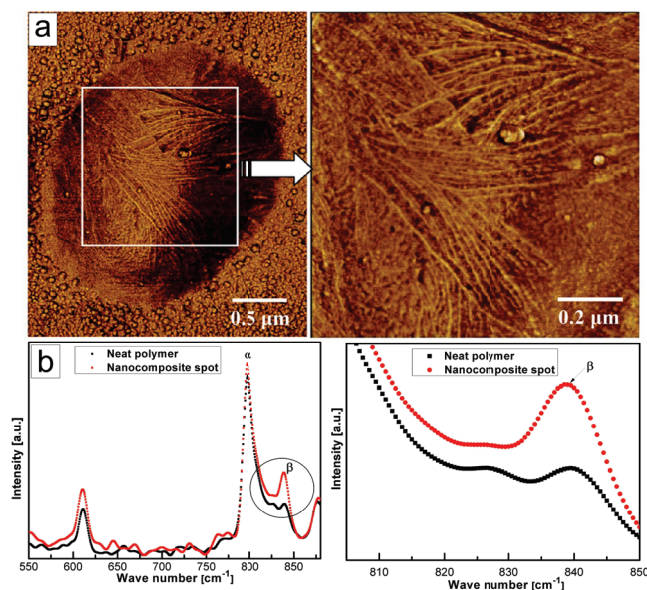


Figure 4.6 a) AFM image of a spot made with 532 nm laser of 10 mW power. The exposure time was 2.5 s. The right-hand side picture is the magnified view of the marked area in the left-hand side picture. b) Raman analysis taken on the neat PVDF film and on the nanocomposite spot made by plasmon heating. Right side graph is the magnified view of the area encircled in the left side graph.

was high enough to melt the polymer subsurface as it is expected from the **Equation 4.10** theoretically. Raman spectroscopy is a sensitive technique to determine changes in molecular conformation and crystal structure of polymers. As shown in **Figure 4.6b**, the Raman analysis of the nanocomposite spot is compared with that of a neat PVDF sheet. It is noteworthy that the analysis was done using a 785 nm laser at 10 mW power, which as previously mentioned had no adverse effect on the spot. A close view at the spectral range between 800 and 850 cm^{-1} is shown in **Figure 4.6b (right)**. An enhancement in the signal at $\sim 840 \text{ cm}^{-1}$ (corresponding to β -phase^[64]) compared with that at 796 cm^{-1} (for α -phase^[64]) indicates that the conformation of PVDF in nanocomposite spot was richer in the β -phase. Our finding demonstrates a local recrystallization along with a generation of β -phase known for its pyro- and piezoelectric properties.^[65] A detailed study of the interplay of several variables on the crystallinity is beyond the scope of the current paper and will be illustrated in a subsequent publication.

A unique feature of our method is that the effect is localized only to the exposed area. Therefore, we can make use of it to repair submicrometer sized defects (cracks, scratches or holes etc.) on the polymer surface by melting only the affected area with much lower laser power input. Cracking is detrimental to the structural integrity of reinforced polymers and can also lead to electrical failure in polymeric microelectronic components.^[66] Heating a polymer above its glass transition temperature (T_g) might be one of the approaches to heal cracks in it. However this approach is neither local nor selective.

We demonstrate here, a plasmonic healing approach to repair defects in polymer in a selective and controlled manner. As previously mentioned the spot size can be controlled by choosing proper parameters; here we choose the spot size according to the size of the defect to be repaired. **Figure 4.7a** demonstrates how one can repair a crack by plasmon-assisted melting. First, a micro fissure was made in the metalized polymer sheet with the help of an AFM tip to simulate a real micro crack. The defect area was then exposed to 532 nm laser at different powers to determine the appropriate power that can produce a melt zone wide enough to cover the crack. It is evident that the spots made with 20 and 10 mW laser power were too big for the purpose, whereas the 2 mW spot (not shown) was insufficiently small. The spot made at 5 mW power was found to be just the right size to fill the void made by crack. The AFM height profile across the crack and the repaired region shows complete filling of the defect, **Figure 4.7b**. A 3D view^[67] taken with AFM elucidates this concept as filling of the crevice with softened polymer is visible, **Figure 4.7c**. The crack was repaired by making numerous overlapping spots over its length, as shown in **Figure 4.7d**.

4.2.3 Conclusion:

In summary, we introduced a novel approach for the fabrication of a “metal-polymer hybrid” utilizing the plasmonic effect for embedding the NPs in a polymeric matrix. Our method demonstrates a quick and efficient

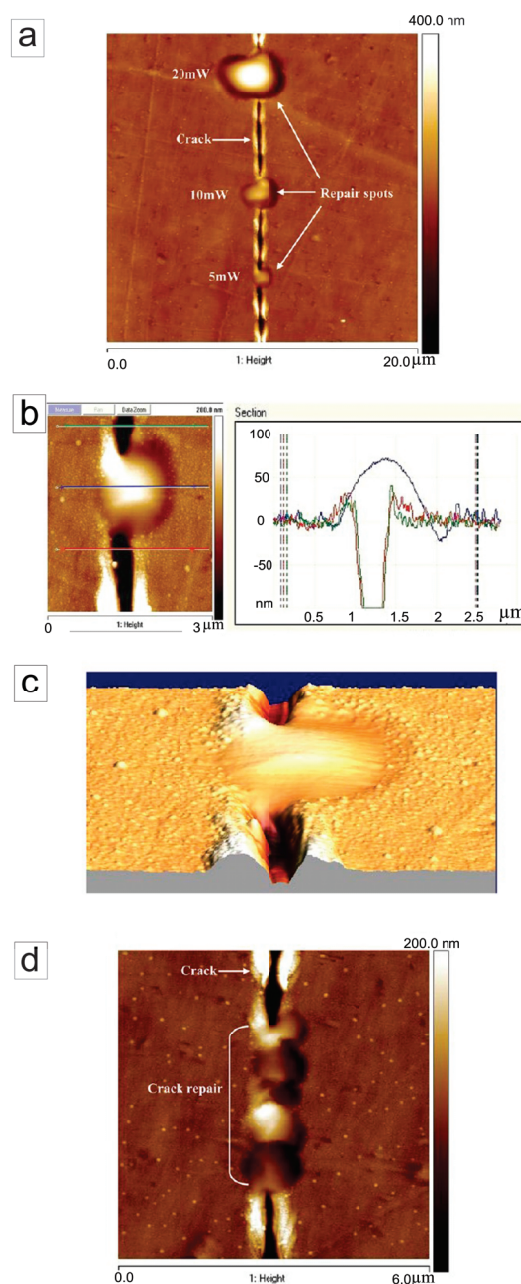


Figure 4.7 a) A crack was simulated by forming a deep scratch, on the silver coated PVDF film, with AFM tip. “Repair spots” were then made by plasmonic melting with 532 nm laser using different laser-powers to determine optimum spot size to fill the crack completely. Picture made with AFM (height contrast). b) AFM height profile across the scratch (red and green line) shows a deep crack. This crack was then filled by making a spot on the crack area. c) 3D view for the concept of crack repair where the softened material fills in the crevice (AFM height profile). d) Multiple overlapping spots made by 532 nm laser using 5 mW power were made to fill in the crack.

way of patterning, writing, and defect healing using light. Selective and localized embedding of NPs in the metalized polymer is expected to open a new route of designing microdevices, for instance, a waveguide or a novel capacitor. A part of these approaches is currently under investigation in our laboratory.

4.2.4 Experiments:

A polyvinylidene fluoride (PVDF) film of thickness 0.05 mm was purchased from Good Fellow Company and used without treatment. It was coated with a 3 nm thick layer of silver with a sputter coater. The sputtering rate was 10 nm/min, and the applied power was 20 W. Its optical absorption behavior was characterized by UV–Vis/IR spectrometer (Lambda 900). Selective embedding (due to plasmonic heating) together with nanocomposite patterning in a lithographic fashion was performed by exposing the coated surface to 532 nm laser beam in Senterra confocal Raman microscope through 100× magnification objective. The spot size of laser through this objective was $\sim 0.8 \mu\text{m}^2$. The Raman microscope was equipped with two types of lasers, that is, red laser (wavelength 785 nm, power range 1–100 mW) and green laser (532 nm, power range 0.2–20 mW). The same microscope was used for determination of any changes in polymer conformation after exposure to plasmonic heat. Plasmon spots were characterized by Veeco Nanoscope IV Multimode atomic force microscope (AFM) and FEI/Philips Tecnai F30 G2 transmission electron microscope (TEM).

4.2.5 Acknowledgements:

We acknowledge the partial financial support through SFB677 funded by the German Research Foundation (DFG) and Deutscher Akademischer Austausch Dienst (DAAD). M.E. thanks The Initiative and Networking Fund of the Helmholtz Association for providing the financial base for the startup of his research group. We would like to thank Prof. Dr. Lorenz Kienle for TEM measurement and Sabrina Bolmer for AFM pictures.

Plasmonic heating of nanofibers:

One of the big advantages of plasmonic heating is that it is contained in a local area and consequently has a minimal collateral damage. That is why it has potential applications in local catalysis and chemistry, tumor treatment and even local melting/welding of tiny objects including electrospun nanofibers. Welding of polymer fibers with ‘embedded’ gold and silver nanoparticles has already been shown,^[68] but the work presented next, systematically explores the effect of silver coating thickness on the absorption and also shows the effects of heat on the local chemistry of the fibers. It is found by UV-Vis spectroscopy and SEM analysis, that as silver particles approach each other due to growth of film thickness, not only there is a broadening and red shift in their plasmon wavelength but also there is an increase in absorption until at a certain film thickness, the enhancement of the electric field confined between them becomes very strong with associated intense thermoplasmonic heat. This results not only in melting and welding of fibers but also in local graphitization. The graphitized fibers find use as electrodes in super capacitors or in hydrogen storage systems etc.

4.3 Thermo-Plasmonics for Localized Graphitization and Welding of Polymeric Nanofibers

*Ahnaf Usman Zillohu, Nisreen Alissawi, Ramzy Abdelaziz and Mady Elbahri**

Published paper: *Materials* **2014**, 7, 323. DOI:10.3390/ma7010323

4.3.1 Introduction:

There is a growing interest in modulating the temperature under the illumination of light. As a heat source, metal nanoparticles (NPs) have played an important role to pave the way for a new branch of plasmonics, i.e., thermo-plasmonics. While thermo-plasmonics have been well established in photo-thermal therapy, it has received comparatively less attention in materials science and chemistry. Here, we demonstrate the first proof of concept experiment of local chemistry and graphitization of metalized polymeric nanofibers through thermo-plasmonic effect. In particular, by tuning the plasmonic absorption of the nanohybrid through a change in the thickness of the deposited silver film on the fibers, the thermo-plasmonic effect can be adjusted in such a way that high enough temperature is generated enabling local welding and graphitization of the polymeric nanofibers.

The use of plasmonic heat in medical therapy is well established and a variety of applications of this phenomenon have already been studied and reviewed,^[69] including targeted hyperthermia, destruction of tumor cells and drug release. In materials science, although its effectiveness has been shown by various applications ranging from catalysis,^[70] to preparation of transparent conductors for solar cells,^[71] or fabrication of sensors based on surface enhanced Raman,^[72] but its full potential still remains to be explored.

The properties of nanohybrids can be tailored by controlling the chemical composition, size, shape as well as the volume fraction and the distribution of the nanoscale particles.^[73,74] Interaction of light with NPs results in its absorption and scattering, where absorption dominates scattering for a particles size smaller than 100 nm.^[75] The light absorption increases with increasing particle size by a power of three and is given by:^[75]

$$\sigma_{abs} = \frac{\pi^2}{\lambda} R^3 \text{Im}\left\{(\epsilon_p - \epsilon_s) / (\epsilon_p + 2\epsilon_s)\right\} \quad \text{Equation 4.11}$$

where σ_{abs} is the absorption cross-section and R is radius of the NPs; ϵ_p and ϵ_s are the wavelength dependent complex dielectric function of metal NPs and the surrounding matrix respectively. The light is absorbed by NPs in the form of coherent oscillations of their electrons. These oscillations, called plasmons, can be of propagating nature as in the case of

thin films, or confined to individual NPs or clusters. The dissipation of these oscillations results in heating of NPs and their surrounding environment. Plasmonic heat generation by pulsed laser (usually nano to femtosecond pulse widths) irradiation has been well studied.^[76-78] The physical picture that arises from these studies showed that, because of low optical quantum yield of metallic NPs, the total heat generated can be roughly equated to the optical energy absorbed. The energy absorbed by the electrons puts the electron gas into non-Fermi electron distribution which thermalizes to equilibrium by electron-electron scattering. At this stage the electron gas may have a temperature of up to several thousand kelvin. The electron gas then cools by electron-phonon coupling with the NP lattice. The NP then cools by heat dissipation to the surrounding matrix through phonon-phonon interaction. Heat transfer equations that govern the temperature T of a sphere and its surroundings are.^[79,80]

$$\frac{\partial T_p}{\partial t} = \frac{\alpha_p}{r} \frac{\partial^2}{\partial r^2} [rT_p(r, t)] \quad \text{Equation 4.12}$$

$$\frac{\partial T_s}{\partial t} = \frac{\alpha_s}{r} \frac{\partial^2}{\partial r^2} [rT_s(r, t)] \quad \text{Equation 4.13}$$

where the subscript p refers to the particles, s refers to their surrounding, α is the thermal diffusivity of the particle or the surroundings and r is the distance away from the center of the nanoparticle. In fact α is related to thermal conductivity k , by the relation, $\alpha = k/\rho C_p$ where ρ and C_p are density and specific heat capacity, respectively. The **Equations 4.12** and **4.13** were coupled with Maxwell's equations and numerically solved^[81] to show that in the steady state regime, the local temperature rise, $\Delta T(r)$, around a single NP is described by the following equation:

$$\Delta T(r) = \frac{V_p Q}{4\pi k_s r} \quad \text{Equation 4.14}$$

where k_s is the thermal conductivity of the surrounding medium, V_p is the volume of the NP and Q is the heat generated in the nanoparticles. Note that **Equation 4.14** is applicable only in case where the distance r is greater than radius of the NP. If the incident light wavelength is much larger than the radius of the NP then the heat generation would be:^[82]

$$Q = \frac{\omega}{8\pi} E_0^2 \left| \frac{3\epsilon_s}{2\epsilon_s + \epsilon_p} \right|^2 \text{Im} \epsilon_p \quad \text{Equation 4.15}$$

Here E_0 is the amplitude of incident radiation and ω is its angular frequency, ϵ_s is the dielectric constant of the surrounding environment of NP and ϵ_p and $\text{Im} \epsilon_p$ are the real and the imaginary parts of the dielectric constant of the NP, respectively. From **Equations 4.11** and

4.15, it is evident that by tuning the particle size and absorption coefficient (which depends on the type of metal), the total light absorption and its conversion to heat can be controlled. The temperature rise of the surrounding not only depends upon Q but also on V_p , as shown in **Equation 4.14**, and thus we expect from a bigger particle to raise the temperature of its surrounding to a higher level than a smaller particle would do. The generated heat can be high enough to cause melting or even decomposition of the surrounding. Since the energy from the incident light is confined to individual NPs therefore the heating effect is also localized to their near vicinity. This not only eliminates the danger of collateral damage by undesired heating but in fact is useful in physical and chemical re-structuring and patterning of matter at submicron scale.^[83-85] Recently we introduced the possibility of NPs incorporation into a polymer film upon low energy laser irradiation to fabricate a metal-polymer nanocomposite.^[85] We showed that selective and precise embedding of Ag NPs in Polyvinylidene fluoride (PVDF) polymeric matrix can be carried out for *in-situ* fabrication of nanocomposites in different forms. That included controlled patterning, writing, defect healing and welding in a controlled manner along with crystallinity control through light irradiation. Indeed, the silver NPs were activated using laser irradiation of only 2–10 mW, causing absorption of photons and the transfer of resulting heat from the NPs to the surrounding polymer matrix. The local heating disrupted the polymer matrix and allowed softening and pre-melting of the subsurface layer of the polymer foil with resulting embedment of Ag NPs in it. Here we introduce our recent progress with the thermo-plasmonics, demonstrating the first experimental proof of light induced local heating and graphitization of polymer-fibers decorated with Ag NPs. PVDF is known for its piezoelectric properties besides high chemical stability and good mechanical properties. Graphitization of PVDF electrospun mats have earlier been demonstrated by conventional heating (800 °C to 1800 °C) in the presence of iron(III) acetylacetonate catalyst.^[86] Graphitized nanofibers are a potential candidate for hydrogen storage^[86] or as electrodes for supercapacitors,^[87] to name a few applications. In this work PVDF electrospun nanofibers were sputter coated with silver NPs and subsequently exposed to laser in a Raman microscope. Graphitization of polymer nanofibers using thermo-plasmonic concept requires significant increase in the temperature of NPs sputtered over them. By tuning the size, shape and interparticle distance, we expect a huge quantity of heat to be generated by the NPs. We demonstrate that the temperature rise is actually high enough to weld the fibers together and even to graphitize the polymer. The novelty of the work presented here is that individual fiber can be graphitized “locally” by plasmonically generated heat.

4.3.2 Results and Discussion:

Electrospinning is a fast and easy method of producing fibers from a variety of polymer solutions. For beadless, uniform fibers it is important to have a solution of sufficiently high viscosity. The PVDF grade used for electrospinning in the present study gives a high viscosity solution of up to 8000 cps.^[88] Moreover, N,N-Dimethylformamide (DMF) was used as the solvent, which has a high dipole moment^[89] of 3.8 Debye and high conductivity^[89] of around 10.9 $\mu\text{S}/\text{cm}$ which improves charge carrying capacity of the jet. As a result, a thin mat of uniform, beadless fibers in submicron size was collected. The fibers were then sputter coated with silver to various layer thickness. Regarding the distribution of silver nanoparticles on the fibers, with the help of scanning electron microscope (SEM), it was found that the NPs almost completely filled the surface and generated a hierarchical structure on top of the fibers, **Figure 4.8**. Obviously, the smallest particles of silver were

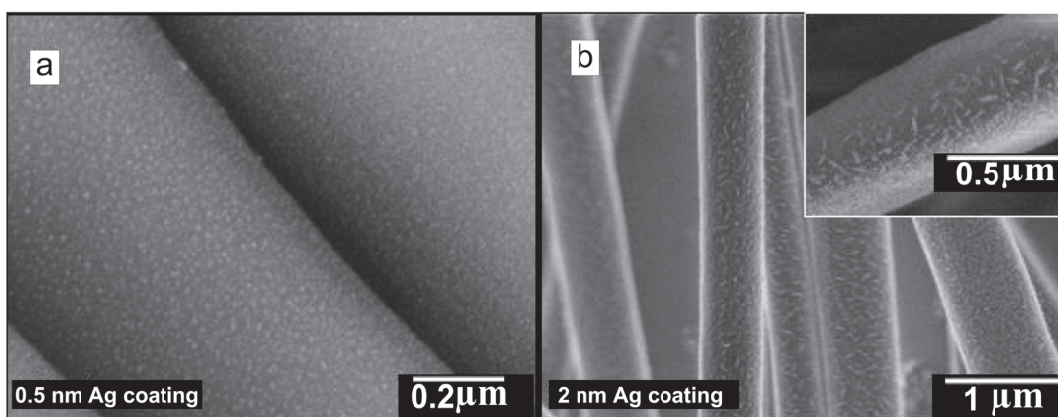


Figure 4.8 Variation of silver nanoparticles' shape and size with increasing sputtering thickness (white particles on darker fibers). **a)** 0.5 nm thick silver coating resulted in isolated round particles; **b)** 2 nm thick coating resulted in elongated agglomerates (inset is a closer view). The micrographs were made by mixing the signal from backscattered electron and secondary electron detectors.

observed for 0.5 nm thick coating and were about 12 nm in size and spherical in shape, **Figure 4.8**. With increasing coating thickness, not only that the particles' size increased but they also got elongated because of joining of incoming neighboring particles. This resulted in a vast size distribution for 2 nm thick coating and up; ranging from small spherical particles to elongated particles with longer axis as big as 150 nm, **Figure 4.8**.

The change in silver coating thickness and a corresponding change in particle size, shape and the inter-particle distance, effects the plasmon resonance wavelength of the system. The plasmon resonance wavelength associated with NPs increases with their size due to retardation effect.^[90,91] This is evident in the UV-Vis results (**Figure 4.9**), where the increase in layer thickness from 0.5 to 1 nm not only increased the extinction maxima but the maxima also shifted to the longer wavelength.

This red shift stems not only from the size increase but also from near field coupling^[92,93] of growing NPs, as they approach each other. By the SEM observation (**Figure 4.8**), it was found that for 2 nm coating thickness (and beyond) the NPs start to touch each other with consequent elongation in overall shape. The elongation of the NPs also results in further red shift^[94] but more interestingly we observe multimode plasmon (plasmon splitting) and extinction in the near IR range. By adding more Ag up to 4 nm, a

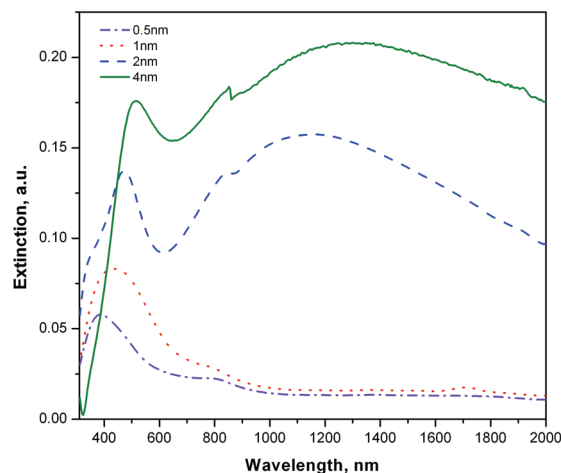


Figure 4.9 UV-Vis spectrum of “polyvinylidene fluoride (PVDF) fiber-Ag composite” with increasing thickness of silver coat (0.5 to 4 nm).

red shift for both peaks (visible and NIR) along with broadening was observed. The appearance of multimode plasmon can be associated to the hybridization of individual plasmon mode as the approaching nanoparticles enter from dielectric proximity to conductively coupled regime.^[95] Presence of a super strong concentration of electric field at the point joining two NPs has been already shown by Atay *et al.*^[95] Indeed, the dissipation of this field into lattice phonons is expected to result in a huge local heat, as mentioned previously. To examine this hypothesis we exposed the fibers to green laser (532 nm wavelength) of 20 mW power, in the Raman microscope. In the case of uncoated fibers, no melting or decomposition was observed, as shown by the optical micrograph in **Figure 4.10a**. Here, it is clear that the portion of the fiber that was exposed to the laser showed no signs of melting/graphitization. However, in the case of fibers with 2 nm thick silver coating, the junction point melted and fused the fibers together, on exposure to the laser, **Figure 4.10b**. This indicates that the plasmonic heat generated by silver nanoparticles was much higher than the melting point of the polymer, which is around 172 °C.^[88] Interestingly, the “joint” also showed blackening which turned out to be local graphitization as seen by the Raman analysis, **Figure 4.11**. The Raman signal scattered by uncoated fibers clearly showed the presence of PVDF as depicted by its finger print peaks at 795 cm⁻¹ for alpha conformation and 839 cm⁻¹ corresponding to beta conformation^[96], **Figure 4.11a**. It is worth noting that there was no evidence of graphitic structure in the Raman spectrum of uncoated fibers. This was supported by the visual observation mentioned above, that the uncoated fibers could sustain laser without melting or graphitization.

With increasing thickness of silver coating, an enhancement in the Raman signal was observed meaning stronger interaction of light with the system, **Figure 4.11a**. This was in accordance with that observed in the UV-Vis analysis (**Figure 4.9**), where an overall increase in absorption of light, including that in the wavelength region of the green laser, was observed with increasing thickness of the silver coating. More importantly, the Raman signal scattered by the fibers coated with 0.5 and 1 nm silver, still confirmed the integrity of the chemical structure of polymer as seen by the presence of peaks corresponding to α and β phase of PVDF.

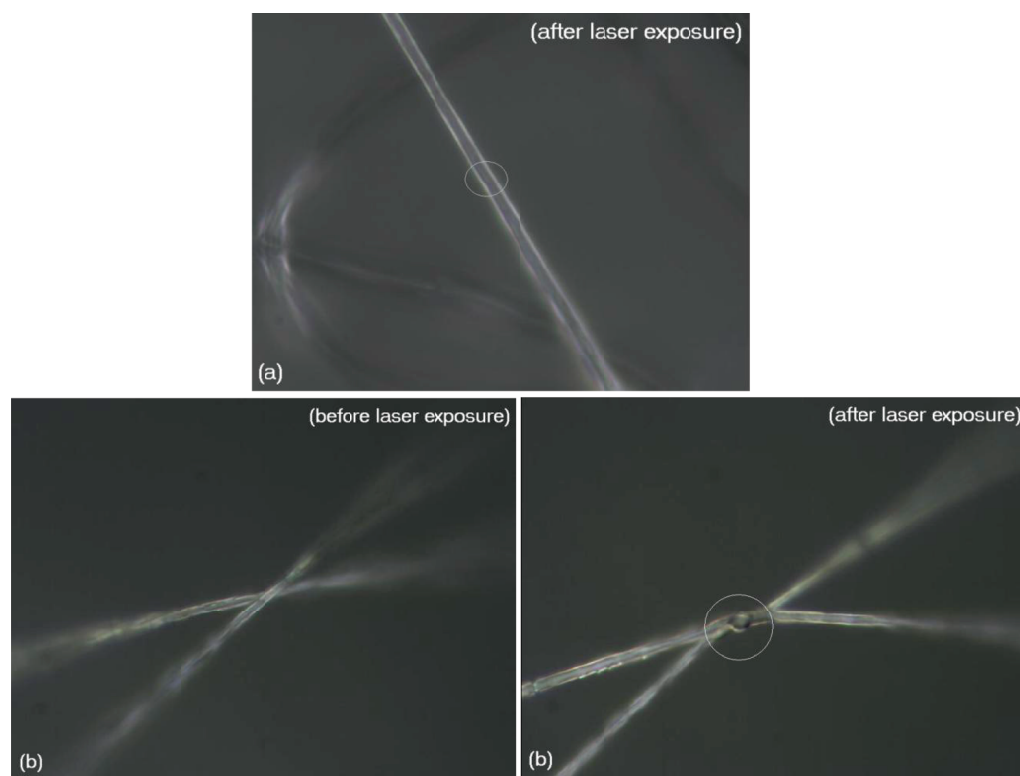


Figure 4.10 Effect of 532 nm, 20 mW laser on fibers. **a)** Uncoated fibers showed no melting on exposure to laser (encircled area); **b)** Fibers coated with 2 nm Ag showed welding/graphitization on exposure to laser.

On the other hand, two additional peaks also appeared, belonging to D and G bands of graphite^[88,97,98] at 1368 cm^{-1} and 1580 cm^{-1} respectively, **Figure 4.11b**. The intensity of these bands got stronger in the case of 2 nm and 4 nm silver coating and indeed, the PVDF peaks diminished and were replaced by strong graphite peaks indicating a complete graphitization of the polymer. Raman analysis during graphitization with 20 mW laser and its reanalysis with a lower power laser (0.2 mW) shows persistent presence of graphite and absence of PVDF, indicating a permanent conversion (data not shown). While this finding is the main scientific message in this communication, we believe that work is still needed to

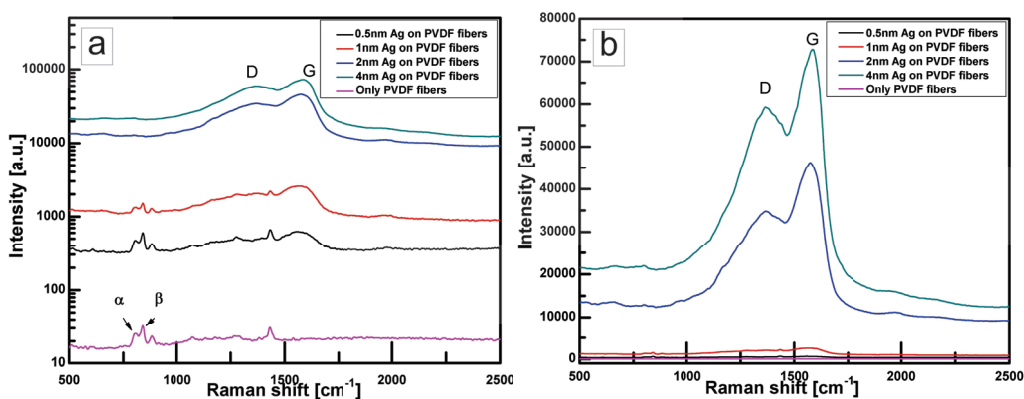


Figure 4.11 a) Raman spectrum of “PVDF fiber-silver NPs” composite with different silver layer thickness (0.5 to 4 nm). b) Same data as in (a), but plotted on “linear” scale to highlight the presence of D and G bands.

explore the chemical transformation as well as the actual temperature rise, which is not a simple task. Nevertheless, we believe that our finding of “thermo-plasmonic based local graphitization” serves only as an example and would open a new avenue in the possibilities of local chemistry and structural control. The applications of such a polymer-graphite hybrid would be diverse, for example, it can be conductive for electrical contacts over a part of its length while piezoelectric over the rest of the length.

4.3.3 Conclusion:

Electrospun PVDF fibers were sputter coated with silver to different film thicknesses ranging from 0.5 to 4 nm. SEM and UV-Vis analysis showed that with increasing coating thickness there was an increase in plasmonic absorption and a red shift in extinction maxima. The heating effect of thermo-plasmonic increased with increasing coating thickness and was ultimately sufficient for a complete local conversion of the polymeric fiber to graphitic fiber.

4.3.4 Experiments:

PVDF (Kynar HSV 900, Arkema Inc., Pennsylvania, PA, USA) solution for electrospinning was prepared by dissolving 11 wt% PVDF in N,N-Dimethylformamide (DMF) (Sigma-Aldrich, Steinheim, Germany). The solution was then pushed through a needle that had 0.8 mm orifice diameter. A target plate, that was covered with glass slides was placed at a distance of 15 cm from the needle and served as collector. The needle was attached to a high voltage (15 kV) supply and target plate was attached to ground potential. As a result of electrostatic force, the polymer coming out of the needle was accelerated and stretched in the form of nanofibers which were collected on the target plate. These fibers were then coated with silver to a thickness of 0.5 nm, 1 nm, 2 nm and 4 nm by physical vapor deposition process, the thickness being controlled with the help of a quartz microbalance. The UV-Vis characterization of the coated fibers was done with “Lambda 900” UV-Vis/IR spectroscope (PerkinElmer, Rodgau, Germany) by normalizing the background to uncoated

PVDF fibers. Raman analysis and welding/graphitization was performed on Bruker confocal Raman microscope (Bruker Optik GmbH, Ettlingen, Germany) equipped with 532 nm continuous wave laser. SEM imaging of the silver coated fibers was performed on LEO Gemini 1550 VP from Zeiss with field emission cathode (Carl Zeiss Microscopy GmbH, Oberkochen, Germany).

4.3.5 Acknowledgments:

We acknowledge the partial financial support by German Academic Exchange Service (DAAD) and also by German Research Foundation (DFG) through SFB677 C9. M.E. thanks the Initiative and Networking Fund of the Helmholtz Association for providing the financial base to start his research group.

4.3.6 References:

- [1] P. P. Edwards and J. M. Thomas, *Angewandte Chemie International Edition* **2007**, *46*, 5480.
- [2] G. Mie, *Ann. Phys.* **1908**, *25*, 377.
- [3] R. H. Ritchie, *Phys. Rev.* **1957**, *106*, 874.
- [4] S. A. Maier and H. A. Atwater, *Journal of Applied physics* **2005**, *98*, 011101.
- [5] H. Ibach, *Physics of surfaces and interfaces*, Springer **2006**.
- [6] V. K. Khanna, *Nanosensors: Physical, chemical, and biological*, Taylor & Francis **2011**.
- [7] S. A. Maier, *Plasmonics: Fundamentals and applications: Fundamentals and applications*, Springer **2007**.
- [8] A. Biswas, T. Wang and A. S. Biris, *Nanoscale* **2010**, *2*, 1560.
- [9] S. Link and M. A. El-Sayed, *The Journal of Physical Chemistry B* **1999**, *103*, 8410.
- [10] W. A. Murray and W. L. Barnes, *Advanced materials* **2007**, *19*, 3771.
- [11] K.-S. Lee and M. A. El-Sayed, *The Journal of Physical Chemistry B* **2006**, *110*, 19220.
- [12] S. Underwood and P. Mulvaney, *Langmuir* **1994**, *10*, 3427.
- [13] D. D. Evanoff and G. Chumanov, *ChemPhysChem* **2005**, *6*, 1221.
- [14] V. I. Klimov, *Semiconductor and metal nanocrystals: Synthesis and electronic and optical properties*, Taylor & Francis **2003**.
- [15] A. Cusano, *et al.*, *Optochemical nanosensors*, Taylor & Francis **2012**.
- [16] K. Kneipp and H. Kneipp, *Frontiers of Surface-Enhanced Raman Scattering: Single Nanoparticles and Single Cells* **2014**, *19*.
- [17] H. Lu, *et al.*, *Optik-International Journal for Light and Electron Optics* **2014**, *125*, 3355.
- [18] S. Chang *et al.*, *Advanced Functional Materials* **2014**, *24*, 3482.
- [19] L. Meng *et al.*, *Optics letters* **2014**, *39*, 1137.
- [20] M. E. Nasir *et al.*, *Advanced materials* **2014**, *26*, 3532.
- [21] K. Yao *et al.*, *Advanced Energy Materials*, DOI: 10.1002/aenm.201400206.
- [22] R. Rodríguez-Oliveros and J. A. Sánchez-Gil, *Optics express* **2012**, *20*, 621.
- [23] M. Zhu *et al.*, *ACS nano* **2012**, *6*, 7227.
- [24] C. Vázquez-Vázquez *et al.*, *Journal of the American Chemical Society* **2013**, *135*, 13616.
- [25] S. Link and M. A. El-Sayed, *Annual Review of Physical Chemistry* **2003**, *54*, 331.
- [26] E. Dulkeith *et al.*, *Physical Review B* **2004**, *70*, 205424.
- [27] C.-K. Sun *et al.*, *Physical Review B* **1994**, *50*, 15337.

- [28] J. H. Hodak, A. Henglein and G. V. Hartland, *The Journal of Physical Chemistry B* **2000**, *104*, 9954.
- [29] M. Malicki, Gold nanoparticles – surface plasmon resonance, http://photonicswiki.org/index.php?title=Gold_Nanoparticles_%E2%80%93_Surface_Plasmon_Resonance, accessed: 07, 2014.
- [30] A. O. Govorov and H. H. Richardson, *Nano Today* **2007**, *2*, 30.
- [31] A. O. Govorov *et al.*, *Nanoscale Research Letters* **2006**, *1*, 84.
- [32] J. R. Dunklin *et al.*, *ACS applied materials & interfaces* **2013**, *5*, 8457.
- [33] Y. Tsuboi Plasmonic optical tweezers can form characteristic micropatterns, <http://spie.org/x92338.xml>, accessed: 07, 2014.
- [34] O. Neumann *et al.*, *ACS nano* **2012**, *7*, 42.
- [35] G. Baffou and R. Quidant, *Chemical Society Reviews* **2014**, *43*, 3898.
- [36] Z. Liu *et al.*, *Nano Letters* **2011**, *11*, 1111.
- [37] Bharat Bhushan, *Springer Handbook of Nanotechnology*, Springer Science and Business Media, **2007**.
- [38] S. A. Maier, *IEEE Journal of selected topics in quantum electronics* **2006**, *12*, 1214.
- [39] M. K. Hedayati *et al.*, *Advanced Materials* **2011**, *23*, 5410.
- [40] H. A. Atwater and A. Polman, *Nature Materials* **2010**, *9*, 205.
- [41] K. Nakayama, K. Tanabe and H. A. Atwater, *Applied Physics Letters* **2008**, *93*, 121904.
- [42] W. A. Murray and W. L. Barnes, *Advanced Materials* **2007**, *19*, 3771.
- [43] M. Elbahri *et al.*, *Advanced Materials* **2011**, *23*, 1993.
- [44] M. Jamali *et al.*, *Advanced Materials* **2011**, *23*, 4243.
- [45] C.J. Murphy *et al.*, *Journal of Physical Chemistry B* **2005**, *109*, 13857.
- [46] P. K. Jain *et al.*, *Plasmonics* **2007**, *2*, 107.
- [47] C. Loo *et al.*, *Nano Letters* **2005**, *5*, 709.
- [48] J.R. Adleman *et al.*, *Nano Letters* **2009**, *9*, 4417.
- [49] I. Pastoriza - Santos *et al.*, *Chemistry–An Asian Journal* **2006**, *1*, 730.
- [50] M. Scalora *et al.*, *Journal of Applied Physics* **1998**, *83*, 2377.
- [51] D. Pissuwan, S.M. Valenzuela and M. B. Cortie, *Trends in Biotechnology* **2006**, *24*, 62.
- [52] G.V. Ramesh, S. Porel and T. P. Radhakrishnan, *Chemical Society Review* **2009**, *38*, 2646.
- [53] F. Faupel *et al.*, *Advanced Engineering Materials* **2010**, *12*, 1177.
- [54] C. Pakula *et al.*, *Nanotechnology* **2010**, *21*, 465201.
- [55] A. D. Pomogaïlo and V. N. Kestel'man, *Metallopolymer nanocomposites*, Springer Verlag Berlin **2005**.
- [56] A. M. Mayes, *Macromolecules* **1994**, *27*, 3114.
- [57] J. Baschnagel and K. Binder, *Macromolecules* **1995**, *28*, 6808.
- [58] V. K. Pustovalov, *Chemical physics* **2005**, *308*, 103.
- [59] V. K. Pustovalov, *Chemical Physics Letters* **2006**, *421*, 142.
- [60] B. Bonno, J. L. Laporte and R. T. d'Leon, *Measurement Science and Technology* **2001**, *12*, 671.
- [61] A. O. Govorov and H. H. Richardson, *Nano Today* **2007**, *2*, 30.
- [62] A. O. Govorov *et al.*, *Nanoscale Research Letters* **2006**, *1*, 84.
- [63] G.J. Kovacs and P. S. Vincett, *Journal of Colloid and Interface Science* **1982**, *90*, 335.
- [64] B.S.I.-Gunduz *et al.*, *Polymer* **2010**, *51*, 1485.
- [65] A. Salimi and A. A. Yousefi, *Polymer Testing* **2003**, *22*, 699.
- [66] S.R. White *et al.*, *Nature Materials* **2001**, *409*, 794.
- [67] I. Horcas *et al.*, *Review of Scientific Instruments* **2007**, *78*, 013705.
- [68] S. Maity *et al.*, *Polymer* **2011**, *52*, 1674.

- [69] S. Lal, S. E. Clare and N. J. Halas, *Accounts of chemical research* **2008**, *41*, 1842.
- [70] J.R. Adleman, *et al.*, *Nano Letters*. **2009**, *9*, 4417.
- [71] E. C. Garnett, *et al.*, *Nature Materials* **2012**, *11*, 241.
- [72] I. Alessandri and L. E. Depero, *Chemical Communications* **2009**, 2359.
- [73] H. Eilers, *et al.*, *Journal of Materials Research* **2006**, *21*, 2168.
- [74] V. Chakravadhanula, *et al.*, *Nanotechnology* **2008**, *19*, 225302.
- [75] A. Biswas, T. Wang and A. S. Biris, *Nanoscale* **2010**, *2*, 1560.
- [76] S. Link and M. A. El-Sayed, *The Journal of Physical Chemistry B* **1999**, *103*, 8410.
- [77] Y.-Y. Yu, *et al.*, *The Journal of Physical Chemistry B* **1997**, *101*, 6661.
- [78] M. B. Mohamed, *et al.*, *The Journal of Physical Chemistry B* **1998**, *102*, 9370.
- [79] F. Cooper, *International Journal of Heat and Mass Transfer* **1977**, *20*, 991.
- [80] S. Kakac and Y. Yenev, *Heat conduction*, Taylor and Francis Washington, DC **1993**.
- [81] A. O. Govorov, *et al.*, *Nanoscale Research Letters* **2006**, *1*, 84.
- [82] A. O. Govorov and H. H. Richardson, *Nano Today* **2007**, *2*, 30.
- [83] I. Alessandri and L. E. Depero, *Nanotechnology* **2008**, *19*, 305301.
- [84] I. Alessandri, M. Ferroni and L. E. Depero, *The Journal of Physical Chemistry C* **2011**, *115*, 5174.
- [85] A. U. Zillohu, *et al.*, *The Journal of Physical Chemistry C* **2012**, *116*, 17204.
- [86] S. E. Hong, *et al.*, *Catalysis today* **2007**, *120*, 413.
- [87] C. Kim and K. Yang, *Applied physics letters* **2003**, *83*, 1216.
- [88] F. Tuinstra and J. L. Koenig, *The Journal of Chemical Physics* **1970**, *53*, 1126.
- [89] T. Jarusuwannapoom, *et al.*, *European Polymer Journal* **2005**, *41*, 409.
- [90] W. A. Murray and W. L. Barnes, *Advanced Materials* **2007**, *19*, 3771.
- [91] K. Lance Kelly, *et al.*, *Journal of Physical Chemistry B* **2003**, *107*, 668.
- [92] K.-H. Su, *et al.*, *Nano Letters* **2003**, *3*, 1087.
- [93] P. K. Jain, W. Huang and M. A. El-Sayed, *Nano Letters* **2007**, *7*, 2080.
- [94] I. Lisiecki, F. Billoudet and M. Pileni, *The Journal of Physical Chemistry* **1996**, *100*, 4160.
- [95] T. Atay, J.-H. Song and A. V. Nurmikko, *Nano Letters* **2004**, *4*, 1627.
- [96] T. Boccaccio, *et al.*, *Journal of Membrane Science* **2002**, *210*, 315.
- [97] M. Matthews, *et al.*, *Physical Review B* **1999**, *59*, R6585.
- [98] M. Pimenta, *et al.*, *Physical Chemistry Chemical Physics* **2007**, *9*, 1276.

Chapter 5

Materials and Methods

This chapter gives a brief introduction about the materials and methods used for synthesis and characterization of nanofiber and film based systems used in this thesis.

5.1 Electrospinning:

As evident by the name, the process uses electric potential to spin fibers from polymer solutions. Because of its dominant electrostatic nature, the process is also called electrohydrodynamic jetting.^[1] 1D nanomaterials have been a subject of great interest due to their unique properties and several methods already exist in competition with electrospinning like, melt spinning, wet and dry spinning, gel spinning or slurry spinning.^[2-6] However, electrospinning is unique in that it can adapt to a variety of polymers, their blends, or composites with metal/ceramic nanoparticles to produce fibers of different surface/internal features in virtually endless length.^[7-9] In contrast to the conventional processes which result in 10 to 500 μm fibers, electrospinning results in 0.01 to 10 μm fibers.^[1] The finer fibers naturally have a higher surface area, which is beneficial in applications like catalysis,^[10] wound scaffolds and drug delivery,^[11,12] sensors,^[13,14] filters,^[15] super capacitors,^[16] etc. Electrospun nanofibers have potential applications in optics too, in particular owing to their scattering effects, as polarizers^[7] or as optical waveguides.^[17,18]

The electrospinning setup in its simplest form is shown in the **Figure 5.1**. In a typical setup, the polymer solution is fed at a suitable rate through a needle, which is at a high electric potential with respect to a ground plate (or target). The charged polymer drop takes the form of electrospinning jet in several steps, i.e., Taylor cone formation, straight jet stage, whipping instability state, jet drying in the form of nanofibers and collection.^[19] A charged pendent drop is thus experiencing various counter acting forces and successful formation of fibers through electrospinning rather than transforming the drop into a spray of droplets as in electro spraying, depends on which forces play a dominant role.

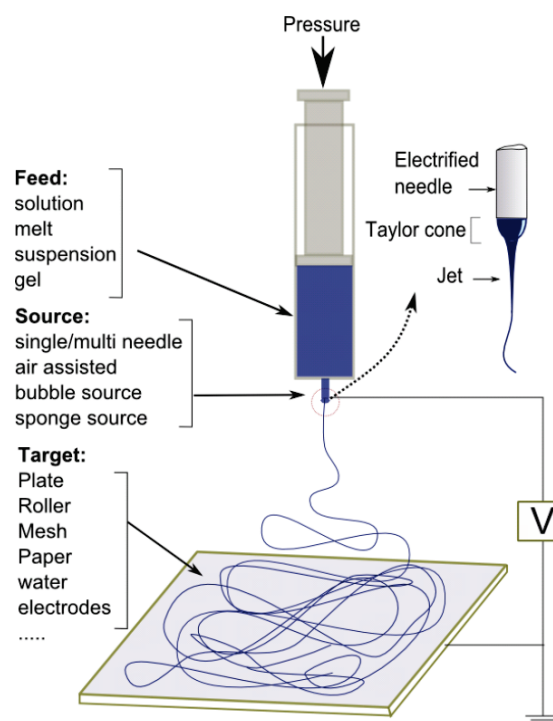


Figure 5.1 Schematic illustrating the electrospinning process in its simplest form. On the right side, the tip of charged needle along with Taylor cone and jet is shown.

As the droplet comes out of the needle orifice, two forces tend to pull it away from the needle and towards the target plate. These are the gravity (if it is downwards spinning) and the electrostatic force. The electrostatic force arises because the contact with the high potential electrode (here, the needle) results in induction charging of the polymer solution.^[1] Mostly, the needle is connected to a positive terminal of high voltage supply and as a result, the negative charges in the solution are attracted towards the needle leaving the pendent drop with the positive charge. The electrostatic force act as two ways, i.e., attraction between the drop and the grounded target as well as mutual repulsion between the charges in the drop itself.^[11] This results in a net force on the drop towards the target. However, the surface tension tried to keep the drop in spherical form. The net effect of different forces acting on the drop is that it takes the elongated form called the ‘Taylor cone’.^[2] For electrospinning to take place the electrostatic force has to overcome the surface tension and viscoelastic forces which resist the elongation of the drop.^[20,21] Gravity may effect the drop shape^[22] but during the flight of the jet towards the target the effect of gravity or other forces like air drag is minimal.^[23] Another effect of gravity may appear when spinning suspensions for longer periods, as gravity may result in separation of blended phases.

An electrospinning jet consists of two parts, i.e., a stable region which starts just after the Taylor cone and extends only a centimeter or two, after which it transforms into the unstable jet which is associated with whipping (or bending) instability. Whipping instability is caused by uneven charge distribution along the circumference of the jet and helps in reduction of fiber size. In fact, the polymer jet may undergo several instabilities like varicose instability and splitting instability, which may result in the formation of drops and multiple jets, respectively.^[1] The final stage in electrospinning is the fibers collection on the grounded target where they loose their charge. Targets may be of many types and influence mainly the fiber layout in the final mat. For example instead of flat plate target, a parallel wire or a rotating drum target may be used for aligned parallel fiber or if paper is used instead of aluminium sheet then one get more fluffy highly charged mat,^[24] etc.

Electrospinning process involves many variables that affect the size, shape and surface features of the fibers. Some of them are related with the polymer solution, i.e., its viscosity, surface tension, rate of evaporation, concentration, charge carrying capacity, conductivity, polymer chain structure, and its molecular weight. Then there are ‘process variables’, like type of solution delivery device, humidity, temperature, distance between target and electrode, flow rate, applied potential and the type of collector. These many variables in a simple looking process give it flexibility and the ability to produce fibers for a variety of applications.

5.2 Spin coating:

It is used for preparing thin films, mostly of polymers, on flat substrates like a glass plate or a silicon wafer, **Figure 5.2**. A pre-cleaned substrate is held in a vacuum chuck that can rotate at a high speed. During or before its rotation, the polymer solution of certain viscosity is deposited on the surface of the substrate. Because of centrifugal force, the solution is pushed outwards, spreading on substrate and covering it in the form of a uniform thin film. This film further thins down during continued spinning as it dries on the substrate.

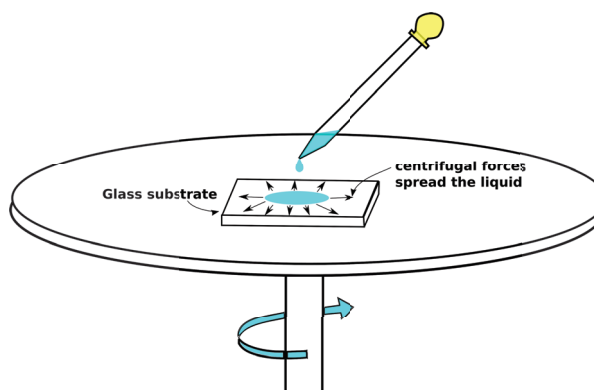


Figure 5.2 Schematic representation of spin coating in its simplest form.

The variables which affect the film thickness and its uniformity include: cleanliness and wettability of the substrate, homogeneity, concentration and viscosity of the solution, solution volume with respect to substrate size, vapor pressure of the solvent, spinning speed and time.

5.3 Sputter deposition process:

Sputtering is used to deposit thin layer of a metal, polymer etc, on a substrate. It is a physical vapor deposition process in which atoms are dislodged from a solid target as it is bombarded with high energy ions. Consequently, these dislodged atoms are deposited everywhere in the chamber including the intended substrate.^[25]

A typical sputtering chamber consists of a pair of an anode and a cathode (with high tension power supply), a provision for high vacuum as well as gas supply, **Figure 5.3**. Cathode is made of the substance whose film is to be coated on the substrate. During the process, plasma of the sputtering gas is generated between anode and cathode and the positively charged gas ions thus produced, are accelerated towards the cathode.

On impact with the cathode, these ions can dislodge atoms from the target plate which deposit every where in the chamber including the substrate. Energy transfer in sputtering may also involve other species like neutral atoms, electrons or photons, however, most relevant sputtering applications are performed involving ions.^[26]

The impact of a high energy particle on the target surface can lead to a variety of events including surface damage, atom ejection, ion implantation etc, depending upon energy of the impinging particle. If the sputtering ion energy is less than the surface binding energy of cathode (typically <50 eV) then the impinging ions can only knock off adsorbed species or

loosely bound atom on the cathode surface. However, in the knock-on sputtering, the energy of impinging ions, i.e., ~ 10 eV-1 keV, is sufficient to eject surface and subsurface atoms and the sputtering yield is directly proportional to the ion energy and current. If the energy of the impinging ions is increased still further, then each ion can eject multiple atoms from the target. However, due to high energy involved and because of ion implantation in the target, this regime is not of interest.^[27]

There are many types of sputtering, e.g., DC sputtering, AC (or RF) sputtering, reactive sputtering, magnetron sputtering, etc. Since magnetron sputtering was used to prepare samples used for this thesis, following introduces it briefly.

Magnetron sputtering is an extension of DC sputtering or RF sputtering. One way to increase sputtering efficiency is to increase the number of Ar^+ ions in the chamber.

However, an increase in the Ar pressure may result in gas incorporation into the sputtered film as well as energy losses by Ar^+ ions after collision with Ar atoms. As a result, with increasing gas pressure, initially there is an increase in the sputtering rate, which then decreases after a certain gas pressure. In order to increase the sputtering efficiency even at low gas pressures, one needs bring plasma close to the target. To do that, magnets are placed at back of the target, which form a kind of magnetic bottle for the electrons. Because of combined effect of vertical electric field and side ways magnetic field, the electrons are forced to move in a toroidal path near the target. This increases the impact efficiency of the electrons with the Ar atoms resulting in a higher number of Ar ions being produced near the target, which in turn increases the sputtering efficiency. Another benefit is that fewer electrons can now reach the substrate, which results in its minimal heating. A disadvantage of magnetron sputtering may be not sufficient electrons near the substrate in order to activate the gas, as required in reactive sputtering. However, this can be dealt with in unbalanced magnetron sputtering, in which some electrons are allowed to escape towards the anode.^[28]

For a normal sputtering experiment, the variables that affect the coating features include sputtering current, gas pressure, distance between target and substrate, substrate temperature and coating duration. For example, a higher sputtering current would mean a

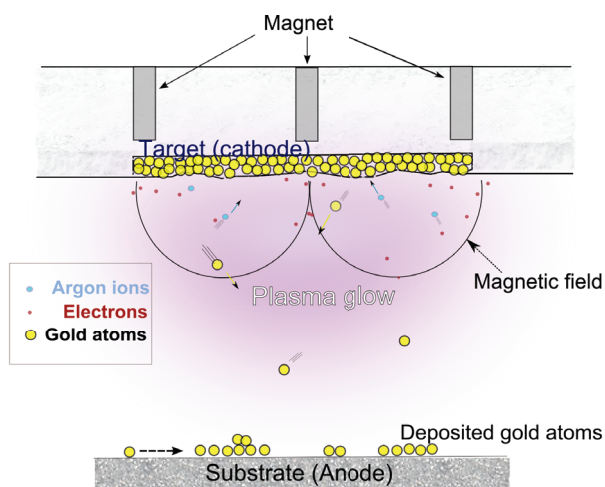


Figure 5.3 Schematic showing the principle of a sputter coater.

higher rate of sputtering which would shift the film deposition trend from surface diffusion and agglomeration on existing nuclei to formation of new nuclei. As a result, the sputtered film would be finer grained. The applied voltage determines the energy with which Ar ions collide with the target. After collision, this energy is either given altogether to one sputter particle (minus its binding energy) or is used in multiple collisions with many particles being ejected but at a lower energy. So it influences the sputtering rate not only by the number of particles produced but also their energy which is important in considering if the particle would stick on the substrate or not and what would be the nucleation and growth path ways. The substrate temperature, which can increase even by the sputtering process without any external heating, determines the sticking coefficient of the incoming particle as well as the crystal structure of the final film they produce. Pressure in the chamber determines the distance a particle can travel before it collides with a gas molecule. Hence, together with the target to substrate distance, pressure determines the number of collisions a particle faces before reaching the substrate. The sputtering angle determines the preferred direction for film growth and has influence on anisotropy of the film. The gas in the sputtering chamber is an inert gas, usually argon. In the case of reactive sputtering, though, it may be another reactive gas as desired according to the required film chemistry.

Sputtering is a widely used coating method because of its easy and precise control over film thickness on large areas, good control over grain structure by application of negative bias and substrate temperature, as well as a good control over film stresses by controlling the sputtering power and gas pressure. However, it has its own drawbacks, such as instability of some materials towards bombardment by high energy ions, or low deposition rates some materials, etc.

5.4 Optical microscope:

Optical microscope is used to observe small objects that cannot be seen by naked eyes. The maximum magnification, which is the product of the powers of eyepiece and objective, available on an optical microscope is x1500 or x2000. Although by using stronger lenses, the magnification can be increased but it does not increase the resolving power of the microscope. Resolving power is the minimum distance that can be observed between two adjacent features. Resolving power is limited by the wavelength of light used for image formation, according to the well known "Rayleigh's diffraction limit":

$$R = \frac{0.61\lambda}{NA} \cong \frac{\lambda}{2NA} \quad \text{Equation 5.1}$$

where, λ is the wavelength of light and NA is numerical aperture, which is given by:

$$NA = n \sin \theta$$

Equation 5.2

Here, n is the refractive index of the medium between objective lens and object, and θ is the half angle subtended by the lens on the object. Thus by using ultraviolet light source (at 405 nm) and an oil immersion lens ($NA=1.25$), the resolving power comes out to be about 197 nm. Since a human eye would see 197 nm features comfortable at x1500 (because it would look like a feature of 0.3 mm size, whereas human eye can resolve 0.1 mm) therefore, it is generally selected as the maximum magnification on a microscope. Any further increase in the magnification would not increase resolution rather image would become grainy. Common viewing modes on an optical microscope are dark/bright field, phase contrast and interference contrast.

5.5 Scanning electron microscope:

Scanning electron microscope (SEM) uses electron beam instead of light for image formation. The beam scans over the sample surface and due to interaction of electrons with the sample surface, a number of effects are produced each of which gives information about the topography or composition of the specimen, **Figure 5.4**.^[29] The interaction of incident electron may result the following:

- the beam may reflect back
- it may knock out electrons of the sample itself
- characteristic X-rays are generated
- Auger electrons are produced
- cathodoluminescence is produced
- electrons are conducted through the sample

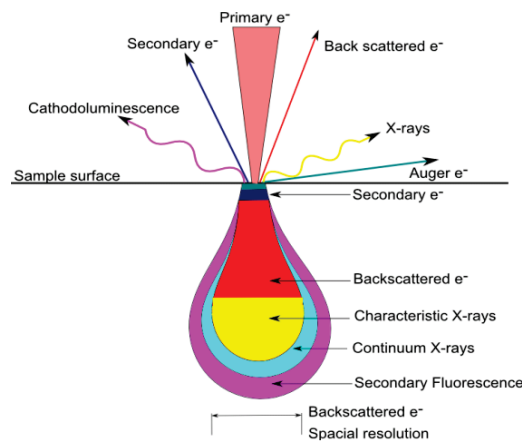


Figure 5.4 Schematic showing the interaction volume of primary electron beam and different signals it generates (source: ISAAC, University of Glasgow).

The SEM is equipped with different detectors to capture these signals, based on which it makes an image on a monitor simultaneously with the scanning beam. The main components of an SEM are thus, an electron source along with electron accelerating system, an evacuated column with magnetic lenses, stigmators and different apertures, detectors and an output setup for image formation and saving, **Figure 5.5**.^[30]

Besides the fact that one can examine so many different properties of a specimen surface, it also has a very high resolution as well as depth of focus. The resolution of an SEM depends upon the size of the electron beam spot, which in turn depends upon the wavelength of the electrons and the electron-optical system. Another factor that determines the limit of

resolution is the beam interaction volume with the sample. With secondary electron mode, the highest resolution so far is 0.4 nm^[31] but ordinarily this lies somewhere between 1-10 nm. Since the interaction volume of backscattered electrons is much higher, the resolution is generally much coarser than that obtained by secondary electrons. One of the reasons why SEM is a good choice for observing rough surfaces, like pollens, fibers etc, even at low magnifications is its high depth of focus. As an example at 100x and a working distance of 20 mm, SEM gives a depth of focus of about 400 μm compared to only 20 μm as offered by an optical microscope.^[32]

Mostly SEM images are those obtained by capturing the secondary electron signal. The topographical image is produced due to an increase in the number of secondary electrons emission by small roughness and edges on the surface and this change in detector signal is plotted on the output screen as the brightness level. The secondary electrons are those, which belong to the sample surface and are knocked out of the sample surface by incident electron beam. These are low energy electrons and are thus ejected only from the top surface of the sample.

In this regard, they present a truer picture of surface morphology than any other type of signal, but at the same time, they are easily affected by surface charge build up which usually occurs for non-conducting samples. In such a case, a thin gold coating on the sample surface is required to make the sample surface conductive and avoid charging. Back scattered electrons, which are the electrons of the incident beam reflected back after elastic interaction with the nuclei of the atoms on the sample surface are not so much affected by the charging effects because of their high energy (more than 50 eV). The number of backscattered electron depends upon the atomic weight of the target atoms from which they reflect, i.e., atoms with higher atomic numbers would scatter more electron than those with lower atomic number. As a result, they can be used for the chemical mapping of the surface. However, since the backscattering event is not frequent, therefore the backscattered signal is weak and noisy.

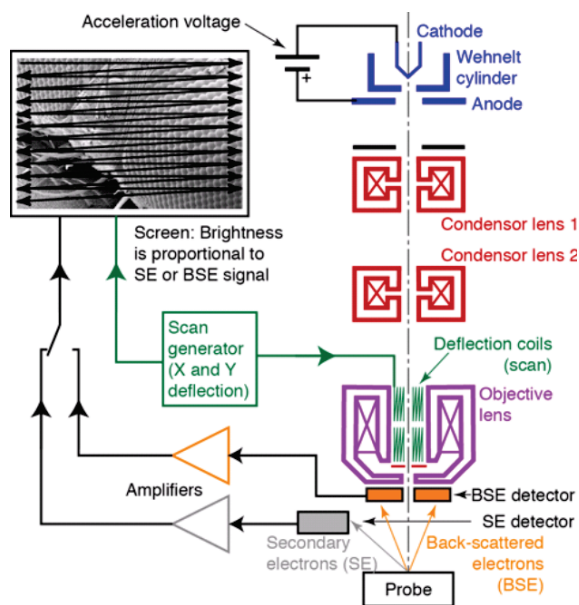


Figure 5.5 Schematic representation of different part of an SEM. Top left, is the representation of raster scan over a sample surface (source: Thomas Ludwig, Heidelberg University).

An atom whose inner shell electron has been knocked out, is not in its equilibrium state until an outer shell electron jumps in, to fill the position. This involves emission of characteristic X-rays or Auger electrons, which are used for quantitative chemical analysis.

For a sample to be examined in an SEM, it needs to be conductive to avoid charging. Moreover, because of high vacuum inside the chamber, the samples need to be dry. They should also be able to withstand electron beam impingement without any damage.

5.6 Transmission electron microscope:

Transmission electron microscope is used to examine structural details inside a sample down to individual atomic planes. Just like an SEM, the image is produced by interaction of an electron beam with the sample; however, here the electron beam transmits through the sample and then forms an image on a fluorescent screen, a photographic plate or on a CCD. The sample for a TEM analysis needs to be very thin (less than 100 nm)^[33] so that electron beam can pass through it. This includes, mechanical milling, ion beam thinning or chemical thinning and staining or fixing. TEM is used to study structural details, like atomic arrangements, stacking faults and dislocations, crystal orientation, electronic structure, sample induced electron energy shifts, layer thicknesses, particles distribution in the matrix etc, in contrast to an SEM that generally gives a surface analysis. The high resolution owes to very high voltage (up to thousands of kV) used to accelerate electrons which in turn results in a very short de Broglie wavelength. A TEM is closer to an optical microscope than an SEM as the image is magnified after the interaction of beam with the sample.

Mostly, the image formation is based on absorption of electrons in the materials depending upon its thickness and nature of material. This forms the conventional bright field image, with thinner areas (or less absorbing materials) appears brighter than the rest, having a direct relation with the Beer's law (see section 5.9). This type of contrast is good for imaging amorphous or biological sample.^[34]

In crystalline samples, the electron beam can undergo Bragg diffraction that forms the basis of diffraction contrast. If the directly transmitted beam is blocked then only those areas take part in image formation, which were scattering a selected reflection and the rest appears dark, which is known as dark field image. Moreover, the Bragg diffracted electron beam is also used for electron diffraction pattern generation which is used in crystal structure study.

Other rather uncommon imaging techniques utilize energy difference (electron energy loss spectroscopy), or phase change (phase contrast) in electron beam as it passes through a sample of uniform thickness.

5.7 Atomic force microscopy:

Atomic force microscope (AFM) is used for high resolution imaging of the sample surface. In principle, a very fine tip (or probe, as it is often called) that is mounted on a cantilever, scans over the sample surface. During the scan, it moves up and down along the surface roughness and this movement of the needle represents the surface topography. The up and down movement of the tip is recorded with the help of a laser which is reflected from the back of the cantilever towards a photodiode which constantly measures the laser signal during a scan,

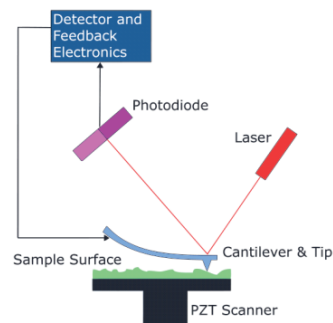


Figure 5.6 Working principle of AFM shown schematically (source:wikipedia.org).

Figure 5.6. This signal is not only plotted in terms of topography but is also fed into the feedback loop which is used to maintain a constant distance of tip with the sample surface. The sample is placed on a piezoelectric scanner that moves the sample under the tip in x-y direction for a complete scan, as well as in the z-direction to maintain a constant distance between the tip and the sample surface.

As is shown in the **Figure 5.7**, there are two types of forces, i.e., repulsive and attractive, acting between approaching atoms. At a relatively larger separation (10 nm or so), van der Waals' forces lead to negative interaction potential with resulting 'attraction'.^[35] These forces, which are always present, originate from zero point quantum fluctuations that are dependent upon local probe and sample geometry, their material as well as the medium between them. As the tip approaches the sample surface even further there is an exponential increase in the attractive forces, **Figure 5.7 (green line)**. This corresponds to the working range for non-contact mode AFM analysis.

After certain proximity, when the electronic wave functions of the outer most atoms on the tip and the surface start to overlap, there is a big increase in the short range repulsive forces, **Figure 5.7 (red line)**. On further approach, the combined effect of both the forces becomes less and less attractive and ultimately enters the repulsive regime, **Figure 5.7 (blue line)**. In the contact mode AFM, the proximity of the tip to the surface is within the repulsive

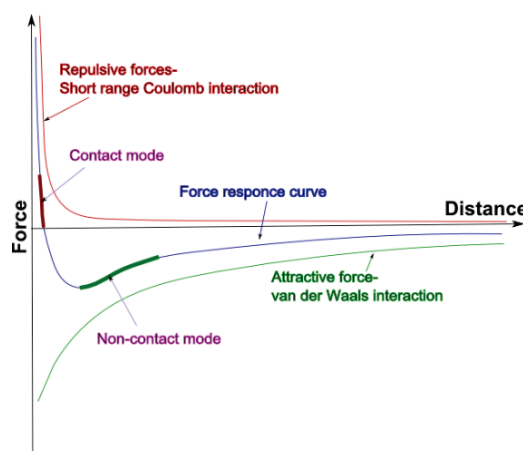


Figure 5.7 Graph showing the varying nature of forces (y-axis) between two atoms as the distance between them (x-axis) changes.

force regime. Further progress of the tip towards the sample surface would result in damage to the tip or the sample. Usually the surface of the tip or the sample is covered with a thin adsorbed layer of water, whose attractive force exceeds both the forces mentioned above and thus can add as a huge background force and overall loading force by the tip on the sample is drastically increased. This can result in a poor lateral resolution in contact mode, hysteresis in the force curve and damage to the tip.

The most commonly used modes in an AFM are, the contact mode, tapping mode and the non-contact mode. In the contact mode, the tip keeps such a close distance with the sample surface that the overall interaction between the tip and surface is always repulsive. There are two types of scans possible, i.e., constant force and variable force.^[36] In the constant force scan, the microscope tries to keep deflection and hence the force on the cantilever as constant. For example, when the tip passes over a hill the distance between the tip and the surface decreases, which results in the increase in the repulsive force and the sample is lowered by an amount determined by the signal of the feed back loop to keep the repulsive force as constant. To keep the deflection in the cantilever as constant, any change in original deflection or set point is compensated with the same change in z , and these changes in z are plotted correspondingly on x - y scale as the image of the sample surface. On the other hand, in variable force measurement, the feed back loop is switched off, which means the z -height remains constant and any deflection in the cantilever is measured as the topography of the sample surface. Although, it produces sharper images than constant force measurement, however, this mode should be better used only for smoother samples.

Since the tip is exerting some force on the sample, contact mode is not suitable for soft samples that can be damaged or whose image can be distorted by the movements in the sample surface by the tip itself. High lateral forces appearing when the tip scans over a slope can also damage the surface. Another source of a lower resolution image is the stick-slip motion of the tip. In order to avoid these problems, dynamic modes, such as intermittent contact or non-contact modes are used.

In the intermittent contact or tapping mode, the cantilever is oscillating close to its resonance frequency. The amplitude of oscillation may change due to repeated engage and disengage of the tip as it scans over the surface. In order to keep the amplitude as constant, the z -height of the piezo-stage is varied and these variations in the height are plotted as the surface structure of the sample surface. Because of negligible contact with the surface, the lateral forces are greatly reduced. Each material, owing to its mechanical and adhesive properties will produce a certain shift in the phase signal between the actual frequency of cantilever oscillation in comparison to the drive frequency. Thus, simultaneously with the

topographical images, the instrument can plot phase images that indicate changes in material properties.

In the noncontact mode, the cantilever is oscillating over the sample surface, just as in tapping mode, but the amplitude of oscillation is very low. On approaching the surface, the van der Waals forces start becoming influential, changing the oscillation frequency of the cantilever. Depending upon the phase shift between drive and oscillation frequency, the z-position of the cantilever is adjusted to keep the tip out of contact with the surface. As the probe does not come in the repulsive regime, the area of contact between the probe and the surface is minimized leading to higher resolution, down to atomic resolution under stable conditions. but in real conditions, the resolution may be lower than the tapping mode, as any water present on the surface would efficiently block the van der Waals' forces as well as it would be difficult for the tip to get itself loose from water layer because of its low amplitude oscillation.

One of the benefits of an AFM is that it can analyze the sample in ambient atmosphere, however, in some special cases, like for high resolution imaging, it can be placed in an isolation chamber. Moreover, sample does not need to be conductive as required for an SEM. The AFM images are three dimensional in contrast to the two dimensional images of other microscope. Some of the drawbacks of AFM are a relatively small scan area, time consuming scans and too frequent contamination/damage of the tip. Moreover, problems like creep, hysteresis, and nonlinearity may cause artifacts in the image. Other sources of artifacts include unsuitable tip shape, bad environment or the sample itself.

5.8 Raman spectroscopy:

Raman spectroscopy gives information about vibrational and rotational modes of molecules. The analysis is done by shining the sample with a monochromatic light and observing the inelastically (or Raman) scattered light. The shift in the energy of the scattered light tells about vibrational or rotational modes of the system. The absorption of light by the molecule puts it to a high energy, virtual level. The molecule then

emits a photon (Raman scattering) to go back to its ground state. The emitted light may be of higher or lower frequency than the incident light (Raman shift), depending upon the initial

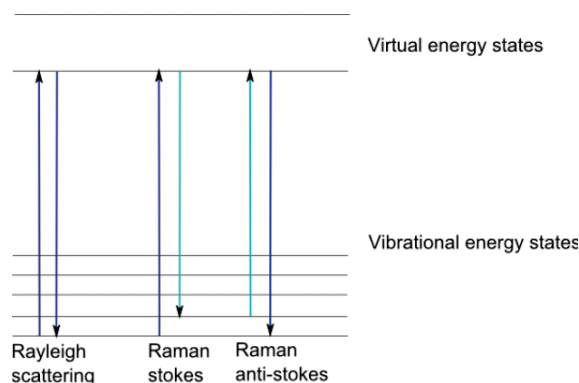


Figure 5.8 Schematic showing the scattering of light as molecule shifts between excited and ground state.

state of the molecule. In the so-called 'Stokes shift' the frequency of the emitted photon is lower than the incident one, and the reverse is true for the 'Anti-stokes' shift, **Figure 5.8**. Since mostly, atoms are in their lowest possible ground state before illumination, therefore, it is very rare that they add some energy to the outgoing photon, that is why mostly stokes spectrum is presented since it is stronger in intensity than an anti-stokes spectrum.

Raman effect can only occur when there is a change in polarizability of the molecules after interaction with light. This is contrast to IR spectroscopy, wherein a change in the dipole moment takes place after absorption of light which is interpreted as vibrational or rotational modes of the molecules. By the rule of mutual exclusion in centrosymmetric molecules, Raman and IR complement each other. Thus modes which are symmetric with respect to center of symmetry are Raman active but not IR active and those with are antisymmetric are IR active but not Raman active. In general, the signal is stronger in Raman when the bond is homopolar covalent, and stronger in IR when it is heteropolar covalent or ionic.^[37,38] The frequency of Raman scattered light is directly dependent upon the force constant (type of bonding between atoms, e.g., single, double or triple) and is inversely proportional to the mass of the atoms involved.

Typically, the sample is excited with UV (244-364 nm), visible (457-660 nm) or IR (785-1064 nm) lasers.^[39] The choice of laser is dependent upon many factors, for example, the intensity of the scattering is proportional to λ^{-4} .^[40] Moreover, blue and green lasers are better for resonance Raman, surface enhanced Raman scattering while IR laser is good for fluorescence suppression.^[39,40] The Raman microscope used in this thesis is shown in the **Figure 5.9**.

Although Raman spectroscopy has some advantages over IR spectroscopy, like a broad spectral range 50 cm^{-1} to 4000 cm^{-1} that can be analyzed in one go, ability to analyze water based solutions or glass sealed samples or selective enhancement of a particular chromophore, however it is not without short comings, like heating of the colored samples, poor resolution of rotational spectra and finally the higher cost of set up.^[37]

5.9 UV-Vis spectroscopy:

UV-Vis or ultraviolet-visible spectroscopy is used to determine the optical absorbance, reflectance and transmittance by the sample in the UV, visible or NIR range of

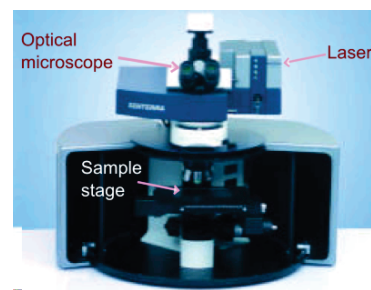


Figure 5.9 Raman microscope used in this thesis.

spectrum. A UV-Vis instrument essentially consists of a light source, gratings or a prism, sample chamber and a detector.

Color is simply a perception felt by our eyes and white light is a mix of different complementary colors in a certain balance. The absorption of one of the colors disturbs the balance and our eyes have a pronounced feeling of its complementary color. Many of the compounds show color because of different reasons, including, high degree of conjugation, excitation of d-shell electrons, charge transfer complexes, plasmon absorption and so on. In any case, a color would mean that a part of light is being absorbed. The spectrophotometer measures the remaining transmitted light, and plots the percent transmittance, given by:^[41]

$$\%T = 100 \left(\frac{I}{I_o} \right) \quad \text{Equation 5.3}$$

Transmittance is related with absorbance by the following relation:^[41]

$$A = \log \left(\frac{I_o}{I} \right) = -\log \left(\frac{\%T}{100} \right) = 2 - \log(\%T) \quad \text{Equation 5.4}$$

Absorbance, according to the Beer-Lambert's law, is related to the concentration of the absorbing species as well as the path length:

$$A = \log \left(\frac{I_o}{I} \right) = \varepsilon.c.L \quad \text{Equation 5.5}$$

where, I_o and I are the incident and transmitted beam intensities, ε is the molar absorptivity or extinction coefficient, c is concentration of the absorbent and L is the path length traversed by the light (sample thickness). Thus, a transmittance or reflectance spectrum would indicate the concentration of absorbing or reflecting species in the sample, which may be plasmonic nanoparticles or molecules of a photochromic compound, etc.

5.10 X-ray diffraction:

X-ray diffraction (XRD) is used to determine the crystallinity, the crystal structure, stresses in the material, disorder, unit cell dimensions etc. The method is used in the study of metal, salts, and a variety of organic and inorganic crystallizable compounds. Simply, the sample is placed on a goniometer and exposed to X-rays through a range of angles. The X-rays would interact with the electronic cloud of atoms in the crystal which due to crystal symmetry behave as a regular arrangement of scatterers or resonators. It should be noted that for an intense diffraction signal, the spacing between resonators should be comparable with the wavelength of the scattered/diffracted light. The regularly arranged scatterers (atoms)

give out spherical waves which interact destructively in most of the direction but in certain directions their interference is constructive. These directions are dependent upon the crystal structure and the wavelength of the X-rays used. Consider the geometrical representation of X-rays of wavelength λ diffracting from the planes of a crystal which are at a distance d apart, **Figure 5.10**.^[42] The diffracted rays QR and TW can interfere constructively only when the path difference between two rays, given by $2d\sin\theta$, is equal to an integer multiple of the X-ray wavelength, i.e., 1λ , 2λ , ...or $n\lambda$. This is the well known Bragg's law, which states mathematically as:^[47]

$$2d\sin\theta = n\lambda \quad \text{Equation 5.6}$$

Normally, X-ray source consists of a metal target that is bombarded with high energy electrons, as a result of which, the source gives off X-rays with a wavelength that is characteristic to the target material. Another source of X-rays is a synchrotron which is one of the brightest sources of inherently collimated X-rays, and is ideal for study of polymers, which are generally poor scatterers.^[43] Here, first the electrons are accelerated to nearly the speed of light and then transferred to a polygonal storage ring. At the end of each side of the polygon, the electrons are forced to change direction, as a results they emit a burst of electromagnetic radiation, including X-rays.

The type of X-ray analysis used in the present thesis is known as ‘Wide angle X-ray scattering’ (or WAXS) which is good for the study of both crystalline and non-crystalline materials especially polymers because polymers always have an amorphous part in their structure.^[44] As it is known that larger diffraction angle leads to a smaller length scale that is probed,^[43] WAXS is useful to determine crystal structure on the atomic scale. The method is used to detect microscopic features which are less than 10 nm in size and diffraction angle measurements are made for $2\theta > 5^\circ$.^[44]

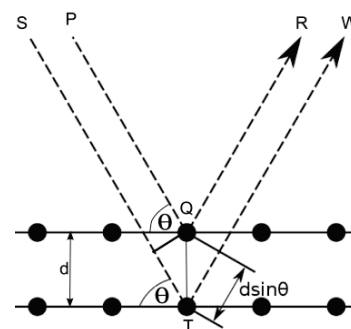


Figure 5.10 Sketch of X-rays, PQR and STW, reflecting from crystal planes, producing a path difference of $2d\sin\theta$ (source: wikipedia.org).

5.11 Contact angle measurement:

Contact angle measurement is used to quantify the wetting behavior of a surface, usually using a water drop, though other liquids can also be used to simulate any real life application. The value of three phase angle (liquid-vapor-solid) shows the wettability of the surface under consideration, **Figure 5.11**. If the surface ‘likes’ the water, it will let the drop

spread over it and consequently the contact angle (θ_c) would be small. In the same way, the contact angle would be very high in the case of a hydrophobic surface on which the water drop would ball up rather than spreading. Quantitatively, a surface on which a water drop makes an angle of $\leq 90^\circ$ is hydrophilic, whereas, one with an angle between 90° and 150° is called hydrophobic and for an angle more than 150° it is known as superhydrophobic.

The contact angle is an indicator of the surface energy and is strongly dependent upon the surface chemistry and surface roughness features. Thus surfaces with high surface energy, for example metals, show a low contact angle and those with low surface energy, like polymers, show a high contact angle.

In the case of partial wetting of a chemically and physically uniform, and smooth surface, the contact angle can be directly related to the surface energy by the Young's relation^[45]:

$$\gamma_{SG} = \gamma_{SL} + \gamma_{LG} \cos \theta_Y \quad \text{Equation 5.7}$$

where, θ_Y is the Young's angle (replacing θ_c in **Figure 5.11**) and γ is the surface energy at the solid-gas, solid-liquid and liquid-gas interfaces, represented by SG, SL and LG subscripts, respectively, **Figure 5.11**. However, most of the surfaces in nature are not smooth and Young's law needs to be modified. In the Wenzel state where the drop penetrates into the surface feature (**Figure 5.12**), the modified contact angle is given by:

$$\cos \theta^* = r \cos \theta_Y \quad \text{Equation 5.8}$$

where θ^* is the contact angle on the rough surface and r is roughness ratio, i.e., the ratio of true area of the solid surface to the apparent area. Thus a hydrophilic smooth surface would show a more hydrophilic behavior after roughening, and a hydrophobic smooth surface would show even higher contact angle after roughening (because $r > 1$).^[46]

Another scenario is where the drop cannot go into the surface features, owing to inter-feature distance and their height, and is sitting on a composite of solid surface and intermittent air pockets, **Figure 5.12**. This reduces the contact area of the drop with the surface and the drop makes a high contact angle due to contribution by air pockets. The modified contact angle would be the partial average of the angle made by the individual phases in the compos state and is given by the Cassie Baxter relation:

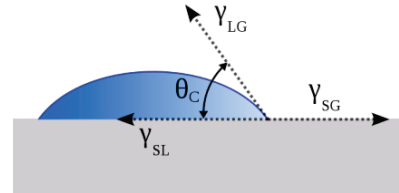


Figure 5.11 Schematic representing the terms used for explaining the behavior of a drop by Young's equation. (source: wikipedia.org).

$$\cos\theta^* = rf \cos\theta_Y + f - 1$$

Equation 5.9

where θ^* is the Cassie modified contact angle, r is the roughness ratio, and f is the area fraction touched by the drop.^[47] A variation in the Cassie state is the impregnating Cassie state, in which the wetting extends into the surface features beyond actual drop contact area. This situation should be distinguished from the Wenzel state where even though the drop penetrates the surface features but still the surface is dry beyond the drop.

In short, Cassie and Wenzel models can give an indication of the contact angle a drop might make on a surface, knowing the roughness of the surface. Due to pinning of the drop that is in the Wenzel state (**Figure 5.12**), a steeper tilt of the surface is required to make the drop slide on it, than that required for a drop in the Cassie state.

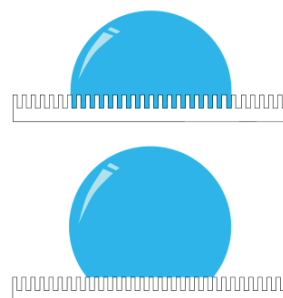


Figure 5.12 Schematic representation of water drop in different wetting state; upper: Wenzel state, lower: Cassie state (source: wikipedia.org).

In a typical sessile drop technique, a drop of water measuring about 5-15 μL is delivered on the surface to be examined from a pipette or an automatic delivery system. The view of the drop from a side is captured by the camera and software determines the profile of the drop and measures the contact angle that the tangent to the drop profile makes with the base line.

5.12 Ellipsometry:

It is a noncontact technique for measuring thickness, crystalline structure, composition and complex refractive index of thin films present on a substrates.^[48] It is a specular technique in which a beam of linearly polarized light impinges on the film surface at a certain angle. The components that are horizontally and vertically polarized with respect to the plane of incidence are reflected with different intensity and phase (change in polarization state), thus making an elliptically polarized beam.^[48,49] Samples can be measured in both

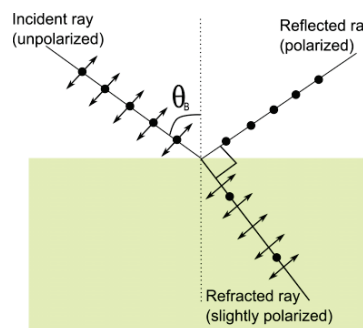


Figure 5.13 Schematic representation of s-polarized reflection at Brewster angle of incidence (source: wikipedia.org).

transmission and reflection, though generally only reflection is used. Ellipsometry is highly accurate as it measures the ratio between R_p and R_s , i.e., p - and s -polarized reflected light. Moreover, due to the presence of phase information (polarization state), films far thinner than the wavelength of light can be analyzed.

As shown in the **Figure 5.13**, that at a certain angle, called Brewster angle θ_B (also called Principal or Polarizing angle), the R_p is completely eliminated and reflection is constituted only by R_s . Knowing Brewster angle, one can easily find the refractive index of the surface,

$$\tan \theta_B = \frac{n_2}{n_1} \qquad \text{Equation 5.10}$$

where n_1 and n_2 are the refractive indices of air and the reflecting surface respectively. Because polarized light is used, it is certainly advantageous for analysis of anisotropic samples. Moreover, it does not need black boxes because stray un-polarized light cannot affect the analysis. Moreover, there is no reference measurement necessary as it measures a ratio and compares the results with a model. This all makes ellipsometry superior to normal reflection based spectroscopy. A disadvantage of the method is the difficulty in fitting appropriate model to solve the data.

5.13 Profilometry:

A profilometer determines a surface profile or the roughness of the surface as well as its contour.^[48] It is a broad term, which includes contact and non-contact (optical) type devices, but in reference to the present discussion, it means a mechanical contact type machine. It consists of a stylus, which scans across the test surface with a certain contact force. Any asperity in the surface is measured by the up and down movement of the stylus as it moves across them. The resolution of the analysis is determined by stylus tip geometry, force and scan speed.

In order to determine the thickness of a film, a scratch is made on the film taking care not scratching the substrate. When the stylus traverses across the scratch, it measures the height difference between the films top surface and the top surface of glass and this gives an indication of the film thickness.

5.14 Materials and other specifications:

Chemical	Remarks	CAS No.	Purity	Source
Polyvinylidene fluoride (HSV 900), powder	-	24937-79-9	-	Arkema Inc.
Polyvinylidene fluoride, film	0.05 mm	-	-	Goodfellow
Polystyrene, pellets	Mw = 280,000	9003-53-6	-	Sigma-Aldrich
Polyethersulfone, powder	Mw = 58,000	25608-63-3	-	BASF SE
Spirophenanthroxazine	MW = 378.47	119980-36-8	-	Sigma-Aldrich
Ammonium hydroxide	28–30 %, NH ₃ basis	1336-21-6	>99 %	Sigma-Aldrich
Hydrogen peroxide	30 %	7722-84-1	>99%	Carl Roth
Ethanol	-	64-17-5	99.8 %	Carl Roth
Toluene	-	108-88-3	99.5 %	Sigma-Aldrich
N,N-Dimethylformamide (DMF)	-	68-12-2	99.8 %	Sigma-Aldrich

All of the experiments were carried out at room temperature. The samples were stored in dark place at a temperature below 10 °C.

5.15 References:

- [1] G. C. Rutledge and S. V. Fridrikh, *Advanced Drug Delivery Reviews* **2007**, *59*, 1384.
- [2] D. Li and Y. Xia, *Advanced materials* **2004**, *16*, 1151.
- [3] X. Sui, C. Shao and Y. Liu, *Applied physics letters* **2005**, *87*, 113115.
- [4] X. Fang and L. Zhang, *Journal of Materials Science & Technology* **2006**, *22*.
- [5] P. a. Hu, *et al.*, *The Journal of Physical Chemistry B* **2004**, *108*, 936.
- [6] M. Lewin, *Handbook of fiber chemistry*, CRC Press **2010**.
- [7] D. Li, Y. Wang and Y. Xia, *Nano Letters* **2003**, *3*, 1167.
- [8] I. D. Kim and A. Rothschild, *Polymers for Advanced Technologies* **2011**, *22*, 318.
- [9] H. Wu, *et al.*, *Nano Letters* **2010**, *10*, 4242.
- [10] E. Formo, *et al.*, *Nano Letters* **2008**, *8*, 668.
- [11] W. J. Li, *et al.*, *Journal of biomedical materials research* **2002**, *60*, 613.
- [12] T. J. Sill and H. A. von Recum, *Biomaterials* **2008**, *29*, 1989.
- [13] J. Yoon, S. K. Chae and J.-M. Kim, *Journal of the American Chemical Society* **2007**, *129*, 3038.
- [14] R. Luoh and H. T. Hahn, *Composites science and technology* **2006**, *66*, 2436.

- [15] S. S. Homaeigohar and M. Elbahri, *Journal of colloid and interface science* **2012**, 372, 6.
- [16] S. Chen, S. He and H. Hou, *Current Organic Chemistry* **2013**, 17, 1402.
- [17] H. Liu, *et al.*, *Small* **2006**, 2, 495.
- [18] Y. Ishii, R. Kaminose and M. Fukuda, "Optical waveguiding in an electrospun polymer nanofiber", presented at *Journal of Physics: Conference Series*, IOP Publishing, **2013**.
- [19] A. Yarin, S. Koombhongse and D. Reneker, *Journal of Applied physics* **2001**, 90, 4836.
- [20] S. Ramakrishna, *An introduction to electrospinning and nanofibers*, World Scientific **2005**.
- [21] H. Fong, I. Chun and D. Reneker, *Polymer* **1999**, 40, 4585.
- [22] D. Rodoplu and M. Mutlu, *J. Eng. Fiber. Fabr* **2012**, 2, 118.
- [23] D. H. Reneker, *et al.*, *Journal of Applied physics* **2000**, 87, 4531.
- [24] H. Liu and Y. L. Hsieh, *Journal of Polymer Science Part B: Polymer Physics* **2002**, 40, 2119.
- [25] M. Ohring, *Materials science of thin films*, Academic press **2001**.
- [26] D. Smith, *Thin-film deposition: Principles and practice*, McGraw-Hill Education **1995**.
- [27] K. Seshan, *Handbook of thin film deposition*, Elsevier Science **2012**.
- [28] H. S. Nalwa, *Deposition and processing*, Elsevier Science & Technology Books **2001**.
- [29] http://www.gla.ac.uk/media/media_249720_en.jpg, accessed:07, 2014.
- [30] http://www.rzuser.uni-heidelberg.de/~hb6/labor/rem/index_en.html, accessed:07, 2014.
- [31] http://www.nanotech-now.com/news.cgi?story_id=42612, accessed:07, 2014.
- [32] <http://www.emal.engin.umich.edu/courses/semlectures/focus.html>, accessed:07, 2014.
- [33] J. Ayache, *et al.*, *Sample preparation handbook for transmission electron microscopy: Methodology*, Springer **2010**.
- [34] García Gutiérrez, Domingo Ixcóatl, *Transmission electron microscopy characterization of composite nanostructures*, The University of Texas at Austin **2006**.
- [35] Tip surface interaction, http://www.doitpoms.ac.uk/tlplib/afm/tip_surface_interaction.php, accessed: 07, 2014.
- [36] W. R. Bowen and N. Hilal, *Atomic force microscopy in process engineering: An introduction to afm for improved processes and products*, Butterworth-Heinemann **2009**.
- [37] J. R. Ferraro, *Introductory raman spectroscopy*, Academic press **2003**.
- [38] F. S. Parker, *Applications of infrared, raman, and resonance raman spectroscopy in biochemistry*, Plenum Press **1983**.
- [39] <http://www.horiba.com/scientific/products/raman-spectroscopy/raman-academy/raman-faqs/what-laser-wavelengths-are-used-for-raman-spectroscopy/>, accessed: 07, 2014.
- [40] I. R. Lewis and H. Edwards, *Handbook of raman spectroscopy: From the research laboratory to the process line*, Taylor & Francis **2001**.
- [41] B. C. Smith, *Fundamentals of fourier transform infrared spectroscopy*, CRC press **2011**.
- [42] P. Naik, *Principles of physics*, PHI Learning Pvt. Ltd. **2010**.
- [43] D. Braun, *et al.*, *Polymer synthesis: Theory and practice: Fundamentals, methods, experiments*, Springer **2012**.
- [44] Y. Leng, *Materials characterization: Introduction to microscopic and spectroscopic methods*, John Wiley & Sons **2013**.

- [45] S. Hartland, *Surface and interfacial tension: Measurement, theory, and applications*, CRC Press **2004**.
- [46] E. Y. Bormashenko, *Wetting of real surfaces*, Walter de Gruyter **2013**.
- [47] A. Marmur, *Langmuir* **2003**, *19*, 8343.
- [48] S. A. Dyer, *Wiley survey of instrumentation and measurement*, Wiley **2004**.
- [49] H. Fujiwara, *Spectroscopic ellipsometry: Principles and applications*, Wiley **2007**.

Chapter 6

Summary and Outlook

6.1 Summary:

With the ongoing advancement in technology and living standards, the materials are required to perform increasingly better. To fulfill these requirements not only that new materials have to be developed but also ways have to be found to utilize the full potential of currently available materials. This thesis aims to do this by highlighting how dimensionality can affect the properties of the materials to meet the needs.

In order to determine the effect of structural shape on optical and wetting properties, polymer based systems in the form of films and fibers were tested; with or without addition of noble metal (Ag) nanoparticles and a photochromic compound, spiropyrone (SPO).

Polyvinylidene fluoride (PVDF) was selected for investigating the effect of dimensionality on the wetting properties, as it is considered to be a hydrophobic polymer. However, it was found that its film was hardly hydrophobic showing a contact angle of around 80° . However, when the same material was formed into nanofibers by electrospinning, the contact angle increased to about 130° , making the same material almost superhydrophobic by mere change of dimensions.

In many applications, for a non-wetting surface, not only a high contact angle is important but also the water drop should be able to slide on its surface. It was observed that where the drop could slide slowly on the polymer film, it could not move at all on the polymer fibers mat and the mat could be tilted up side down without letting the drop fall, thus presenting artificial rose petal surface, i.e., one which is highly hydrophobic but still sticky towards the drop. The stickiness was attributed to pinning of the drop into the micropores between the fibers after partial infiltration due to capillary forces.

The same nanofibers were turned into highly hydrophobic and slippery surface (grass leaf effect) again by playing with the dimension of the system. The fibers were rolled into the form of yarns which were then laid side by side on the random fiber mat. On the yarn like structure, the water drop could roll on a tilt of around 45° as it had a minimum contact with the fibers and was, in a way, floating on the air pockets between the yarns.

A nice feature of this approach was that the yarn structure was mobile and could be removed from one surface and placed on any other surface to make it hydrophobic slippery without bringing any permanent change in it. Moreover, the interyarn spacing could be changed in real time, changing the state of the structure from hydrophobic slippery to hydrophobic sticky, reversibly.

The control over wetting properties was demonstrated also by chemical restructuring by blending SPO with the polymer. SPO molecule can reversibly switch between its open (highly polar) state and its closed state on exposure to UV and white light respectively. In

literature, SPO is generally shown to increase the hydrophilicity of the host polymer matrix as it switches into its open/polar state on exposure to UV, however, in the present case affinity of the system towards water actually decreased as indicated by about 9° (maximum) decrease in the sliding angle even without UV exposure. This could be explained on the basis of the effect of SPO on the crystal structure of the host polymer. When SPO was added to PVDF solution for electrospinning, the resulting fibers which were otherwise (i.e., without SPO addition) semicrystalline with β -conformation, lost their crystallinity as revealed by wide angle X-ray spectroscopy (WAXS). The loss of crystallinity was attributed to the intercalating SPO molecules that hindered regular arrangement of PVDF chains required for a crystalline structure. A random chain arrangement in an amorphous structure results in no net polarity of the polymer or in other words a low affinity towards water. Since most of the SPO molecules were already in their open state, just by the matrix effect, exposing this system to UV did not significantly affect the wetting behavior.

It was observed, during contact angle measurements along with the UV exposure, that the drop of water acted as a lens for UV, amplifying the UV intensity at the drop-fiber interface due to multiple reflections and interference within the drop. This led to the use of water as a removable template for patterning and erasable writing on the fiber mat. Since UV is intensified only at a certain point, the method can be used for UV driven local reactions without unwanted damage to the neighboring material. Moreover, the intensity of the blue spot made under the drop can be used as a visual indicator of any UV absorbing species suspended in the drop.

The interaction of photochromic molecule with its matrix was further studied regarding the optical properties. According to the commonly known solvatochromic effect, the absorption wavelength of a solution of photochromic compound is an indicator of the matrix polarity and is mostly determined by the UV-Vis transmission spectra. Since photochromic molecules act as oscillating dipoles when irradiated with electromagnetic waves, the light given off (i.e., reflection) by these radiating antennae is a very sensitive indicator of polarity of their surrounding, as revealed by ellipsometry results. It was found that, where the transmittance method (by UV-Vis spectroscopy) showed only 11 nm/D sensitivity, the reflective method showed up to 40 nm/D difference in reflectance minima of p-polarized light at Brewster condition. It was further demonstrated that the color reflected by a polymer film containing photochromic compound is not solely based on the chromophore, rather it can be manipulated by real and imaginary parts of refractive index and, the interference effects offered by the substrate, on which the coating is prepared. When there was an interlayer of silicon oxide between the silicon substrate and the 'chromophore-

polymer' film, the color of the film resulted from reflection minima being in the imaginary part of the refractive index of chromophore-polymer film, resulting in absorption in yellow part of spectrum and a blue reflected color. Obviously, upon exposure to UV this color simply intensified from earlier light blue to darker blue. No splitting in absorption spectrum was observed, meaning that the imaginary part of refractive index was dominant. However, in the absence of a spacer layer, a reflection maximum existed in the range of real part of refractive index of 'chromophore-polymer' film resulting in scattered color (brown). Upon exposure to UV, not only that a reflection dip appeared due to typical absorption of photochromic compound, in orange color part (around 600 nm) of the spectrum resulting in perceived color of green, but also the reflection peak red shifted by 50 nm and reflection dip blue shifted by 12 nm owing to modulation of real part of refractive index. A change in coloring range of the same system of 'chromophore-polymer', simply based on substrate, has never been earlier shown.

On the other hand, in the case of SPO loaded nanofibers, a novel behavior of increased transmittance after UV exposure was observed. The size of the fibers was controlled in such a way that the resonance coincided either with the real or with the imaginary part of refractive index. In the latter case there was simply an increase in the absorption intensity after UV exposure, at a wavelength where SPO open form typically absorbs when it is present in thin polymer films (i.e., at around 600 nm). However, in the former case, i.e., when the resonance of fibers matched with the real part of their refractive index, there was an increase in transmittance at the same wavelength where SPO shows absorbance. A splitting was observed in the transmittance peaks, indicating molecular photonic coupling analogous to molecular plasmonic coupling.

The control over optical properties by molecular photonic coupling naturally raised interest in molecular plasmonic coupling effect. In this study, the SPO loaded polymer film was coated on sputtered thin metal film to produce a photoswitchable omnidirectional transparent conductor. At a certain filling factor of SPO, the hybrid system showed a transparency increase up to 100% relative to intrinsic value of thin metal film together with inherently high conductivity coming from the metal film. The increase in transparency was due to wave vector coupling between the photochromic molecules and their dipole image in metal film which resulted in plasmonic tunneling. Such a hybrid system is a good candidate for transparent conductor applications. The transmittance could be blocked by exposure to UV. Although the recovery of open state SPO molecules to their initial closed state was slow but it could be accelerated by exposure to solvent vapors, thereby demonstrating a chemical vapor sensor.

The final part of the thesis was concerned with thermoplasmonics, which result from interaction of light with metal nanoparticles. The substrate was PVDF, in the form of sheet and electrospun fibers, both forms sputter coated with silver. The samples were exposed to green (532 nm, 0.2-20 mW) and red (785 nm, 1-100 mW) lasers. Whereas, the uncoated film could withstand both lasers up to their maximum power without melting, the silver sputtered PVDF film could be melted by as little power as 2 mW (green laser). It was found that green laser needed much lesser power to melt the film, compared to red one, because its wavelength was much nearer to the plasmon absorption of silver (which is nearly at 400 nm). TEM and UV-Vis analysis of the melting spots that had a size down to 500 nm showed embedding of nanoparticles in the polymer thus locally forming a nanocomposite. These spots could be overlapped to form patterns, submicron writing, etc. Raman analysis of the nanocomposite spots showed an increase in β -chain conformation thus indicating a local control over polymer chemistry. The plasmonic heat was also used for welding/repairing of microcrack and defects in the film.

Thermoplasmonics, because of its localized heating, can be used to heat tiny and thin structures such as nanofibers. To study the thermoplasmonic effect on electrospun fibers, the same were sputter coated with different thickness of silver. With increasing coating thickness, the particle size increased with consequent decrease in interparticle distance. This increased the absorption intensity, as well as shifted the plasmon absorption to longer wavelength due not only to the size growth of particles but also due to near field coupling between them. At a certain coating thickness, the particles started to touch each other with a consequent appearance of multimode plasmon which was split in optical and NIR wavelength. At this stage the nanoparticles were in conductively coupled regime and the electric field between them was highly intensified. The thermoplasmonic heating in such a condition was very strong, which was not only used to melt/weld two fibers together but also local control over chemistry was demonstrated by graphitizing the polymer using plasmonically generated heat. Such a huge containment of heat was not observed in the case of films and may be attributed to the less efficient conduction of heat in fibers because of dimensionality.

6.2 Outlook:

Another interesting aspect is the effect of fibrous structure on the conductivity switching of a blend of a conductive polymer, PEDOT-PSS, with a photoswitchable azobenzene (PAZ) compound. The blend was spread in the form of a film on top of electrospun PES fiber mat as well as on PES cast film. An excellent photoswitching of conductivity was observed when the fiber based system was exposed to repeated UV

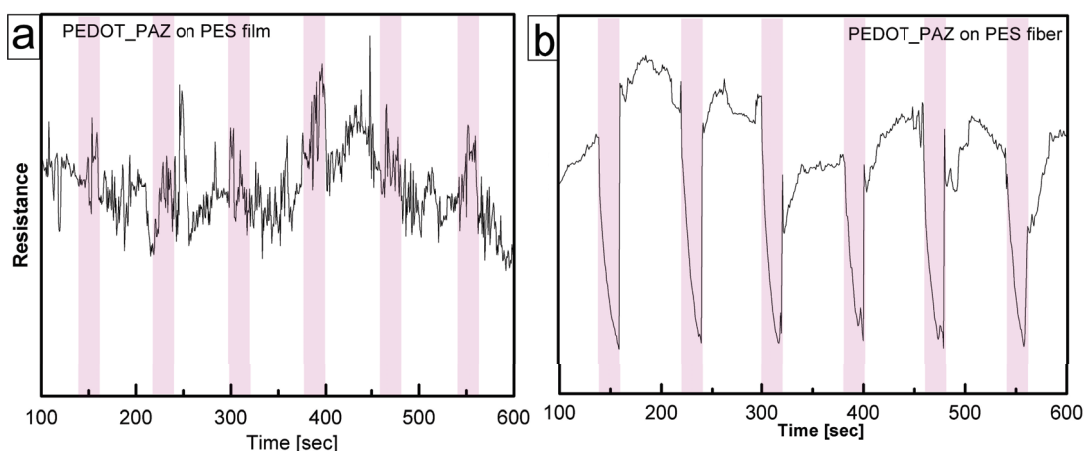


Figure 6.1 Photoswitching of electrical properties of PEDOT-PAZ film prepared on **a)** PES film, **b)** PES fibers. The time interval of UV exposure is shown by a violet band.

exposures, while no switching was observed for the film based system, **Figure 6.1**. In order to confirm that dimensionality of the substrate (PES fibers vs film) rather than the presence of PAZ was playing a decisive role for the appearance of a prominent switching, the PES fiber mat and film were coated with only PEDOT-PSS layer and the experiment was repeated in similar conditions. Here again appearance of a prominent switching in the case of fiber based

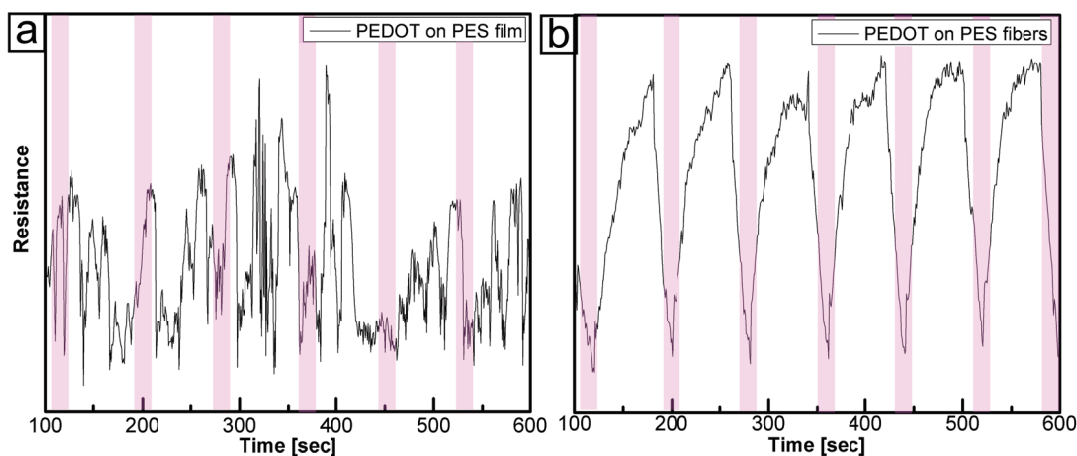


Figure 6.2 Photoswitching of electrical properties of PEDOT film prepared on **a)** PES film, **b)** PES fibers. The time interval of UV exposure is shown by a violet band.

system and absence of this effect in the case of a film type substrate confirmed that a

prominent switching in resistance on exposure to UV originated because of the substrate dimensionality, **Figure 6.2**. A probable explanation of this novel effect maybe the roughness and consequent higher surface area of the conductive layer that was laid on top of the fibers. However, more investigation is needed to understand the effect and its practical application.

Publications

Submitted papers

- Specular Reflection by Oscillating Photochromic Molecules with Tailored Photoswitchable Brewster Wavelength and Molecular Photonic Coupling
M. Elbahri*, **A. U. Zillohu**, B. Gothe, M. K. Hedayati, R. Abdelaziz, H. J. El-Khozondar, M. Bawa'aneh, M. Abdelaziz, A. Lavrinenko, S. Zhukovsky, S. Homaeigohar

Presently under peer review in "*Light: Science & Applications*", (reference number: LSA2014133).

Published papers

- Biomimetic Transferable Surface for a Real Time Control over Wettability and Photoerasable Writing with Water Drop Lens
A. U. Zillohu, R. Abdelaziz, I. Krasnov, M. Müller, T. Strunskus, Mady Elbahri*
Scientific Reports, **2014**, *4*, 7407.
- Thermo-plasmonics for Localized Graphitization and Welding of Polymeric Nanofibers
A. U. Zillohu, N. Alissawi, R. Abdelaziz, M. Elbahri*
Materials **2014**, *7*, 323.
- Photo-driven Super Absorber as an Active Metamaterial with a Tunable Molecular-Plasmonic Coupling
M. K. Hedayati, M. Javaheri, **A. U. Zillohu**, H. J. El-Khozondar, M. S. Bawa'aneh, A. Lavrinenko, F. Faupel, M. Elbahri*
Advanced Optical Materials **2014**, *2*, 705.
- Plasmonic Tunable Metamaterial Absorber as Ultraviolet Protection Film
M. K. Hedayati, **A. U. Zillohu**, T. Strunskus, F. Faupel, M. Elbahri*
Applied Physics Letters **2014**, *104*, 041103.
- Green Chemistry and Nanofabrication in a Levitated Leidenfrost Drop
R. Abdelaziz, D. Disci-Zayed, M. K. Hedayati, J. Pöhls, **A. U. Zillohu**, B. Erkartal, V. S. K. Chakravadhanula, V. Duppel, L. Kienle, M. Elbahri*
Nature Communications **2013**, *4*, doi:10.1038/ncomms3400
- Plasmon-mediated Embedding of Nanoparticles in a Polymer Matrix: Nanocomposites Patterning, Writing and Defect Healing
A. U. Zillohu, R. Abdelaziz, M. K. Hedayati, T. Emmler, S. Homaeigohar, M. Elbahri*
The Journal of Physical Chemistry C **2012**, *116*, 17204-17209.
- Bionanocomposite: Smart Metal-Polymer Bionanocomposites as Omnidirectional Plasmonic Black Absorber Formed by Nanofluid Filtration
M. Elbahri*, S. S. Homaeigohar, T. Dai, R. Abdelaziz, R. Khalil, **A. U. Zillohu**
Advanced Functional Materials **2012** (Inside Front Cover), *22*, 4626.

- Smart Metal–Polymer Bionanocomposites as Omnidirectional Plasmonic Black Absorber Formed by Nanofluid Filtration
M. Elbahri*, S. S. Homaeigohar, T. Dai, R. Abdelaziz, R. Khalil, **A. U. Zillohu**
Advanced Functional Materials **2012**, 22, 4771.
- Photoresponsive Transparent Conductive Metal with a Photobleaching Nose
M. Jamali, M. K. Hedayati, B. Mozooni, M. Javaherirahim, R. Abdelaziz, **A. U. Zillohu**, M. Elbahri*
Advanced Materials **2011**, 23, 4243.

Conferences:

- Poster presentation: “Electrospun Nanofibrous Affinity Membrane: a Modern Cleaning Method”
A. U. Zillohu, B. Gothe, T. Strunskus, M. Elbahri
International Symposium on Photochromism 2013, September 23 – September 26, 2013, Humboldt-Universität zu Berlin, Campus Mitte, Germany.

Acknowledgements

Studying in Germany was my dream ever since I was a school-going because German education, German people, their scientists and industry are famous around the world and I thank Allah who gave me opportunity to fulfill my dream and brought my PhD to a successful end. Since I started my studies after nine years of gap, many a time I did not feel myself up to the mark and I thank my parents for their prayers (and patience with my progress) and my friends for their ever ready support which led me successfully through this difficult task. I also find myself very thankful and indebt to the government and people of Germany for offering a free education to all. I feel proud that I spent a part of my life within this great nation and it will always be a source of good memories for me.

I would like to say my sincere gratitudes to Prof. Dr. Mady Elbahri, for supervising my PhD work. I feel lucky to work in his group, Nanochemistry and Nanoengineering, where I worked in a friendly environment and my work received his personal attention despite his tight schedule. Without his guidance I could not have completed this huge task.

I would also like thank Prof. Dr. Volker Abetz, Head of Center for Polymer Research, Helmholtz Zentrum Geesthacht (HZG), for giving me the opportunity to do my experimental work using the well renowned facilities of his institute.

My stay in HZG, which started from my Master thesis to more than the middle of my Ph.D., was probably the best part of my life. I would like to thank Joachim Koll for his ever ready help. My special thanks to PMC group, Clarissa Abetz, Karen-Marita Prause and Sabrina Bolmer for their patience and help in teaching me different characterization techniques. I also remember with gratitude, the kind help of Dr. Thomas Emmeler with Raman analysis technique. My special thanks to Silvio Neumann, Heinrich Böttcher for their help in thermal analysis, FTIR and mechanical testing. Help from Berthold Wendland for instrumental setup is also appreciated. I also thank Holger Pingel and Gunter Lühns for keeping the environment safe for work. My special thanks to Ilona Zillich, Dr. Karin Kirstein, Katja Quetschke, Ingrid Hagge, Christine Plath and Peter Kummerow for helping me out with managerial problems. My hearty thanks to my friends, Dr. Shahid Majeed, Aurangzeb Khan, Muntazim Khan, Mushfequr Rahman, Shehzad Khan, Husnul Maab, Rakibul Kabir and Shahin Homaeigohar for their nice company which made me feel Geesthacht as my home.

A third of my PhD duration was spent in TF, CAU Kiel where I came to know with many good colleagues. I want to thank Bastian Gothe, Zahwa Kareh, Usman Saleemi, who did their master thesis with me, for their hardwork and patience with me. I also want to thank

Acknowledgements

my group fellows Duygu Disci, Rania Khalil, Mehdi Hedayati, Moheb Abdelaziz, Jason, Fabian Schütt, Worley and Ramzy Abdelaziz for all their support and good time. My sincere gratitude to Burak Erkartal, Viktor Schneider and Alexander Hinz for the useful discussions and Stefan Rehders, Peter Sommer, Mathias Hoppe, Kay Rath and Christoph Ochmann for their invaluable help and for providing me with a nice working environment. I wish all of them a successful future and best of everything.

I would also like to thank German Educational Exchange Service (DAAD), especially Monika Osman, Kerstin Richter, Hellen Sahlmann, Angela Becher and Patricia Guzman, for giving me financial support and looking after me during my stay in Germany. I would also like to appreciate the Higher Education Commission of Pakistan, especially Irfan Abbas, for the financial support and taking care of my case. Financial support from DFG for the project SFB C09 is also appreciated. Last but not least, my special thanks my supervisors and colleagues in Pakistan for supporting me during my studies abroad.

Finally, I would say that staying and studying in Germany was one of the best experiences in my life and my best wishes for all my friends and colleagues in Germany.

List of Figures:

Figure 2.1	Comparison of wetting behavior of loose fiber with fiber yarn	18
Figure 2.2	Mobile ‘yarn device’ with real time control over wetting properties.....	19
Figure 2.3	Amorphousization of PVDF due to intercalating SPO molecules	21
Figure 2.4	Water drop as a UV lens.....	23
Figure 3.1	Spectral change during photochromic effect.....	32
Figure 3.2	Photoexcitation of electron into higher energy level (schematic).....	33
Figure 3.3	Structure of SPO with ring opening mechanism (schematic).	34
Figure 3.4	Positive and negative solvatochromism of photochromic compounds.	35
Figure 3.5	Positive solvatochromism of SPO.....	35
Figure 3.6	Oscillating dipoles of SPO as a radiative antenna, along with absorption spectra of different polymer matrices containing SPO.....	39
Figure 3.7	Ellipsometry analysis of angular reflectance, of p- and s-polarized light, from SPO loaded polymer films.	41
Figure 3.8	UV exposed samples showing a significant, matrix dependent change in Brewster wavelength. Real and imaginary parts of refractive index of PS-SPO Film.	42
Figure 3.9	Color and transparency by refractive index modulation in thin films and fibers.	45
Figure 3.10	Reflectance and transmittance spectra of silver film coated with PS-SPO blend	51
Figure 3.11	Dipole-dipole interaction of SPO molecules with their image in metal film (schematic).....	52
Figure 3.12	Photograph showing switchable optical transparency of the hybrid system.	53
Figure 3.13	Photo-reversion and vapor assisted reversion of SPO into its closed form.....	54
Figure 4.1	Oscillation of electron cloud relative to nucleus upon irradiation	61
Figure 4.2	Silver sputtered PVDF film (AFM height contrast).....	69
Figure 4.3	Thermoplasmon assisted patterning on silver coated PVDF film. AFM surface profile and color of pattern depict embedment of silver nanoparticles..	69
Figure 4.4	UV-Vis spectrum before and after silver embedment.....	70
Figure 4.5	Melting feature size control by laser power and time of exposure.....	71
Figure 4.6	Recrystallization features on resolidified spots. Raman analysis showing conformation modification in the resolidified area	72
Figure 4.7	Repair of a simulated microcrack with thermoplasmonic welding.	73
Figure 4.8	Size growth and shape elongation of silver particle sputtered on nanofibers with increasing coating thickness	80
Figure 4.9	UV-Vis spectrum of PVDF fiber-Ag composite, with increasing thickness of silver coat.	81
Figure 4.10	Welding and graphitization of silver coated nanofibers.....	82
Figure 4.11	Raman confirmation of graphitization in the heat affected spot.	83
Figure 5.1	Basic electrospinning process (schematic).....	89
Figure 5.2	Basic spin coating process (schematic).	91
Figure 5.3	Principle of a sputter coater (schematic).	92
Figure 5.4	Volumetric distribution of different signals generated from a sample during SEM analysis (schematic).	94
Figure 5.5	Essential parts of an SEM (schematic).....	95
Figure 5.6	Working principle of AFM (schematic).....	97
Figure 5.7	Nature of forces in different working modes of AFM.	97
Figure 5.8	Energy level diagram for Raman scattering phenomenon.	99
Figure 5.9	Raman microscope used in this thesis.	100
Figure 5.10	Bragg’s law presented schematically.	102

Figure 5.11	Water drop with Young's interfacial energy terms.	103
Figure 5.12	Water drop in Cassie and Wenzel states.....	104
Figure 5.13	Polarization of reflected light at Brewster angle.	104
Figure 6.1	Photoswitching of electrical resistance of PEDOT-PSS:PAZ film on PES film and fibers.....	115
Figure 6.2	Photoswitching of electrical resistance of PEDOT-PSS film on PES film and fibers.....	115

List of Tables:

Table 2.1	Tilt angles required to initiate the drop rolling on surfaces with different roughness.....	20
Table 2.2	Tilt angles required to initiate the drop rolling on different surfaces with added SPO.....	22
Table 3.1	Refractive indices and dipole moments of the polymer matrices.....	40